COMPENSATION OF GERMANIUM BY RADIATION DEFECTS

by

LIONEL COOPER KIMERLING

S.B. Massachusetts Institute of Technology (1965)

Submitted in partial fulfillment of the requirements

for the degree of

DOCTOR OF PHILOSOPHY

at the

Massachusetts Institute of Technology

1969

Signature of Author
Department of Metallurgy

Signature of Professor
in Charge of Research

Signature of Chairman of
Departmental Committee on
Graduate Students

ABSTRACT

COMPENSATION OF GERMANIUM BY RADIATION DEFECTS

by

LIONEL COOPER KIMERLING

The electronic behavior of radiation defects in high purity germanium was studied in order to evaluate the role of irradiation in the mechanism of carrier compensation. In particular, the role of impurities as defect stabilizing agents was investigated.

A technique was developed for the growth of highly perfect, high purity germanium single crystals by the Czochralski method. Antimony doped n-type crystals were grown with impurity concentrations as low as 6×10^{12} cm^{-3}. Undoped p-type crystals were prepared with acceptor concentrations as low as 2×10^{11} cm^{-3}. Dislocation densities in these crystals were kept below the level of 1000 cm^{-2}. Most crystals exhibited the well known tendency to contain a highest impurity content in the center of their cross section (core).

Hall coefficients and minority carrier lifetimes were measured as a function of temperature for n- and p-type samples irradiated with cobalt 60 gamma rays. Defect energy positions were determined at 0.20 eV below the conduction band edge (i.e., E_c - 0.20 eV), E_c - 0.09 eV, and E_v + 0.26 eV, in n-type material. A defect level at E_v + 0.16 eV was found in p-type material. The level at E_c - 0.09 eV was correlated with the presence of oxygen in the lattice. The level at E_c - 0.20 eV was found to be in a neutral charge state at room temperature and acted as a recombination center for holes. The E_v + 0.26 eV state was found to possess a double negative charge at room temperature and functioned as a temporary trap at low temperatures. Measurement on a variety of n-type samples indicated that energy states located below the middle of the energy gap became more stable as the initial donor concentration increased. The E_v + 0.16 eV level in p-type material was determined to have a negative

charge state at room temperature and acted as a recombination center for electrons. The stability of this state was observed to increase with initial acceptor concentration. A small net decrease in the hole concentration upon irradiation indicated that both donors and acceptors are introduced in p-type material.

The net defect introduction rate was measured in terms of the carrier compensation rate for a fixed dose of radiation. In as-grown material the initial donor concentration was observed to have a strong influence on the defect introduction rate for n-type crystals. A model was developed for the stabilization of defect vacancies by association with donor impurities in the lattice. Interpretation of the experimental results on the basis of this model indicates that 50 percent of the vacancies introduced by irradiation undergo annihilation with the interstitials with which they were originally associated.

P-I-N radiation detection devices were constructed as an application of the radiation compensation process. These structures yielded an energy resolution of 1.6 percent for the cesium 137 spectrum which compares favorably with a .5 percent resolution obtained with the best detectors produced using the lithium-drift process. The compensation by radiation defects was found to be stable at room temperature. The role of materials parameters in device construction and performance was considered.

Thesis Supervisor: H.C. Gatos

Title: Professor of Electronic Materials

TABLE OF CONTENTS

LIST OF FIGURES

This is the most complete text of the
thesis available. The following page(s)
were not included in the copy of the
thesis deposited in the Institute Archives
by the author:

$$\# \; X - X I$$

LIST OF TABLES

ACKNOWLEDGEMENTS

Radiation Facilities at Massachusetts General Hospital.

The M.I.T. library system was of great help in the use of their facilities.

A major role in every aspect of this work was contributed by my wife, Linda, who typed the rough and final copies of this thesis and whose interest and enthusiasm were limitless.

I. INTRODUCTION

The unique electrical properties of semiconductors have long been studied and appreciated. However, the intrinsic properties of these materials are rarely entirely utilized and have been studied in only a limited range. The reason for this situation rests with the presence of structural defects in the lattice.

In an ideal germanium crystal all atomic valence electrons are involoved in localized covalent bonds. Thus, no conduction can exist unless carriers are excited into a conduction state by the application of external energy. For the case of germanium, the thermal energy supplied at room temperature will excite approximately 3×10^{13} carriers per cubic centimeter; at liquid nitrogen temperature ($77^{\circ}K$) practically no excitation occurs.

However, the presence of chemical impurities and crystal imperfections cause localized perturbations of the bonding scheme which introduce states requiring very little energy for ionization. Thus, relatively high concentrations of conduction electrons exist which " freeze out " only in the vicinity of absolute zero temperatures.

The most modern purification and crystal growth techniques are able to produce material which is only intrinsic at room temperature. Most semiconductor devices do not even require

this degree of perfection for starting material. However, striking, recent advances in the detection of nuclear radiation have been achieved employing very high resistivity germanium material as an ionizing medium. The remarkable success of these devices has stirred considerable interest in structures with less than 10^{10} free carriers per cubic centimeter.

As mentioned earlier, the highest purity single crystal material available contains, still, 10^{12} - 10^{13} carriers per cubic centimeter at $77^{\circ}K$. The free carrier concentration, in this case, can be reduced only by the introduction of compensating imperfections into the crystal structure. These imperfections are characterized by energy states which electrically ionize in an opposite sense to those initially present in the material. In n-type material conducting electrons would be removed from circulation by the ionization of acceptors. Donors would act similarly to reduce conduction by holes in p-type material. A simplified energy level diagram is shown in Figure 1. It is evident that only the net excess states of the majority type of imperfection will contribute to conduction.

In semiconductor materials science, the process of compensation is usually associated with a degradation of electronic properties. This association is based on the observation that the introduction of ionized centers tends to increase the number of scattering events that a carrier

will experience and, thus, decrease its effective mobility. It has also been noted that impurities with deep levels (high ionization energies) such as gold, produce a drastic decrease in minority carrier lifetime by acting as intermediate states for recombination. Very high levels of compensation, though, have been recently achieved by ion-drift techniques (see section II-C) while having the above mentioned parameters basically unchanged. The compensation level, however, tends to degrade above 77°K.

The current study is undertaken with these aspects in mind. Although the exact mechanism is still unclear, it is believed high energy particles displace germanium atoms from their normal lattice positions leaving behind deep acceptor states in the form of vacancies and vacancy complexes. Besides tightly binding electrons from donor states initially present in the material, these levels can also act as scattering centers, recombination centers, and temporary traps for non-equilibrium carriers. However, there is good reason to believe that these effects are secondary to the process of carrier removal for low doses of radiation.

The attraction of this method is that it represents probably the fastest and cleanest means yet devised for the modification of semiconductor properties. In addition, radiation defects have been shown to be stable well above room temperature; and, the use of deep levels eliminates the concern for precise concentrations because such levels are not ionized at low

temperatures (77°K).

Radiation effects may possibly be considered as the current enigma in semiconductor science. The major conceptual difficulty has been the absence of an exact mechanism for the formation of stable defect configurations.

The purpose of this investigation is to develop an understanding of the effects of radiation induced defects on the electronic behavior of germanium. The nature of the compensation process is studied for low dose levels in carefully grown, high purity material, and an attempt is made to correlate these results with proposed defect structures in the germanium lattice.
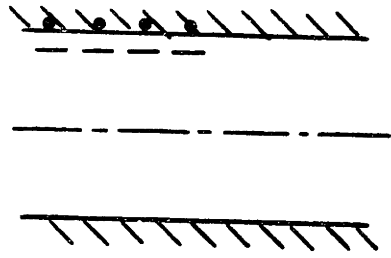
a) Conduction by electrons.
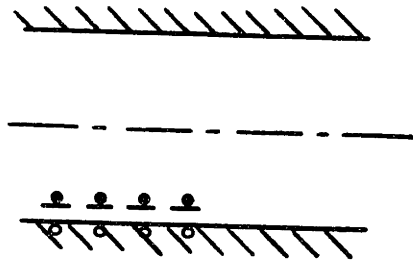
b) Conduction by holes.
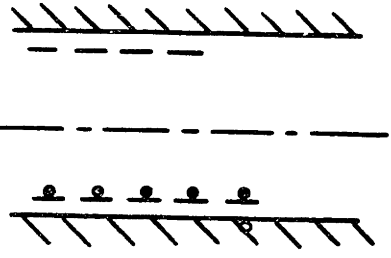
c) Compensation with excess shallow acceptors.
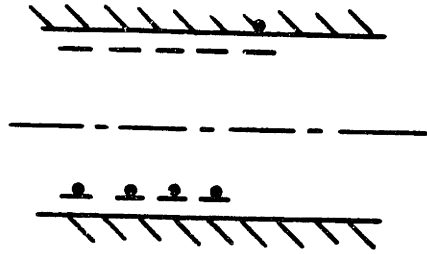
d) Compensation with excess shallow donors.
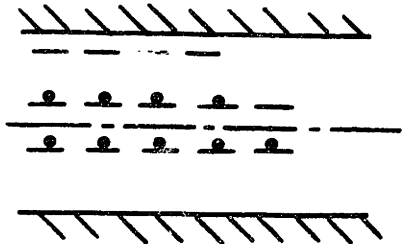
e) Compensation with excess deep levels.
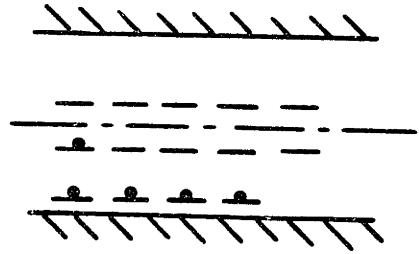
f) Compensation with excess deep levels.

Figure 1.   Schematic Representation of Compensation Effects
in N-Type (a,c, and e) and P-Type (b,d, and f)
Materials at $77^\circ K$.

II. BACKGROUND AND PREVIOUS WORK

A. Radiation Defects in Germanium

The study of the effects of energetic radiation on semiconductor properties has been expanding greatly since the early 1950's. However, as mentioned earlier, few unambiguous results have been obtained. Recent findings, indicating long range motion of defects below 77°K, have put many earlier conclusions in doubt.

The predominant effect of irradiation on the electronic properties of germanium is the introduction of deep energy states in the forbidden gap. This result has provided a most sensitive means of observing displacement effects. However, analyses of early experiments were inconsistent and inaccurate because occupation statistics had not yet been developed to describe correctly the effects of deep levels. Only recently have experimental techniques and analyses been apparently modified to handle this unique problem. For this reason, early work will be noted sparingly and qualitatively, and only recent results will be given full consideration. The literature concerning the effects of gamma radiation on Ge is primarily considered.

Energetic photons introduce lattice damage by means of high energy electrons produced as energy is absorbed from the radiation. The dominant interaction for gamma rays with energies in the range of 1 to 2 MeV is the Compton process.

The energy spectrum of the Compton electrons extends from very low values to a maximum given by

$$E_c(\text{max}) = 2E_\gamma^2 \, (m_e c^2 + 2E_\gamma)^{-1},$$

where E_γ is the gamma ray energy, m_e the electron rest mass, and c the speed of light. A pertinent example is cobalt 60 radiation which consists primarily of two photons of energies 1.17 and 1.33 MeV. The resulting $E_c(\text{max})$ has a value of about 0.95 MeV.

For energies of about 1 MeV or more, these electrons produce displacements via direct interaction with the Coulomb potential of the nucleus in the solid. A discussion of this process is given by Seitz and Koehler[1].

For energies much below 1 MeV long range Coulomb interactions come into play as atomic electrons effectively screen the nucleus from collision. The higher energy electrons, in this case, dissipate energy via photoelectric ionization and low energy Compton scattering.

The threshold energy for defect production (E_t) is defined as the energy required to impart displacement energy (E_d) to a lattice atom. Values for the threshold electron energy in germanium have varied with the effect being measured and the experimental technique. The values most acceptable today are $E_t = 400$ keV and $E_d = 15$ eV which were determined by lifetime[3] and resistivity[2] techniques.

Oen and Holmes[4] have calculated displacement cross sections for gamma rays of energies up to 5 MeV in solids

with a variety of atomic masses and displacement energies.
The observed defect yield[5] is about an order of magnitude
less than predicted by calculations.

A collision of a sufficiently energetic electron with
an atomic nucleus will result in the displacement of the
atom to a metastable interstitial site leaving behind a
vacancy. Silsbee[6] has estimated that focusing of collisions
along nearest neighbors in a close packed direction should
be significant in the relatively open diamond cubic lattice.
It is also expected that if electron energies are not much
greater that the threshold energy (as for Co^{60} irradiation,
E_c(max) = 0.95 eV), the recoiling atom will be displaced
only a few lattice spacings. Therefore, it is expected that
the irradiation of germanium by cobalt 60 gamma rays will
produce, primarily, closely spaced vacancy-interstitial
pairs. Furthermore, the penetration power of gamma rays
indicated, that these defects should be homogeneously
distributed.

The lack of correlation between calculated and observed
damage rates implies that a relaxation effect of some kind
has been overlooked.

Several notable attempts have been made to relate primary
damage with the deep energy levels found in irradiated material.
H.M.James and K. Lark-Horovitz[7] have given a qualitative
argument relating acceptor levels to vacancies and donor
levels to interstitials based on the hydrogenic behavior of

these defects. Blount[8] proposed a similar explanation
from a tight-binding description of the defects. Both points
of view tend to describe the observed effects, but they are
limited in that they are qualitative and do not consider the
relaxed defect configurations that actually exist.

The spectrum of energy levels in gamma irradiated
germanium has been investigated rather intensively but not
conclusively. Fan and Lark-Horowitz[9] observed, early, the
change of conductivity with radiation of n-type material.
The conductivity decreased to a minimum and then increased
to a constant value. The minimum was associated with a change
in conductivity type from n- to p-type. The dose required to
reach the minimum was found to vary directly with the initial
conductivity. It was observed, independently[10], that
in p-type germanium, the hole concentration tended to
approach a limiting value upon irradiation. The behavior of
n-type material has become well established over the years,
but there is still considerable discussion concerning p-type
germanium.

The determination of the energy positions of these
levels in the enegy gap has not always yielded consistent
results. The recent work, mentioned below, is the most
generally accepted. All irradiation was with cobalt 60
gamma rays at room temperature unless otherwise stated. In
n-type antimony doped germanium, Crawford and Cleland[11]
observed two deep levels, one at 0.23 eV below the conduction

band (E_c - 0.23 eV) and one near or below the middle of the gap. These were studied with Hall measurements and found to be introduced in essentially equal concentrations.

Ishino, et al[12] observed levels in antimony doped germanium at E_c - 0.21±.01 eV, E_c - 0.09 eV, and at or below midgap; and in arsenic doped material at E_c - 0. 25 eV, E_c - 0.09 eV, and at or below midgap.

Vitovskii, et al[13] used a variety of antimony concentrations with a variety of radiation doses in initially n-type material to sweep the Fermi level through the energy gap. Levels were located at E_c - 0.2 eV, E_v + 0. 26 eV, E_v + 0.11 eV, and E_v + 0.02 eV with Hall coefficient-temperature profiles. By extension of measurements to liquid helium temperatures (4°K), they concluded that E_c - 0.2 eV was the uppermost level.

Using lifetime-temperature profiles, Ryvkin, et al[15] observed a recombination level at E_c - 0.2 eV and a trapping at E_v + 0.24 eV in antimony doped material.

Curtis[16], using the same technique, found a recombination level at E_v + 0.36 eV for antimony doped material. and at E_v + 0.28 eV in arsenic doped material.

Recently, Streetman[17] continued the work of Curtis and found a recombination level at E_v + 0.35 eV and a trap at E_v + 0.21 eV which increased in concentration upon annealing in antimony doped germanium. In arsenic doped material, a recombination level at E_v + 0.32 eV was found

with a trapping level at E_v + 0.16 eV.

By analyzing the photoconductivity spectrum of irradiated antimony-doped germanium, Mashovets and Khansevarov[18] observed the production of levels at E_c - 0.20 eV, E_c - 0.34 eV, E_v + 0.27 eV, E_v + 0.22 eV, and E_v + 0.11 eV. It was concluded that the E_c - 0.20 eV and E_v + 0.27 eV were different ionization levels of the same defect because the upper level was not observed when the lower level was partly filled, and the lower was not observed when the upper was completely filled.

More recently in the U.S.S.R.[19], a level at E_c - 0.09 eV was identified in oxygen doped germanium with photoconductivity analysis.

Frequent attempts have been made to assign these levels to various defect structures based on the James and Lark-Horowitz scheme, but it still remains to be shown that they are associated with the simple point defects.

It is certainly of interest to consider, also, the stability of these defect states. The activation energy for self diffusion in germanium has been determined to be about 3 eV[20]. The rate at which thermal quenching introduces acceptor defects in germanium indicates an energy of formation of about 2 eV[20]. If it is assumed that simple vacancies are involved in both cases, the activation energy for vacancy motion would be about 1 eV. Thus, one would not expect major annealing to occur until well above 100°C.

Two annealing stages at very low temperatures in n-type germanium have been observed by Klontz and MacKay[21]: one stage at 35°K and one at 65°K. Together they account for about 50 percent recovery in carrier concentrations. Supplementary data on these levels indicate that the charge state of the defects is of primary importance.

Brown, et al[22], in n-type and p-type germanium, (irradiation at 80°K) have found annealing stages beginning at 200°K. This also coincided with the emptying of electron traps indicating, again, that the charge state of the defect is important. Dependence on impurity type was also demonstrated.

Annealing in the room temperature range was further studied in depth[22] and indicated a maximum recovery in carrier concentration of about 20 percent (50 percent mobility recovery) in the range of 0 to 70°C. This behavior was strongly dependent on impurity type and concentration. It was noted during this annealing stage that a level was introduced at E_c - 0.09 eV. Further annealing did not occur until temperatures above 150°C.

Two conclusions can be drawn from these results: (a), defects resulting from room temperature irradiation, which usually involves "gamma heating" to about 60°C, are stable to at least 150°C; (b), these defects are not simple vacancy-interstitial pairs.

In concluding, some new findings are mentioned that are

currently leading to a reinterpretation of many previously proposed defect configurations. Whan[24] has detected two infrared absorbtion bands in oxygen doped germanium (irradiated at 25°K) which have been conclusively identified with a form of oxygen-vacancy complex. These bands were observed to appear at about 65°K! The diffusion of oxygen in germanium has been studied extensively, and it appears that oxygen is not the mobile species (The energy of migration is 2 eV[25].). This result implies that vacancies are in motion at these low temperatures, with a migration energy of about 0.2 eV! Watkins had previously drawn similar conclusions based on E P R measurements on silicon. He proposed migration energies of 0.33 eV for the neutral vacancy[26] and 0.18 eV for the doubly negative vacancy[27] in the silicon lattice.

It appears that the past fifteen years have served as an incubation period in the study of point defects in solids. Recent studies on the identification of defects using electron paramagnetic resonance techniques in silicon[28] (not amenable to germanium) and infrared absorbtion spectra[24] in both silicon and germanium have provided the first break-throughs in the field. However, the theory concerning the mechanisms of defect formation and annealing is still in a rather unsatisfactory state and not much help in guiding experiments. It is expected that as the understanding of defect configurations is developed, similar studies of the processes involved will prove fruitful.

The effects of radiation induced defects on the electrical properties of germanium have received considerable attention but are still not well characterized. In the author's opinion, this is due to varying experimental techniques and analyses, and unidentified microscopic variances in the materials being considered. It is felt that accurate characterization of the virgin material should give more coherence to these findings.

Excellent reviews summarizing the present state of the study of radiation defects in semiconductors have been recently published by Crawford[29] and Corbett[30].

B. Growth of Germanium Single Crystals

One of the most important steps in the study of the effect of any outside influence on a material is the accurate characterization of the starting material. As has been previously indicated, the electrical and physical properties of a semiconductor are highly sensitive functions of the perfection of the crystal structure. One distinguishes between foreign atoms, point defects, and line defects, but, as a general group, all must be characterized if the behavior of the material is to be understood. Purification takes place in the initial phase of preparation and must be maintained through crystal growth where the avoidance of physical imperfections is of primary concern.

1. Crystal Purity

Commercial high purity germanium contains approximately 10^{12} donor and/or acceptor impurities per cubic centimeter. The purification process consists, generally, of the following steps:

(a) Fractional distillation of chlorides from various ores in which germanium is a main constituent. This initial, crude $GeCl_4$ contains arsenic and boron as main impurities and is further purified by fractional distillation in an oxidizing medium (8N HCl + Cl_2) in quartz stills.

(b) Hydrolysis with doubly distilled water according to the reaction

$$GeCl_4 + 2H_2O \rightarrow GeO_2 + 4HCl$$
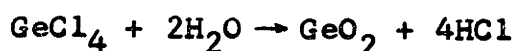
(c) Reduction of the washed and dried GeO_2 powders in silica or graphite crucibles in purest hydrogen at about $660^{\circ}C$ and melting down to bars at about $1000^{\circ}C$.

The resulting germanium is then purified to commercial levels by multipass zone refining[31]. With the exception of boron which is effectively removed during the fractional distillation of the chlorides, the commonly encountered impurities in germanium are more soluble in the melt than the solid ($k = C_s/C_l < 1$) so that the method is extremely effective.

The residual impurities in commercial high purity

germanium are frequently unidentified but generally attributed to boron. The material is usually p-type, and boron is the most common element not affected by zone refining. Aurich and co-workers[32] found that exhaustive zone refining of commercial high purity material could not reduce the impurity level below 5 x 10^{11} per cubic centimeter. They postulated that boron was reintroduced during the purification process by the attack of germanium chloride radicals, existing temporarily during the hydrolysis process, on the quartz or glass vessel containing the reactants. By inserting a high purity paraffin liner in the glass vessel and employing a float-zone process as a final stage, they claim that material with an impurity concentration of less than 10^{10} per cubic centimeter was produced. However, the dominance of surface conduction in their measurements and the detection of deep levels complicate the interpretation of their data.

Very recently, Hall and co-workers have begun an intense effort to produce high purity single crystals of germanium[33]. Using a specially modified Czochralski furnace to minimize handling, germanium has been grown at purity levels of 2 to 5 x 10^{11} per cubic centimeter. They, too, presumed the identity of a frequently appearing, non-segregating acceptor to be boron. It appears that these impurities are not present in the source material, but, rather, are introduced during growth. Here, also,

the presence of deep levels in cases where "boron" is not found denies a unique characterization of the material.

Purification is the natural result of the normal freezing process where impurities have a distribution coefficient ($k = C_s/C_l$) of less than unity. This, as stated earlier, is the basis for zone refining. However, the conditions of crystal growth are not usually those defined at equilibrium. Therefore, some concern with growth kinetics is necessary to maximize this segregation effect.

Classic studies on Czochralski growth from the melt have been performed by Burton et al[34], Thurmond[35], and Hall[36]. Their theoretical models cannot be regarded as rigorous because an atomic mechanism for crystal growth has not yet been established. However, their conclusions regarding the departure from equilibrium do rather accurately describe the observed behavior.

Basically, it is maintained that equilibrium can exist only for very slow rates of growth. If this is not the case, impurity atoms are rejected faster than they can diffuse into the bulk of the melt. This creates an enriched boundary layer just ahead of the growth interface which leads to an effective k greater than the equilibrium value. It has been predicted and confirmed by experiment that k will approach its equilibrium value under the conditions of slow growth and efficient stirring in the

melt. A high rate of stirring is also expected to give a more homogeneous distribution of impurities by reducing radial temperature gradients at the growth interface.

2. Structural Perfection

Liquid germanium has a higher density than it solid. As a result, imperfections are frequently introduced during solidification by stresses generated as the melt expands against the crucible walls. Therefore, techniques which provide for a free expansion of the melt are preferred for highest structural perfection.

Recently, zone melting methods have been modified with the use of pre- and after-heaters and magnetic stirring so that a high degree of structural perfection can be achieved. These methods are limited, however, to the growth of crystals with a rather small diameter. For applications such as the radiation detectors mentioned in the introduction, which require large volumes of highly perfect material, the Czochralski technique[37] as modified by Teal and Little[38] is the most desirable. (This procedure will be discussed here.)

Their method consists of vertical pulling from the melt beginning with an oriented seed. Using this technique, Runyan[39] has reported the growth of crystals up to 15 centimeters in diameter. Since the growing crystal is not in contact with a crucible, the method is desirable from the standpoint of both purity and crystal perfection.

The prerequiste for a physically perfect crystal
is the maintenance of a flat liquid-solid interface during
growth. This is a direct result of the absence of radial
temperature gradients. While a detailed discussion will
not be given here, it is mentioned that in order to minimize
these gradients, one must be concerned with the following:

(a)   isotherms in the melt,

(b)   radiation losses at the growth interface,

(c)   dissipation of latent heat of fusion.

It is believed that dislocations are generated in
order to relieve radial thermal stresses that result
during the growth process. Dash[40] has suggested a
method to limit dislocation formation by reducing the seed
diameter to about 1 millimeter before growth. This is
based on the idea that most of the dislocations present
in the seed will grow out during this stage; and new
dislocations will not easily be generated, in later stages,
without a significant concentration of "sources" present
to permit glide.

A number of experiments have been undertaken to
measure the electrical properties of dislocations in
germanium[41,42]. Early results must be interpreted
with some reservation.because of the failure to adequately
consider the generation of point defects and polygonization
occuring at the high temperatures required for deformation.
Also, analysis of the data is somewhat complicated because

the occupation probabilities of states on a single dis-
location line are interrelated[43]. Acceptor levels have
been located between E_c - 0.2 eV and E_c - 0.35 eV in n-
type material[44] and donor levels at about E_v + 0.09 eV
in p-type material[45].

Wertheim and Pearson[46] made a detailed study of the
effect of dislocations on lifetime. It was found that
in p-type material the variation was described by

$$\tau = .7 N_d^{-1}$$

where N_d is the number of dislocations per square centimeter.
In n-type material the relation was

$$\tau \approx 2.5 N_d^{-1}.$$

Vogel[47] has shown that tilt boundaries encourage
recombination processes to an even greater extent.

Logan, et al[48] have demonstrated that dislocations
can effect carrier mobility in n-type material at low
temperatures. The mobility of carriers traveling parallel
to the dislocation line was unchanged, while the mobility
perpendicular to the line was greatly reduced.

It is well known that point defects, such as vacancies,
are present in all crystals, even at equilibrium. Tweet[49],
using dislocation free germanium, concluded that vacancies
tend to cluster upon cooling (in crystals of low dislocation
content) to configurations which are electrically neutral.
Letaw[50] observed similar effects and proposed a theory
for vacancy precipitation. Recent work by Hiraki and

Suita[51], and Fuller and Wolfstirn[52] provide further evidence that vacancy clusters are present in as-grown crystals.

Early work concerning the electrical activity of quenched-in defects is believed to be in error due to the undetected presence of copper impurities. Surveys of the primary studies have been given by Letaw[50], and Hiraki and Suita[51]. Penning[53] observed an acceptor level at $E_v + 0.02$ eV by the study of the precipitation kinetics of copper and nickel in germanium. Fuller and Wolfstirn[52] located an acceptor level at $E_v + 0.02 - 0.03$ eV, and Hiraki and Suita[51] found levels at $E_v + 0.03 - 0.05$ eV and $E_v + 0.19$ eV with quenching studies. Recently, Mashovets, et al[54], using gold as a getter for copper, found levels at $E_c - 0.2$ eV and $E_v + 0.04$ eV in germanium quenched from above 500°C.

As in the case of radiation effects, it must be mentioned that the determination of the mobility of the monovacancy is critical to the interpretation of these results.

Stojic and Hasiguti[55], and Swanson[56] have recently reported an appreciable amount of recovery upon quenching to 77°K and warming at room temperature.

The one remaining concern in crystal growth is the homogeneity of the distribution of defects in the crystal cross section. Struthers, et al[57] showed very early

that resistivity and lifetime can vary rather sharply within an as-grown crystal. A survey of work on this subject is given by Schafft, et al[58].

In conclusion, it is emphasized that methods for the exact characterization are still not well developed. While valuable observations have been made regarding the production and properties of some crystal defects during growth, a detailed discussion must still be based partly on speculation. The electrical properties of growth defects must be considered specifically, in high purity materials. The increasing demand for high crystalline perfection (radiation detection devices, for instance) requires that a much more in depth understanding of the principles involved be developed.

The behavior of point defects in the solid, as discussed earlier with regard to radiation damage, has revealed, clearly, that a semiconductor crystal cannot be accurately characterized merely by its dopant concentration.

C. Semiconductor Radiation Detectors

The advantages of using semiconductor structures for radiation counters are now well known. The high stopping power of the semiconductor solid and the relatively small energies required for ionization lead to an ideal device for high resolution spectroscopy.

For the detection of high energy radiation such as

beta and gamma rays, large sensitive volumes are required
for maximum counting and energy resolution. The most
widely used structures are p-i-n devices employing a
large volume of "insulating" or highly compensated semi-
conductor ("i") as the depleted or sensitive region. It
is desired that the semiconductor have a large atomic
number and small band gap so that it exhibits a large
cross section of interaction to the incident radiation. The
radiation absorbed by the crystal produces a charge by
photoelectric ionization proportional to the particle
energy. For highest resolution, all of the charge must
be collected. Consequently, very high mobility and long
lifetime are required.

The most widely used method (which has resulted in
good detectors) for producing the "i" region consists
in drifting lithium interstitial atoms into p-type germanium
under an electric field[59]. In this way precise compen-
sation is accomplished through the ion-pairing of the
positively charged lithium donors with the negatively
charged acceptors present in the crystal. However, long
times are required for drifting (usually months) and low
storage temperatures are necessary to maintain the stability
of the donor-acceptor pairs and thus, prevent diffusion
of the highly mobile lithium to sinks which leads to the
degregation of the detector [60,61].

The concern for compensation within a reasonable

amount of time has led to the consideration of using
deep traps in an n-type material. The tedious process
of exact compensation is not necessary because the deep
acceptor levels will remove the electrons from the shallow
donor levels but will, themselves, not be electrically
active at the low temperatures of the device operation
(77°K). Recent reports from the Soviet Union[62,63] have
discussed the compensation of n-type germanium by irradiation
and the subsequent construction of a structure suitable
for radiation counting. According to these reports, the
resolution of such counters is almost as high as that
of counters prepared by lithium drifting. A resolution
of about 3 percent for the 662 keV cesium 137 gamma photo-
peak was originally reported for the new detectors and
was subsequently improved to 2.2 percent for the 122 keV
peak of cobalt 57 and .4 percent for the 1.33 MeV peak
of cobalt 60. The energy resolution of the best lithium
detectors is .5 percent for cesium 137 and 3 percent for
cobalt 60[64]. Very recently, preparation of the same
detector was announced in this country[65].

The fabrication of the lithium drifted detectors has
met with major difficulties with regard to the yield of
finished devices and the consistency of their energy
resolution[66,67]. The difficulties are apparently
associated with the starting germanium crystals (crystalline
perfection, impurity concentration and homogeniety). The

materials problems in the radiation compensated counters are equally acute[68] and probably result from similar effects.

Since the introduction of germanium radiation detectors in 1964, the performance of these detectors has been well characterized. However, the understanding of the processes involved has not made similar progress. If the potential performance of these counters is to be fully realized, the influences of structural and chemical defects on device performance must be identified and understood.

III. OUTLINE AND PLAN OF WORK

The compensation of germanium by radiation defects introduced by cobalt 60 gamma radiation is studied in precisely characterized material. The general method is summarized as follows:

Highly perfect germanium single crystals were grown under carefully controlled conditions. Samples from these crystals were characterized by resistivity homogeniety, dislocation density, carrier concentration, and minority carrier lifetime.

The samples were then irradiated at room temperature with cobalt 60 gamma rays and re-analyzed as above.

The energy positions of the defect levels were determined from the variation of the Hall coefficient with temperature. The role of these defects in electrical behavior was further studied with lifetime and mobility temperature profiles.

A series of quenching experiments was performed to study the effects of initial defect concentration on the introduction rate of stable defects by irradiation.

Conclusions are drawn concerning the introduction rate

of radiation produced defects. A model process for the formation of stable defects is proposed based on the observed behavior.

The above methods of crystal growth and compensation by radiation defects are applied to the preparation of a nuclear radiation detector. The device is evaluated by its energy resolution of the 662 keV line of the cesium 137 spectrum. Recommendations are made concerning crystal growth and compensation processes for materials used in these devices.

IV. DESCRIPTION OF APPARATUS AND PROCEDURE

A. Single Crystal Growth

Germanium single crystals were pulled in a Czochralski type furnace employing high purity polycrystalline ingots obtained from Eagle Pitcher, Inc. (resistivity greater than 45 ohm-centimeter at 27°C). The crucible was made of spectrographically pure graphite and the ambient gas was prepurified electrolytic hydrogen (less than .001 percent oxygen) which was passed through DeOxo unit (catalytic purifier).

The seed was oriented using the Laue back-reflection technique and etched in 2 parts (70%)HNO_3 + 1 part (48%)HF until the surface appeared smooth. It was then mounted in a molybdenum holder, re-etched, and mounted in the pulling furnace.

The charge was etched as the seed, quenching with distilled and deionized water, and then rinsed in spectrographic grade isopropyl alcohol. It was frequently necessary to etch more than once when the etch did not attack the underside of the charge homogeneously.

The crucible was not treated, but was removed using Kimwipes when the seed holder was mounted to avoid contamination.

Using teflon tweezers, the charge was taken from the isopropyl alcohol and placrd in the crucible. The

furnace was then closed and evacuated to 5×10^{-5} Torr, drying the charge.

The furnace was cycled three times between vacuum and purge with hydrogen. It was outgassed at about $600^{\circ}C$ under vacuum and purged for 30 minutes with hydrogen. The charge was then melted and held at about $1000^{\circ}C$ under high flow of hydrogen for 30 minutes. The flow was then reduced and the crystal pulled using varying rates of pulling, seed rotation, and crucible rotation.

The crystals were pulled in the $\langle 111 \rangle$ and $\langle 100 \rangle$ directions using low dislocation seeds. In some cases the melts were doped with up to one gram of a germanium alloy containing 10^{17} atoms per cubic centimeter of antimony.

During all preparation procedures care was taken to avoid any contact with metal or boron containing glass. All etching and rinsing was performed in teflon beakers.

It must be noted that the furnace was originally purified by several months of growing undoped crystals followed by baking out at high temperatures. In the early stages the furnace was often completely dismantled to remove volatile products.

B. Resistivity Measurement

Room temperature resistivity measurements were made in order to assess crystal homogeneity by using the four point probe technique[69]. Measurements were made along

the length of as-grown crystals and across slices cut

perpendicular to the growth direction   Areas to be measured

were lapped flat with 600 grit abrasive and cleaned

with distilled water and acetone.

Probe spacings of .159 centimeters and .0635 centi-

meters were used for large and small samples, respectively.

The measuring circuit employed a 0-1 milliampere current

source and a Rubicon portable precision potentiometer

as shown in Figure 2.

Voltage readings were averaged for current flow in

each direction and resistivity was determined by the relation

$$\rho = \frac{2\pi Vs}{I}$$

V= voltage
s= probe spacing
I= current

Corrections for the variation in sample thickness were

taken from reference 69.

C. Etch Pit Counting

It has been shown that there is an exact correspondence

between the density of dislocations and the density of

pits revealed on etched germanium surfaces[70]. This

technique is now well established. Etch pits were counted

in this work in order to determine the dislocation densities

in as-grown crystals.

Slices were cut from as-grown germanium single crystals

perpendicular to the direction of growth, ground with

600 and then 1600 grit abrasive, cleaned in ultrasonic
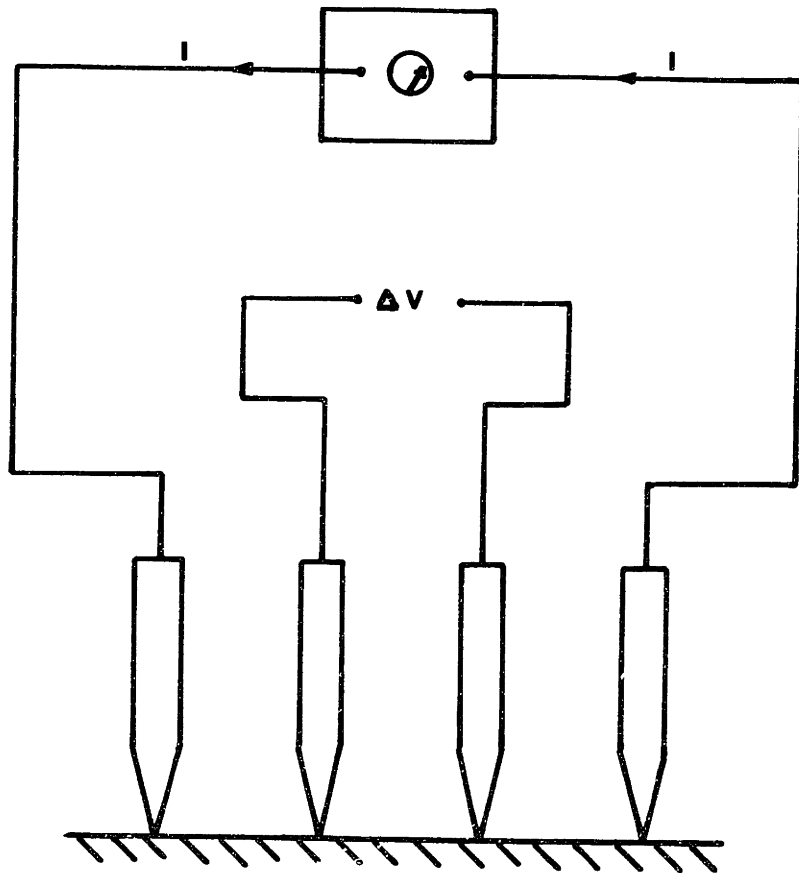
Figure 2. Four Point Probe Arrangement

baths of distilled water and then acetone, and etched in
CP4 (15 parts (48%)HF + 25 parts (70%)HNO_3 + 15 parts
(glacial)CH_3COOH + .3 parts Br_2 dissolved) for about 5
minutes.

Etch pits were counted by averaging five readings
at 57X magnification.

D. Hall Effect Measurement

Hall effect samples were prepared from the germanium
single crystals described in section III A. Slices were
cut perpendicular to the growth direction and scanned with
a four point probe (section III B) to assess cross sectional
impurity gradients. Samples were taken only from areas
in which the resistivity variation was less than 5 percent.

The samples were cut, either with an ultrasonic die
to a bridge configuration or with a thin diamond wheel
(.3 millimeters thickness) to dimensions of 15 x 4 milli-
meters, so that the long dimension (path of current flow)
was parallel to the $\langle 110 \rangle$ direction. The samples were
then lapped with 600 grit abrasive to a thickness of 1.5
millimeters and etched in CP4 for 2 minutes, displacement
quenching with distilled water.

Ohmic contacts were applied using indium metal (MP
156°C) and no flux. For the quenching experiments ohmic
contacts were formed using a gallium-indium eutectic alloy
(MP 16°C) which does not require heating. The samples

were then mounted on Al_2O_3 plates, as shown in Figure 3, using gold wire (3 mil) held to the plates with Ecco- bond 56C conducting paste and using silver paint as a conduction path to the Hall probe circuitry. Once mounted, the samples were handled no more, with the exception of those used in quenching studies.

The Hall probe and cryostat are shown in Figure 3. Sample temperature was controlled isothermally in the range of 80-300°K by means of nitrogen gas ambient, liquid nitrogen in the cryostat jacket, and a counter-wound heater adjacent to the sample chamber. A copper-constan- tan thermocouple was placed directly below the sample for measurement, regulation, and stabilization of temperature.

Two circuits were employed for the measurement of Hall coefficients as shown in Figure 4. For carrier concen- trations above about 5×10^{12} per cubic centimeter an automatic mode was used which employed a cam-driven switching circuit. Within a two minute cycle the specimen current and magnetic field were reversed and values of the conduct- ivity, Hall, and thermocouple voltages were fed into a Sargent recorder. A Harrison 6202A power supply was used, and a Keithley 149 milli-microvoltmeter in parallel with a precision one ohm resistor measured specimen current.

At very low carrier concentrations the high sample resistances and signal levels required an alternative circuit. As shown in Figure 4, a Keithley 610B grounded
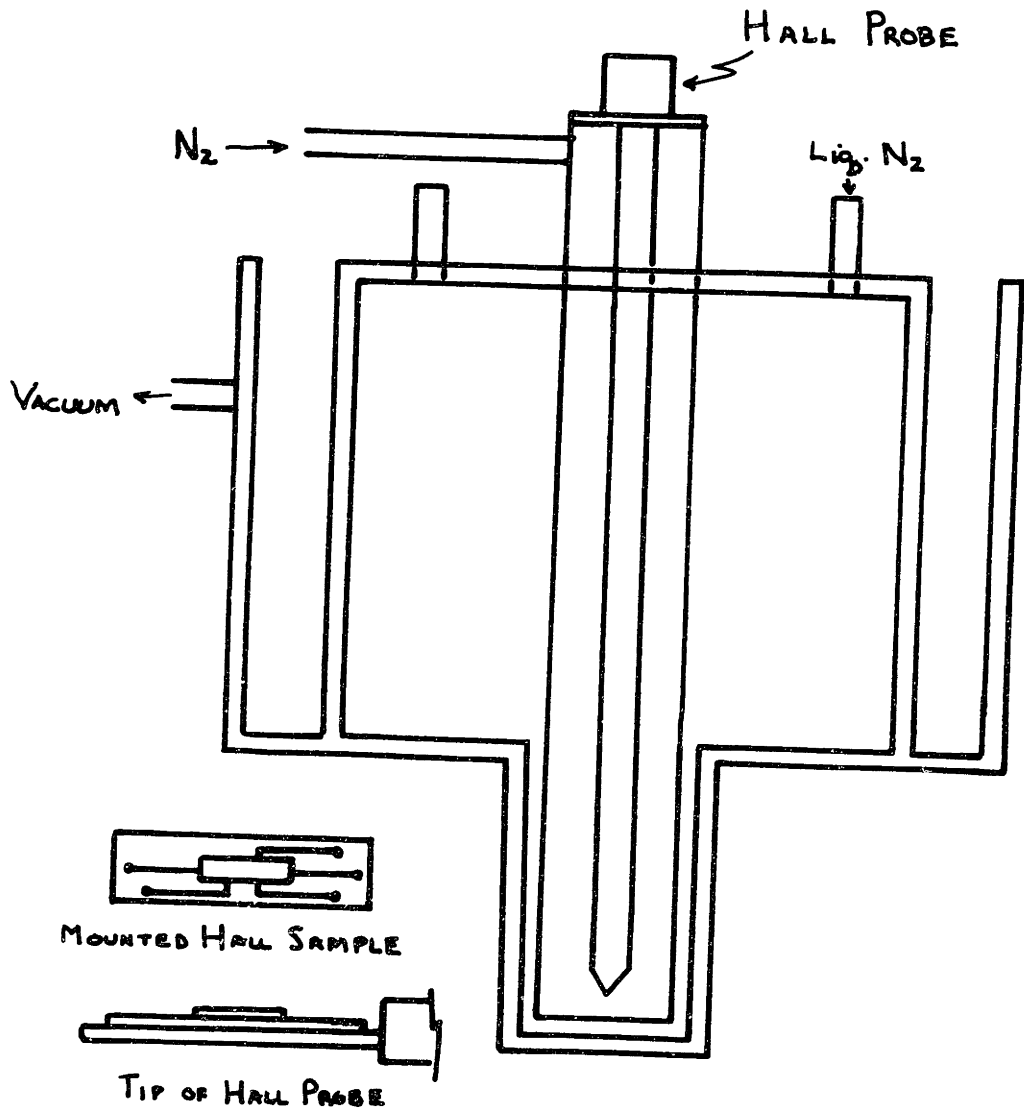
Figure 3. Schematic Diagram of Hall Probe, Cryostat and Mounting Plates
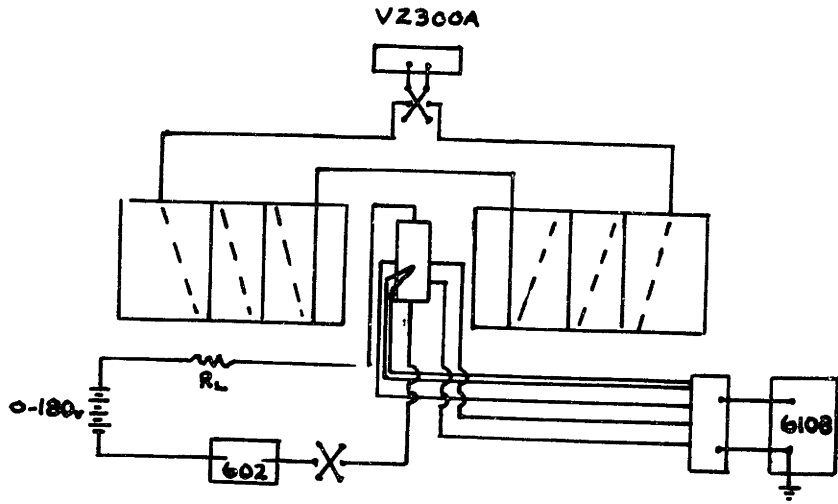
(a) High Resistivity Samples
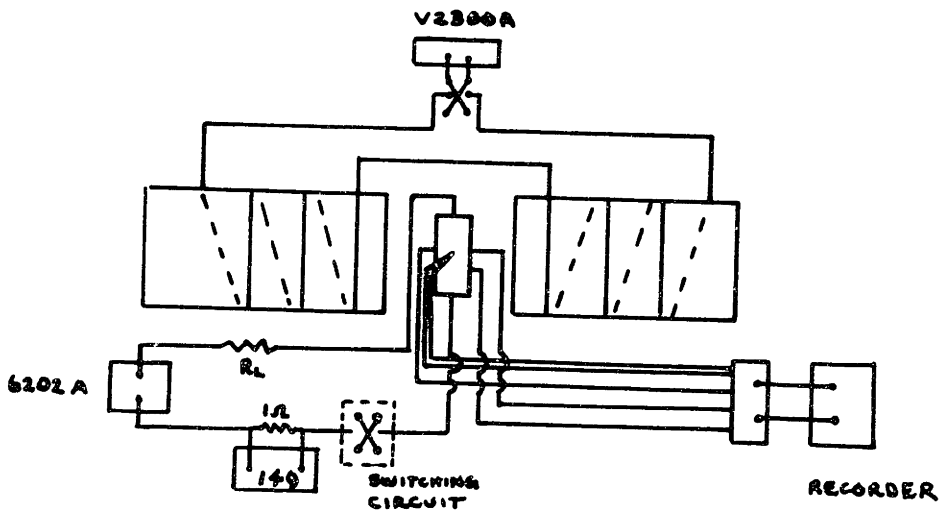
(b) Medium Resistivity Samples
(a automatic mode)

Figure 4. Hall Coefficient Measuring Circuits

electrometer (10^{14} ohm rated input resistance) was used
to measure voltages, a Keithley 602 battery-powered electro-
meter to measure specimen current, and a battery pack
making available 0-180 volts in 22.5 volt intervals for
a power supply.

In both circuits a Varian electromagnet Type V2300A
with a V2301A current regulator was used to provide magnetic
fields in the range 0-5000 gauss.

An in depth discussion of measurement procedure and
analysis is given in Appendix A.

The precision of these measurements is estimated to be
better than ± 5 percent.

E. Lifetime Measurement

Lifetime samples were prepared exactly as the Hall
specimens with the exceptions of dimensions which were
15 x 5 x 5 millimeters and etching which was in CP4 for
5 minutes with a methyl alcohol quench. Ohmic contacts
were applied using the gallium-indium alloy, and the samples
were mounted on a copper block as shown in Figure 5.
General Electric Co. glyptal (#7031) cement was used to
hold the samples in place. It was found to have adequate
thermal conductivity to allow an equality of temperature
between the sample and the copper block in a short period
of time, and it is readily soluble in acetone so that
the sample could be easily removed for re-etching when

desired

The sample holder was a block with a thin piece of mica or Al_2O_3 providing electrical insulation. The electrical feedthroughs were copper pins mounted in bakelite. The unit was attached to a copper chamber, as shown in Figure 5, using liquid gallium-indium metal as a gasketing material to insure heat transfer.

A 10 x 3 millimeter radiation slit was cut in the chamber and covered with a 1 millimeter thick piece of n-type germanium by means of indium solder. The slit dimensions were such that the edges and ends of the sample were masked from the incident light in order to minimize carrier losses through surface recombination and sweep-out by the measuring field. The 1 millimeter germanium filter had the effect of filtering out short wavelengths which would have been absorbed within about 1 millimeter of the surface. This insured a more uniform penetration of the radiation and further inimized surface effects. Two small holes in the side walls allowed the sample to be maintained under vacuum by continuous pumping. A detailed explanation of this design is given in Appendix B.

Temperature control was achieved with a Cryotip AC1 - 110 cold finger unit which cooled by means of a Joule-Thompson expansion of nitrogen gas. Temperature stability was rated at $.1^{o}K$ in the range of 80 - $110^{o}K$ (regulation by back pressure on liquified nitrogen) and

HEAT
EXCHANGER

TO
VACUUM
PUMP

VACUUM
SHROUD

SAMPLE
HOLDER

GAS
FLOW
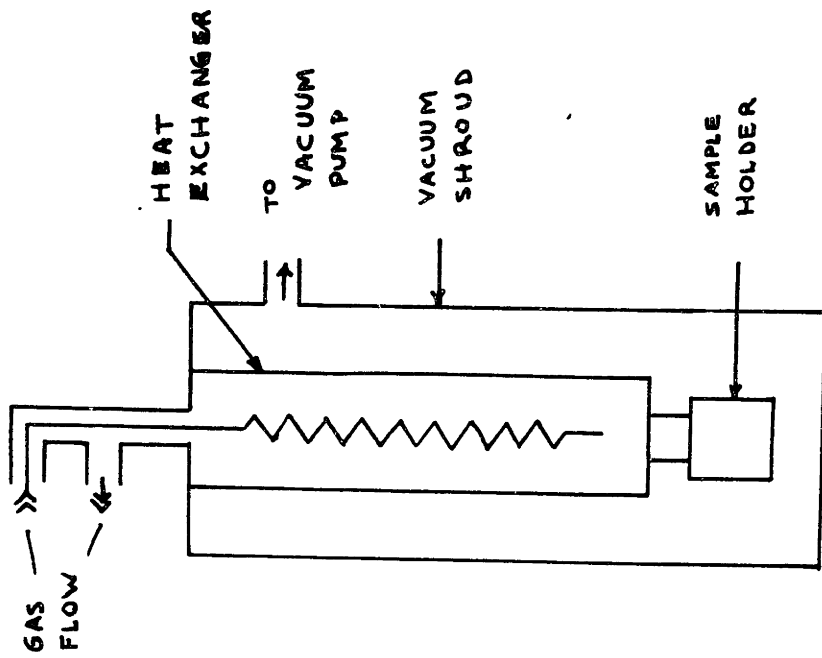
b) Schematic of Cryotip Unit

Ge

SAMPLE

Ga-In
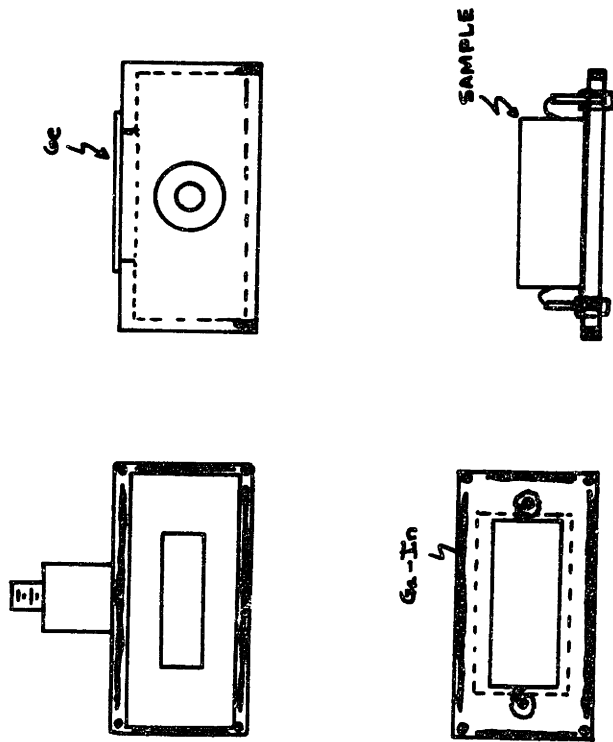
a) Sample Holder and Mounting

Figure 5. Lifetime Measurement, Sample Mounting, and Temperature Control

SAMPLE

50Ω

1.5v

OSCILLOSCOPE
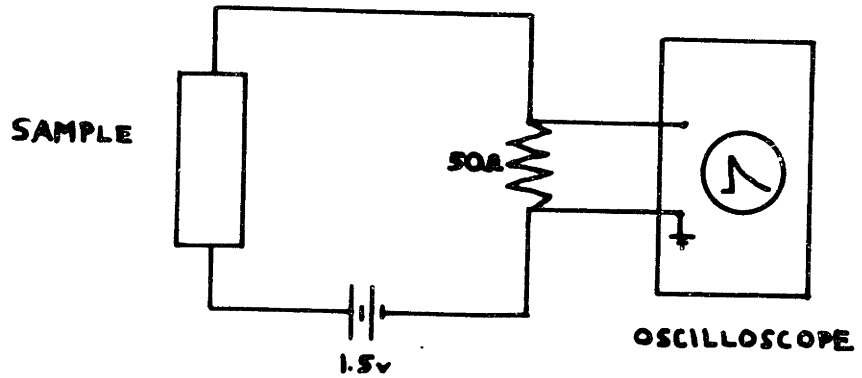
a)   High Level Lifetime Circuit for High
     Resistivity Samples

SAMPLE

$R_L = 10$ KΩ
     100 KΩ
     1 MegΩ
     10 MegΩ

12.5v

OSCILLOSCOPE
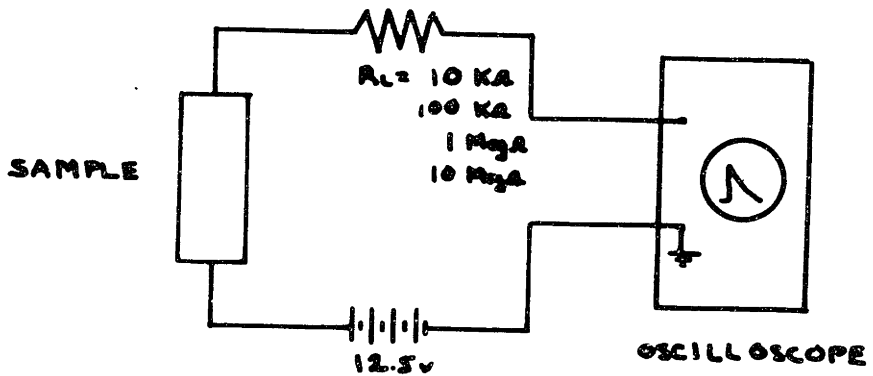
b)   Low Level Lifetime Circuit for Low
     and Medium Resistivity Samples

Figure 6.   Lifetime Measuring Circuits

.3°K in the 110 - 300°K range (regulation by nitrogen gas flow).

Prior to measurement, the mounted sample surface was given a mild swab etch with (30%)H_2O_2, quenched with distilled water, and washed with methyl alcohol. The sample unit was then placed immediately into the cold finger chamber and evacuated to 10^{-5} Torr.

Nonequilibrium carriers were excited optically using a short pulse from a Xenon discharge tube (General Radio 1538A) in conjunction with the germanium filter mentioned above. The pulse duration was measured at half-maximum to be .7 microseconds.

The decay of the sample conductivity after excitation was monitored on a Techronics 564 storage oscilloscope with a 3A3 plug-in unit (DC - 500kc frequency responce) in conjunction with the circuits shown in Figure 6. The decay constant was determined by measurement on the final 10 percent of the curve. For exponential decays, the decay constant was calculated from the half signal decay point (see Appendix B). For apparent nonexponential decays, the very late decay was found to be approximately exponential and was measured on semilog paper from a photograph.

F. Radiation of Samples

Lattice imperfections were introduced into germanium

test samples by means of irradiation by cobalt 60 gamma rays. The cobalt 60 decay spectrum consists primarily of two photons with energies of 1.7 and 1.33 MeV.

All gamma radiations were performed using 10,200 curie cylindrical cobalt 60 source at the Massachusetts General Hospital. The samples were irradiated at room temperature at a dose rate of 1.7 megarads per hour with a maximum of heating to about 60°C for long irradiations.

Following removal from the source chamber, the samples were not analyzed for 48 hours in order to allow any subsequent room temperature annealing processes to take place.

G. Detector Fabrication and Analysis

1. Fabrication Procedures

Germanium radiation detectors were constructed as an application of the crystal growth and compensation processes developed in this work. Concern in fabrication was mainly with the formation of a uniform, highly rectifying p-type contact and an etching procedure to produce passive, non-conducting surfaces.

Initial sample preparation was the same as outlined for the Hall effect samples. The dimensions in this case were 5 x 5 x 3 millimeters. An n-type contact region was formed on one face by diffusion of lithium donors, and a p-type contact was formed on the opposite face by

the alloying of gallium and indium acceptors in the germanium or by a metal-semiconductor surface barrier contact using nickel or gold. The procedure is outlined in the following paragraphs.

Alloyed p-type contact

Gallium-indium alloy is applied to one of the large faces and a suspension of lithium in mineral oil is applied to the opposite face. Subsequently, the sample is brought to $425^{\circ}C$ for five minutes in an atmosphere of helium at which the lithium diffuses about 1 millimeter, and the gallium and indium alloy with the germanium. The excess lithium is then removed by washing in distilled water, and the lithium contact face is lapped smooth with 600 grit abrasive. The gallium-indium contact is protected with polystyrene ("Q-Dope) or an Apiezon "black wax", and the sample is etched for 1 minute in CP4. The lithium contact is then similarly protected.

Surface barrier p-type contact

A diffused lithium contact is applied and protected as above. The sample is then etched for 1 minute in CP4, quenched with distilled water, and left with the unprotected face up in a partially opened desecator overnight. The gold contact is applied by vapor deposition of a layer about 10^{-5} centimeter thick in a vacuum of about 4×10^{-7} Torr at room temperature. The nickel contact is applied by electroless plating as described in Appendix D.

The resulting structures were then irradiated with cobalt 60 gamma rays employing doses up to 60 megarads.

Following irradiation, the sample edges were lapped with 600 grit abrasive, etched in CP4 for 2 minutes, rinsed in electronic grade methyl alcohol, etched in 6 parts (70%)HNO_3 and 1 part (48%)HF for 10 seconds, and rinsed again in methyl alcohol. The contact protection was then removed and the device was tested in an evacuated Dewet (10^{-5} Torr) at 77°K.

2. Testing Procedures

Capacitance

The behavior of a p-n junction is similar to that of a capacitor having n-type and p-type material as parallel plates. Given the properties of the two electrodes, the capacitance of the junction indicates the separation of the "plates" or how wide the junction depletion region must be in order to accomodate the voltage difference existing across the barrier.

In a p-i-n structure employing an n-type base, the depletion region will spread from the p-type junction when the "i" region is not perfectly compensated. The device capacitance is given in this case by

$$C = 1.05 \ A\left(\frac{\epsilon q \ N_D}{8\pi(V_o - V_a)}\right)^{\frac{1}{2}} \text{ microfarad}$$

where A is the junction area (cm^2), ϵ is the dielectric constant (=16 for germanium), q is the charge on an electron

(coulombs), N_D is the net donor concentration in the "i" region, (cm^{-3}), V_o is the junction contact potential at zero bias (volts), and V_a is the applied bias (volts).

When the applied bias is large enough, the depletion region will "punch through" to the n-type contact and the capacitance value becomes constant. In this case the capacitance is given by

$$C = \frac{\epsilon A}{4\pi W} \quad \text{picofarad}$$

where W is the depletion width which is now the separation between the n- and p-type contacts.

It is desired that detector structures have a low value of capacitance which is independent of applied bias. This would indicated accordingly a large depletion region (sensitive volume) and a well compensated "i" region. Capacitance was measured employing the circuit shown in Figure 7. The load capacitor, C_L, served to shunt possible contributions to the measured capacitance from the power supply. The capacitance bridge was a Boonton Model 74C.

Device leakage current

The current flowing through the device under back bias is an indication of both the contact uniformity and the surface condition. As discussed later, a minimum leakage current results when the space charge region spreads uniformly from the p-type contact under the

application of back bias.

The curcuit given in Figure 8 was used to obtain
the reverse-bias current-voltage relations for the detector
structures. A reverse current of 10^{-9} amperes at -360
volts was a minimum requirement before the structure could
be tested for resolution.

<u>Detector energy resolution</u>

The energy resolution of a detection device is the
best means of evaluating its overall performance. As is
discussed later, this test indicates the effects of both
fabrication and initial material parameters.

Resolution was determined from a pulse height analysis
of signals generated by a 150 microcurie source of cesium
137 as shown in Figure 9. Pulse signals from the detector
were amplified by a Sturrup 1408C field effect transistor
preamplifier and a Sturrup 1416 passive filter RC amplifier
(Canberra Industries) and fed into RIDL Model 3412 multi-
channel analyzer. The radiation energy spectrum was
displayed on an oscillographic screen as well as paper
print out.

Resolution was measured as the full peak width at
one half maximum height (FWHM). The electronic circuitry
was designed for a maximum resolution of about 5 keV
(FWHM).
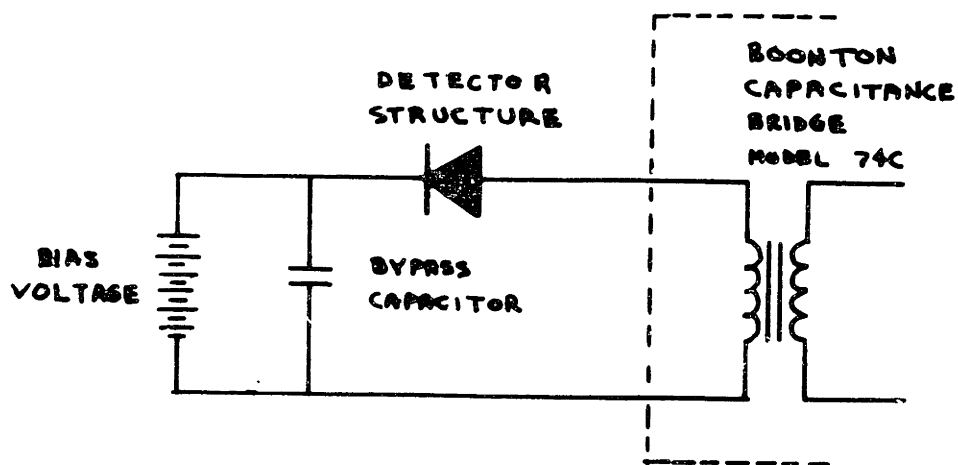
Figure 7.   Device Capacitance Measuring Circuit

DETECTOR
STRUCTURE

610B

BIAS
VOLTAGE
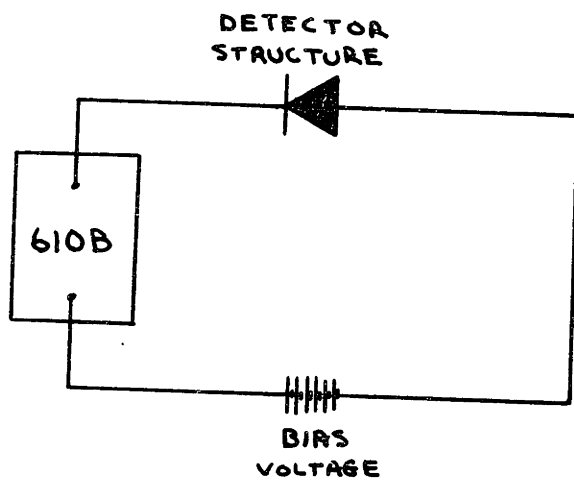
Figure 8.   Circuit for Measurement of Device Leakage
Current
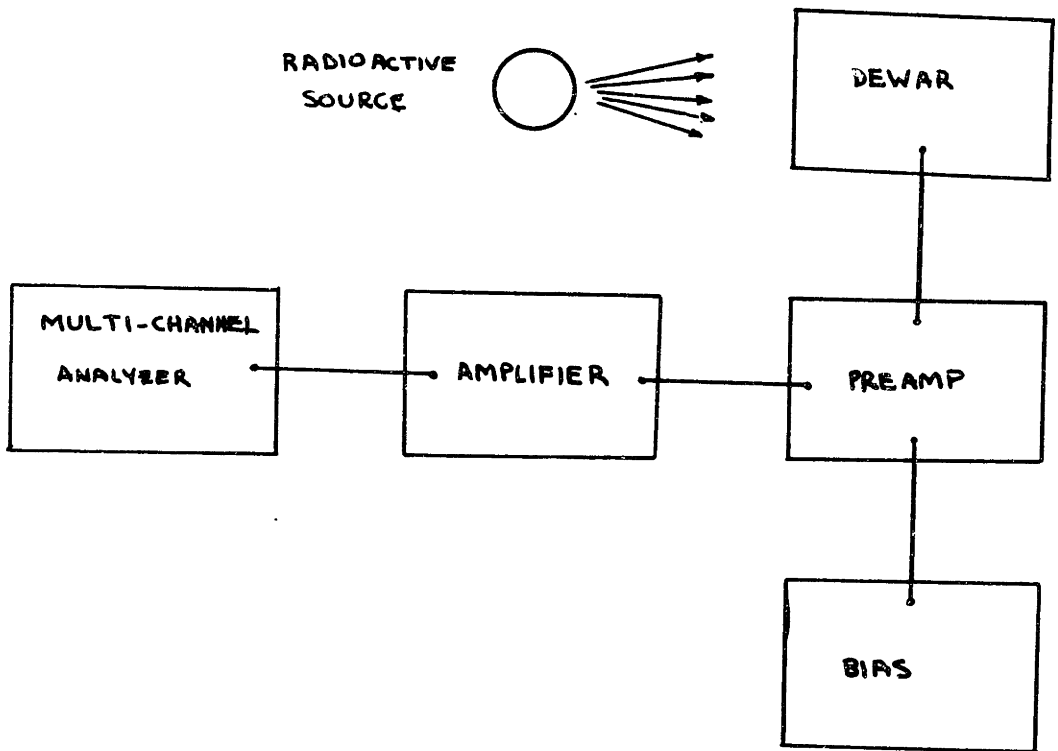
Figure 9.   Detector Resolution Measurement

H. Quenching Procedure

Quenching experiments were performed in order to
evaluate the effects of initial defect concentration on the
introduction of stable defects by radiation. The primary
concern in experimental technique was to avoid contamination
of the sample by fast diffusing impurities (notably copper)
during heat treatment.

All quenching studies involved Hall effect samples
prepared as described in section IV C. After Hall co-
efficient measurement, the gallium-indium contacts were
carefully removed with cotton swabs, and the sample was
degreased with ultrsonic washes in trichloroethelene and,
then, acetone. This was followed by washing in deionized
water; etching in 2 parts (70%)HNO_3 + 1 part (48%)HF,
with displacement quenching by deionized water; and,
washing in deionized water, (70%)HNO_3, and deionized water.
The samples were then blotted clean with filter paper to
remove any ordinary Cu on the surface. Any intermittent
handling was done with teflon tweezers to further minimize
contamination by metallic elements.

The samples were then sealed in quartz ampoules under
a vacuum of 10^{-6} Torr.

The ampoule-sample package was heated in a vertical
wire wound tube furnace in an argon atmosphere and quenched by
dropping into a room temperature water bath as shown in
Figure 10. Testing for a gas discharge in the ampoule

with a tesla coil confirmed the maintenance of a high vacuum.
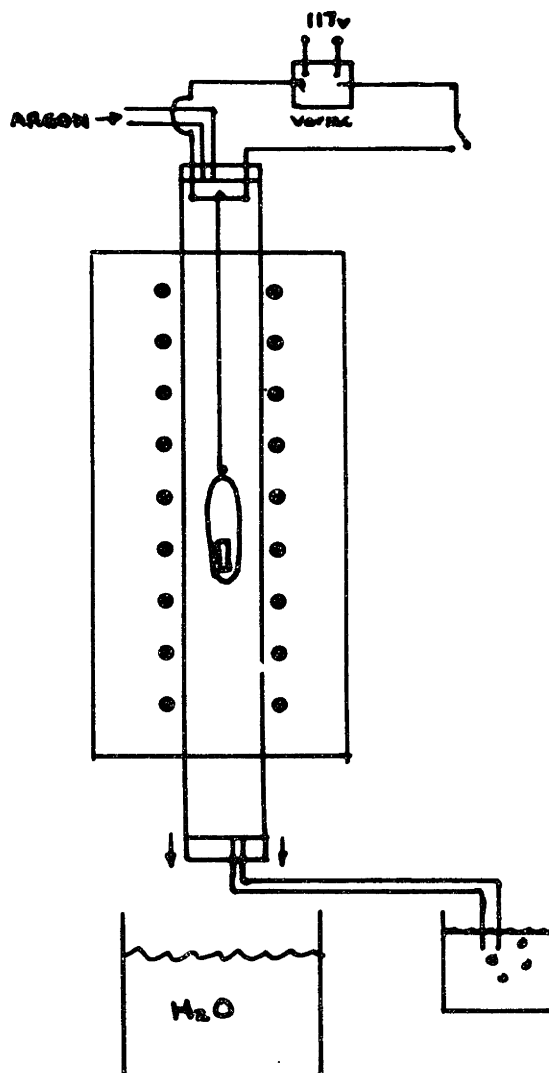
Figure 10. Quenching Apparatus

For quenching, the bottom tube cap is removed and the wire supporting the ampoule is melted with a high current.

V. EXPERIMENTAL RESULTS AND ANALYSIS

Introduction

A series of controlled experiments was performed to study the electrical properties of germanium irradiated with cobalt 60 gamma photons. The chief objective of these studies was to develop a coherent representation of the defect structures in these materials. In particular, it was necessary to characterize accurately the state of the initial material in order to identify native sources and sinks that may effect the final defect configuration. In this way, perhaps, the intrinsic influence of the radiation defects may be understood.

A set of high purity, germanium single crystals were carefully grown and characterized for this purpose. It was assumed that any constituent present in a finite concentration (greater than 10^{11} cm^{-3}) would be noted in this high purity material. Radiation defects were then introduced into the bulk of the material and the effects were carefully observed.

The energy positions of states introduced into the forbidden gap by the local interruption of lattice periodicity were determined by Hall coefficient and minority carrier lifetime measurements. The charge state of the defects was investigated through the behavior of the lifetime and carrier mobility in the irradiated material.

The relaxation of defect structures was examined by studying the defect introduction rate in a variety of samples. A discussion of these results and a correlation of the electrical behavior of the bulk material with its physical structure is presented in the following section.

A. High Purity Crystal Growth

1. Crystal Purity

Germanium single crystals were grown according to the procedure outlined in section IV-A. This procedure was developed during the growth of 28 germanium crystals prior to the preparation of those used in this study. A brief summary of this preliminary work is given below to underline the important steps of the process.

A clean furnace is of primary importance. It was found that baking out the system for 5 hours at $1000^\circ C$ under vacuum (10^{-5} Torr) was very effective in this respect. Particulary after doping with a highly volatile element, such as antimony, the bake out would result in a thin deposite on the furnace walls. This deposit was removed by partially dismantling the furnace and cleaning with acetone. The bake out process was repeated until no deposite was noticed. Before growth a final bake out was performed under the high purity ambient atmosphere. When using low doping levels, it was found that furnace purity could be maintained for extended periods.

The crucible was most effectively purified by continual growth using high purity melts. The effectiveness of this process could be monitored through the increasing resistivity of the pulled crystals. In each case, the entire melt was pulled from the crucible to avoid back diffusion of contaminants into the crucible walls during cooling down of the furnace. The residual impurities usually had the form of shallow acceptors. For n-type crystals, the maximum acceptor concentration permitted before growth was five percent of the anticipated final donor concentration.

A prepurified hydrogen ambient was found to be superior to a nitrogen ambient of the same relative purity. The addition of a DeOxo purifier unit further improved the hydrogen results.

A noticable improvement occured when the handling procedures described in section IV-A were adopted. It was found that a greater degree of control and reproducibility resulted from the use of teflon beakers and tweezers.

Spectrographic grade isopropyl alcohol was used in the final stages, mainly, because it was the purest solvent available. It also possesses the advantage of a high vapor pressure. This permits the germanium charge to be dried under vacuum in the furnace and greatly reduces handling.

The appearance of a scum on the melt surface usually resulted in a crystal of inferior purity. This contam-

ination was traced to the etching process and normally occured when the underside of the charge, not directly exposed to the etch, was not attacked evenly. Consequently at least two etching steps were normally employed.

Table 1 gives a summary of the results for the crystals used in this study. In _all_ cases the resistivity increased toward the bottom of the crystal indicating a distribution coefficient ($k = {}^{C}s / C_1$) for the impurity of less than unity. This effectively rules out boron ($k = 20$) as a major contaminant.

All crystals doped n-type were grown twice, resulting in further purification by impurity segregation during the normal freezing process. A crystal was initially grown using a very slow growth rate and high rate of rotation to insure maximum segregation of impurities (as discussed in section II-B). The bottom end of the resulting crystal was then cut off and discarded and the upper part was remelted and regrown. The effect is similar to zone refining and results in a much higher degree of purity than could reasonably be achieved by a single doping stage. It is assumed that small amounts of residual acceptor impurities are, also, removed in this process.

Figures 11 and 12 show Hall effect measurements on typical high purity crystals. Measurements between room temperature and 77°K effectively sweep the fermi level from midgap to about 0.05 eV from the band edge. The

TABLE 1

Characterization of As-Grown Crystals

Crystal	Dopant	$n_o, (p_o)/77°K$ (cm^{-3})	$\mu/77°K$ $(cm^2/V\text{-}sec)$	Dislocation Density (cm^{-2})	Lifetime $(\mu\,sec)$
I	Sb	1.1×10^{13}	33,100	0 center 2000 edge	600
II	Sb	6.6×10^{13}	24,800	1200 center 12000 edge	700 250
III	Sb	5.6×10^{13}	31,350	0	800
IV	Sb	2.2×10^{13}	34,000	3000	850
V	Sb	9.7×10^{12}	34,330	700	900
VI	Sb	7.5×10^{12}	34,000	0	600
VII	Sb	1.8×10^{13}	34,000	0	800
GE*	-	4×10^{11}	32,300	13,000	500
VIII	Ga	(9.3×10^{13})	35,000	500 center 13000 edge	200
IX	Ga	(7.6×10^{12})	39,000	90	600
X	-	(8.0×10^{11})	48,000	1800	400
XI	-	(3.0×10^{12})	45,300	300	650
XII	-	(2.2×10^{11})	48,000	0	700
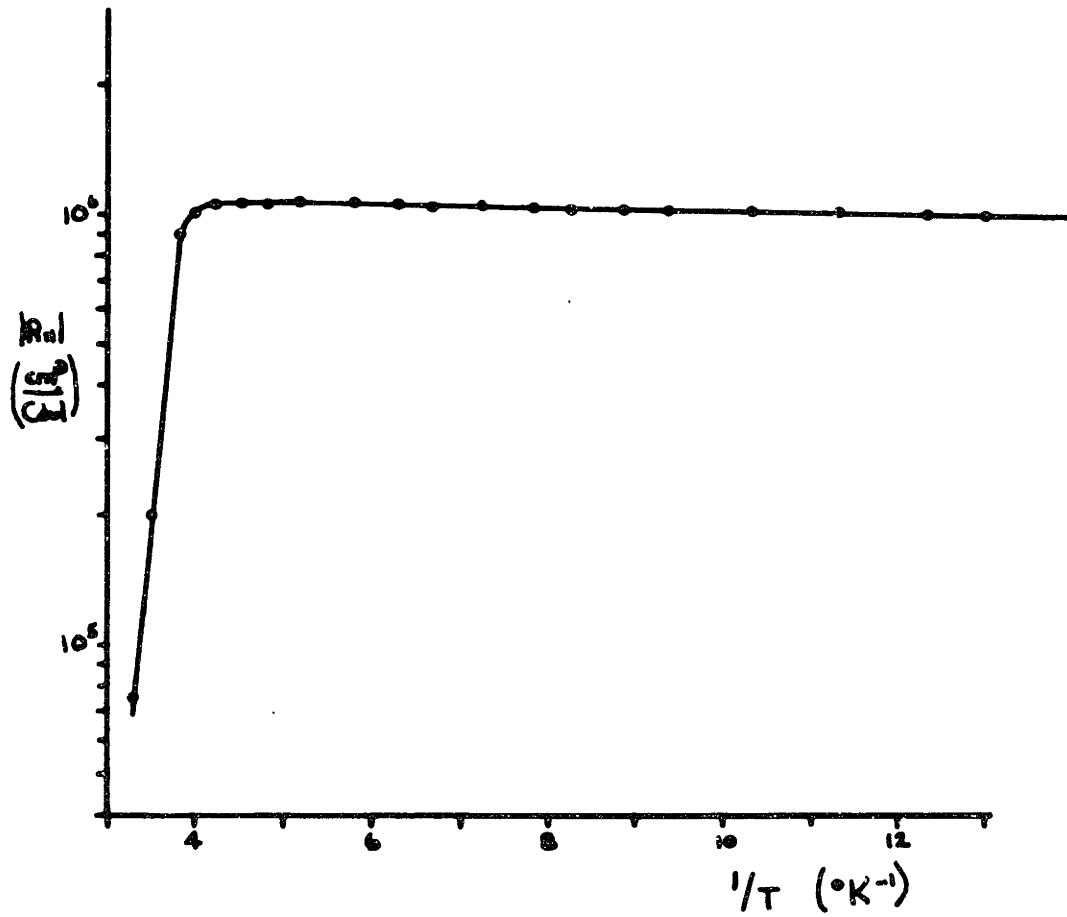
Figure 11.   Typical Hall Curve for a High Purity N-Type
             Sample (Crystal VI)
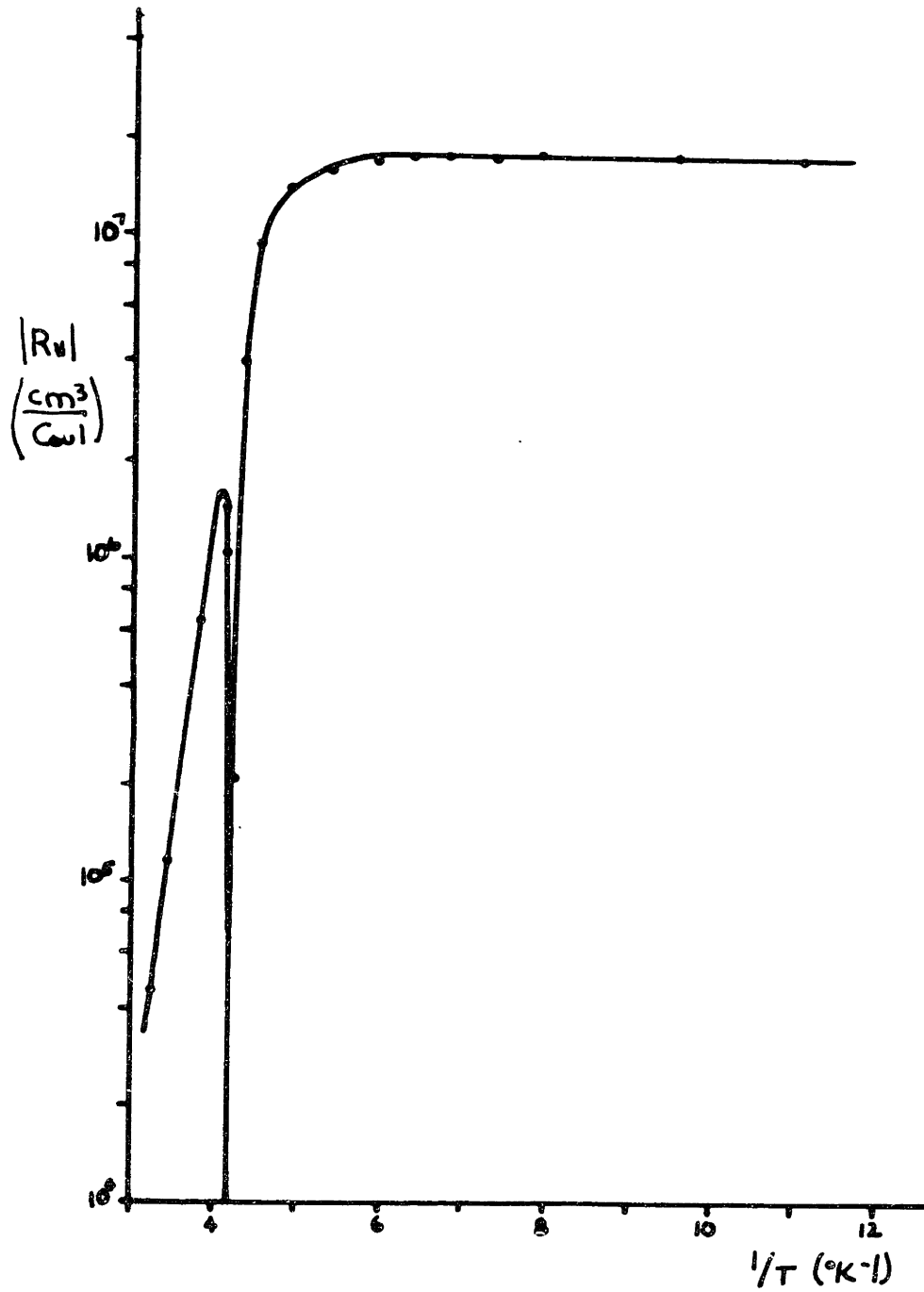
Figure 12. Typical Hall Curve for High Purity P-Type Sample (Crystal 12)

absence of any sloping portions in these curves, in the exhaustion range, indicates that only shallow levels contribute to the residual carrier concentration. Common contaminants, such as copper, introduce deep states in the energy gap and would be apparent in a measurement of this kind.

The mobility values at 77°K (Table 1) are near the theoretical values predicted for lattice scattering by Morin[71]. This result indicates that the low carrier concentration is derived from a very small concentration of impurities rather than compensation by large concentrations of both donors and acceptors.

The minority carrier lifetime, as noted in Table 1, appears to be limited only by the dislocation density. The room temperature variation generally follows the inverse dependence on dislocation density predicted by Wertheim and Pearson[46].

The temperature dependences of the minority carrier lifetime (Figures 13 and 14) exhibit no temporary trapping effects as discussed in Appendix B. This provides a very sensitive indication that there are no deep centers in the energy gap.

From the preceeding it may be concluded that the only electrically active centers that need be considered in these crystals are the small concentrations of shallow impurities, which give rise to a finite carrier concentration
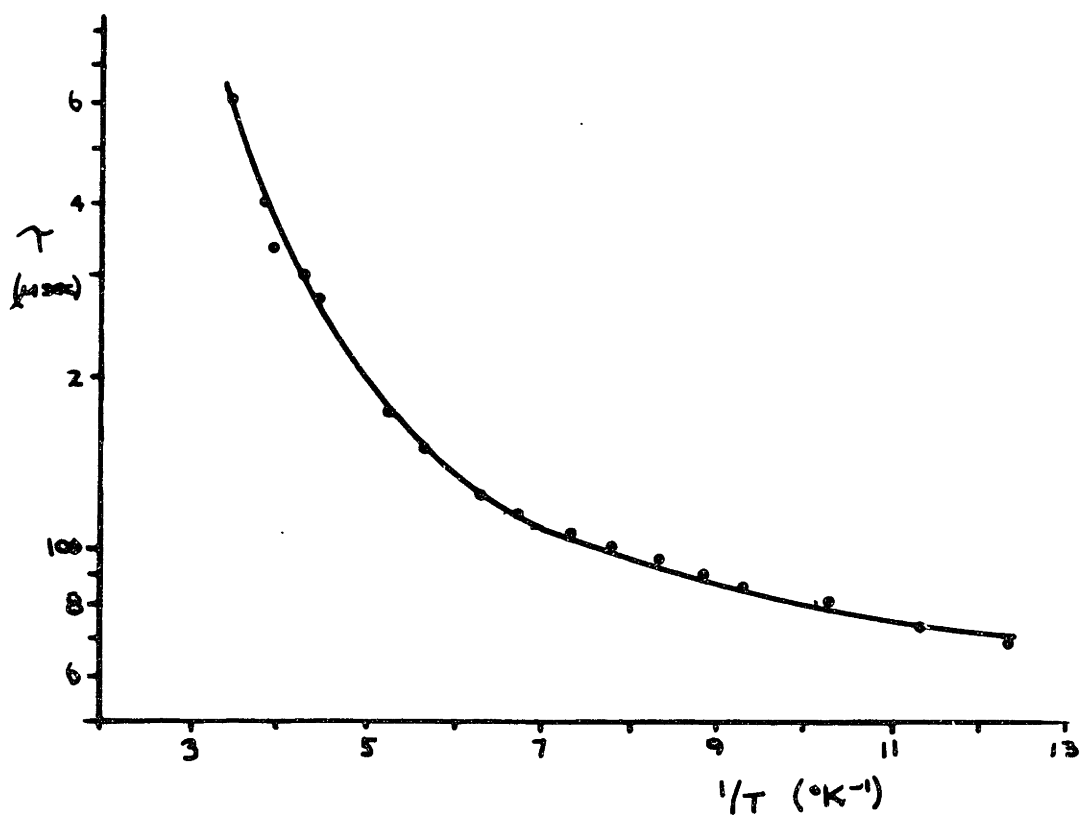
Figure 13. Typical Lifetime Behavior of a High Purity
N-Type Sample (Sample V)
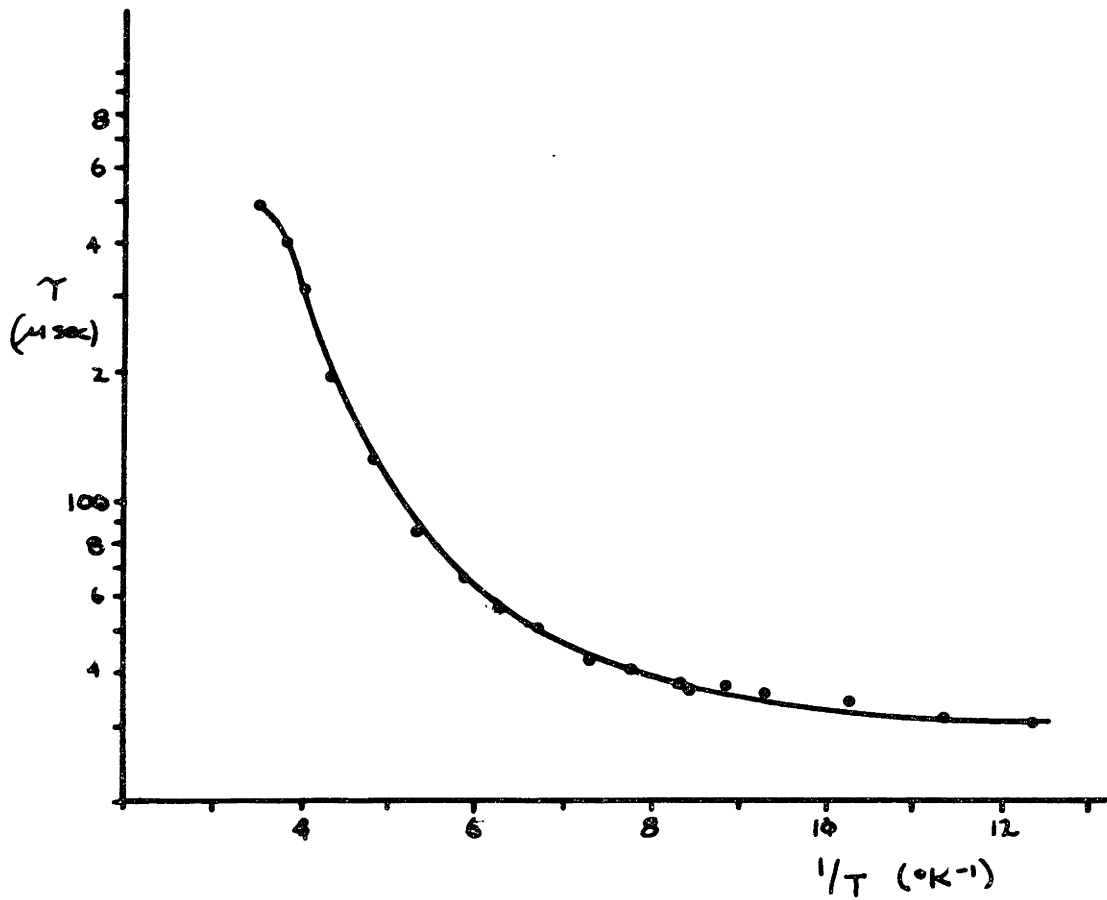
Figure 14.   Typical Lifetime Behavior for a High Purity P-Type Sample (Sample XI)

at 77°K, and dislocations which limit the initial minority carrier lifetime.

The one possible variable remaining is the concentration of electrically inactive impurities, of which oxygen is the most probable. Thurmond, et al[72] reported that germanium grown under a hydrogen ambient could contain as much as 10^{18} oxygen atoms per cubic centimeter. It must be considered, however, that this work was done in 1956 and that normal tank hydrogen was used. The electrical activity of oxygen in germanium is not well characterized, but there are indications that it can act as a donor in high concentrations[73]. While the oxygen content of the crystals used in this work was not assessed, there is reason to believe that the oxygen concentration was very low[74].

2. Structural Perfection and Homogeneity

There are very few circumstances when structural perfection and homogeneity are not required of a single crystal. However, there is still no overall scientific approach to obtaining these desired results. This, perhaps, is why the growth of single crystals is still considered to be an art.

Good results were obtained by using the method suggested by Dash[40] to grow essentially dislocation free crystals. In most cases, reduction of the seed diameter to about one millimeter in the early stages of growth

was sufficient to yield a dislocation density below 3000
per square centimeter. In large crystals, however, the
dislocation density tended to be very high at the edges
(note crystals I, II, and VIII in Table 1). It appears
that this increase is related to thermal stresses generated
by radial heat flow in the form of radiation from the
crystal edge. It was found that this heat flow could be
controlled by growing-in or reducing the crystal diameter
slightly during growth (Figure 15a). When a crystal is
growing-in, there is an excess of heat at the crystal
interface. Apparently, this excess tends to replace heat
lost by radiation in large diameter crystals and retards
the build up of thermal stresses.

No attempt was made to ascertain vacancy concentration
and distribution in the crystals. There is evidence that
vacancies are present in the form of clusters in Czochralski
grown crystals of low dislocation content[49,50,51,52,].
These clusters would be expected to be homogeneously
distributed provided that no preferred nucleation sites
are present. If such sites were present, they would
probably be,in the absence of dislocations, impurity atoms.
Then, the particular impurity distribution would determine
the vacancy distribution.

Figure 16, 17, and 18 indicate the resistivity homo-
geneity of the crystals used in this study. There is a
definite tendency for the impurity concentration to increase

Figure 15a. Typical as-grown crystal
              (crystal XII).

Figure 15b. Growth facet on the liquid-
              solid interface of crystal
              VIII.

toward the center of the crystal. This cannot be simply explained from the contour of the growth interface.

In Figure 17, the resistivity contours have the general shape of a slight decrease at the edges and a flat, very low valued region in the middle. This flat, low resistivity region is associated with the existence of a "growth facet". Facet formation represents flat sheet-like growth initiated by two dimensional nucleation. This is to be compared with a random atomic attachment process in the off-facet region. Since the growth processes are basically different in these two regions, it is not surprising that impurity incorporation varies. Figure 15b shows the actual solid-liquid interface of crystal VIII obtained by quickly pulling the growing crystal from the melt. The flat facet region is evident and may be compared with the resistivity profile in Figure 17a.

Figure 16 shows the resistivity contours of samples V and IX. Seed and crucible rotation were varied as indicated during the growth of these crystals to assess the effect on the homogeneity of the cross section. It was found from these and similar studies that the overall rotation rate and not component rotating was the determining factor for the slope of the contours (in the absence of a facet). Table 2 indicates that both seed and crucible rotation are desirable for the production of optimal electrical

properties.

Figure 18a, b, and c represent the cross sections of
the highest purity crystals. Carrier concentrations
determined by measurement of the Hall coefficient are
noted so that the constant intrinsic resistivity value
will not be misleading. A gradient is apparent but its
absolute magnitude is small because of the low impurity
level.

Figures 18d, e, and f show crystals I, IV and X. The
excellent homogeneity of I and X is attributed to a high
rotation rate (60 rpm) during growth. Crystal IV was
grown with a moderate rotation rate (20 rpm), but is
believed to have had a concave interface.

Whereas the purpose of this investigation was to
characterize the grown crystal, it has underlined the need
for an in depth understanding of the liquid-solid interface
kinrtics. A high rotation rate apparently reduces in-
homogeneity in the diffusion boundary layer at the inter-
face. At slow rotation rates, the boundary layer increases
in thickness toward the crystal center. The effect of
high rotation could possibly be interpreted in terms of
theoretical proposals by Cochran[75] and Goss[76] predicting
a vertical flow of the melt under these conditions. This
would tend to effect more mixing in the center and, thus,
homogenize the boundary layer thickness.

The ideal circumstance would, of course, be a perfectly
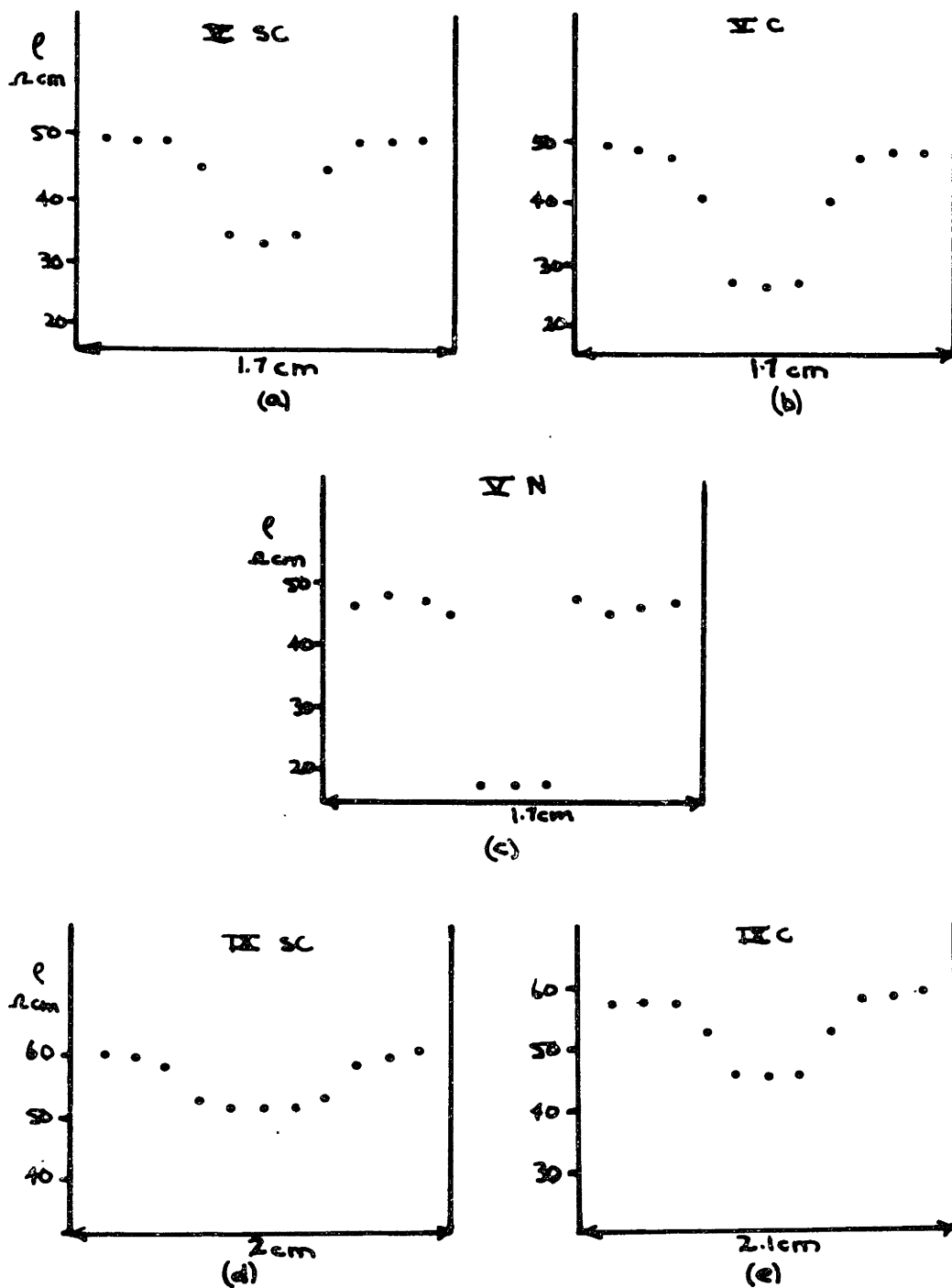
Figure 16. Cross Sectional Resistivity Profiles in As-Grown Crystals. Seed and Crucible Rotation, SC; Crucible Rotation, only, C; no Rotation N.
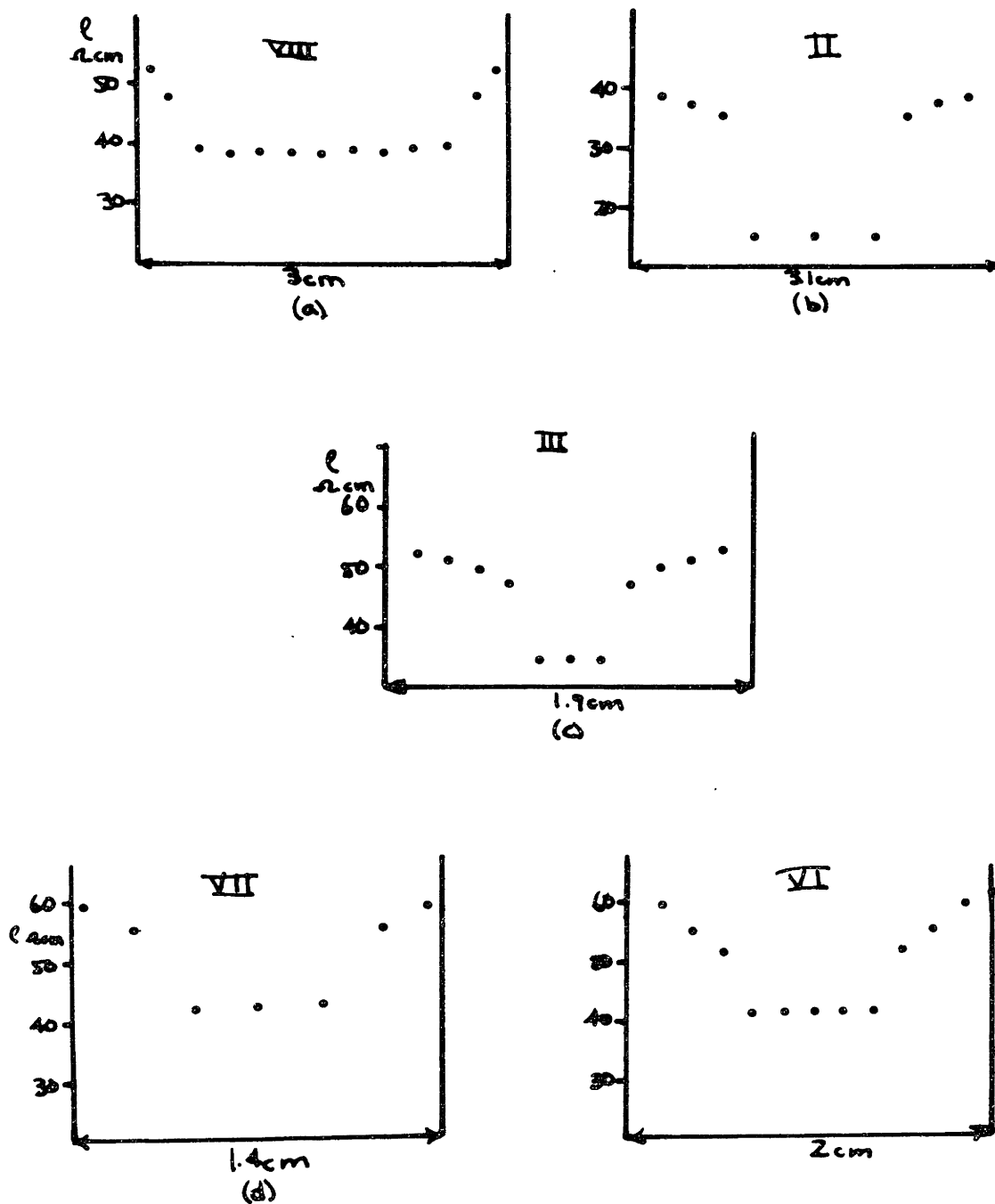
Figure 17. Cross Sectional Resistivity Profiles in As-Grown Crystals
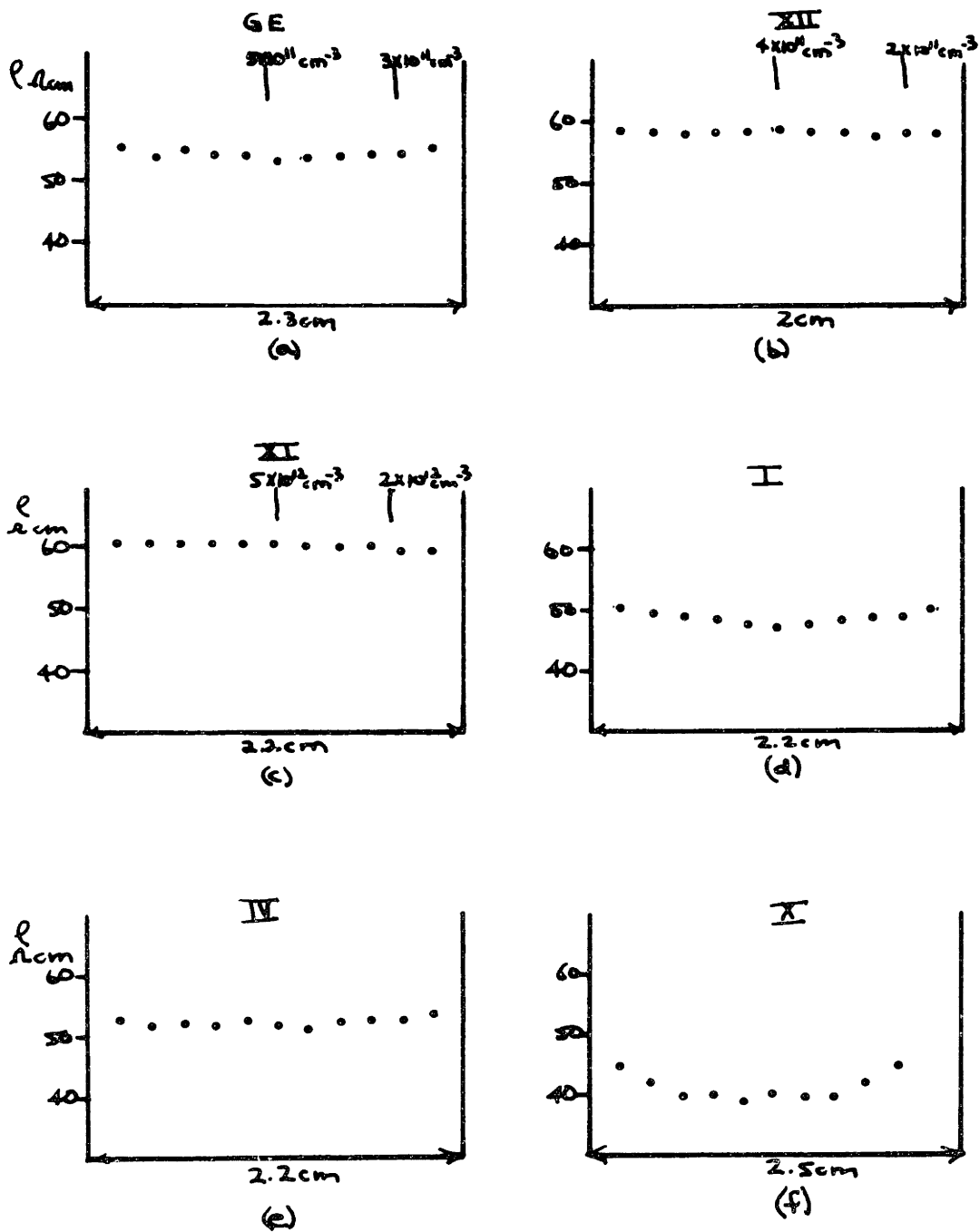
Figure 18. Cross Sectional Resistivity Profiles in As-Grown Crystals

TABLE 2*

Effects of Rotation During Growth on the Electrical Properties

of Crystal V

Rotation	Total Rotation Rate (rpm)	N_D (cm^{-3})	μ (cm^2/v-sec)	Dislocation Density(cm^{-2})	Lifetime (μ sec)
seed and crucible	30	1.1×10^{13}	35,000	680	900
crucible	25	1.2×10^{13}	27,800	850	550
none	0	1.3×10^{13}	25,600	1370	500

flat "facet" interface. However, no complete concept
exists for the conditions of facet formation. Crystal
VIII was grown with a relatively slow rotation rate
(18 rpm).

B. Radiation Defects in Germanium

    1. <u>Electronic Characterization of Radiation Defects</u>

        a. Determination of energy positions by Hall

           effect analysis

The Hall coefficient and conductivity were measured as a function of temperature in order to determine the energy positions of the defect states. The method of analysis is discussed in Appendix A. Typical curves for a number of different crystals and radiation conditions are given in Figures 19 through 22.

For all n-type crystals, the Hall coefficient shows an increase in the extrinsic region after irradiation. This indicates a net introduction of acceptor states into the system which decrease the concentration of free electrons. This behavior did not deviate for any of the crystals measured.

Table 2 summarizes the important results noted in the n-type crystals. A number of trends are evident among these samples. The increase in the Hall coefficient, R_H, is primarily due to the acceptor-like behavior of a level at E_C -0.20 eV. This behavior, however, does not definitely establish that this level corresponds to an acceptor state.

The true identity of a state as a donor or acceptor determines its charge state under different ionization conditions. A donor is neutral when it is occupied by

an electron, whereas an acceptor state is negative in the occupied condition. There are indications that the charge state of a point defect plays a major role in determining its structural behavior. In this case, the E_c -0.20 eV level may correspond to either an acceptor state or a donor state which has lost an electron to an acceptor in the lower half of the energy gap.

Levels at E_c -0.20 eV and E_c -0.10 eV were evident from irradiation of sample A. This sample was taken from an antimony doped crystal grown before the high purity growth procedure was established. While the chemical and structural details of this material are not known, the appearance of a level at E_c -0.10 eV in this crystal, only, serves to emphasize the importance of accurately characterizing the starting material.

A level at E_c -0.09 eV has been apparently associated with a vacancy-oxygen complex[19]. This association was derived from the relatively high density of these levels in oxygen-doped crystals. A similar experiment was performed in this work. A sample from crystal III was placed on a hot plate at about 350°C for five hours. Figure 23 shows the effect of irradiation on this sample. The E_c -0.20 eV level has apparently been replaced by a level located at E_c -0.09 eV. (Subsequent to this experiment, only "cold" processes for crystal mounting were employed.) The absolute identification of the E_c -0.09 eV as a

vacancy-oxygen complex is not yet conclusive, but results such as these support the idea that the presence of oxygen is related to this state. The fact that this level has been observed to increase in density upon annealing[13] gives further support to the idea that it represents a secondary and not a primary form of defect.

The level at E_c -0.20 eV has been evident in practically every study with antimony doped germanium irradiated with gamma rays (see section II-A).

The effects of defects which do not ionize in the range of the Hall measurements must also be noted. In Figures 19 through 23 the samples appear to remain intrinsic to a lower temperature after irradiation. This behavior is due to states at or below the middle of the energy gap which are acting as acceptors. Since these levels are always below the Fermi level in an n-type material, they are always filled with electrons. Therefore, no ionizing step is present in the ln R_H vs. 1/T curve, but there is a net increase in the extrinsic Hall co-efficient. In Table 2, N denotes the number of acceptor states represented by the ionization step in the Hall curve. These curves indicate that only one level is introduced in the upper half of the gap in "clean" material. N_T is the net total concentration of acceptor states introduced by irradiation. This value is found from the total change in the Hall coefficient at $77^\circ K$. If it

is assumed that a fixed set of acceptor levels is introduced by each damage event, the ratio of N_T/N should give the number of different acceptor levels introduced by each event. However, since some relaxation of the primary defect configuration does occur, the ratio would more accurately indicate the tendency of the level in the upper half of the gap (E_c -0.20 eV) to "anneal" relative to the acceptor levels in the lower half of the gap. The results in Table 2 indicate that N_T/N decreases with the increase in the purity of the samples (decrease in N_D). Similar results were found by Vitovskii, et al[6]. Thus, the E_c -0.20 eV level appears to become more stable with decreasing carrier concentration. However, when it is noticed that the carrier removal rate, $\Delta n/\Delta \phi$, also decreases with N_D and N_T/N, a more acceptable explanation would be that the states in the lower half of the gap are becoming actually less stable.

It is intuitively unacceptable that as many as ten different acceptor levels (as indicated N_T/N for samples II and IIIa) are introduced by irradiation. However, the apparent lower limit of two for N_T/N (sample VI) is appealing because of the parallel with the James - Lark-Horovitz model[7]. This model, as mentioned in section II-A, relates vacancies to defect acceptor states and interstitials to the defect donor states. It is predicted that isolated vacancies will possess two acceptor type
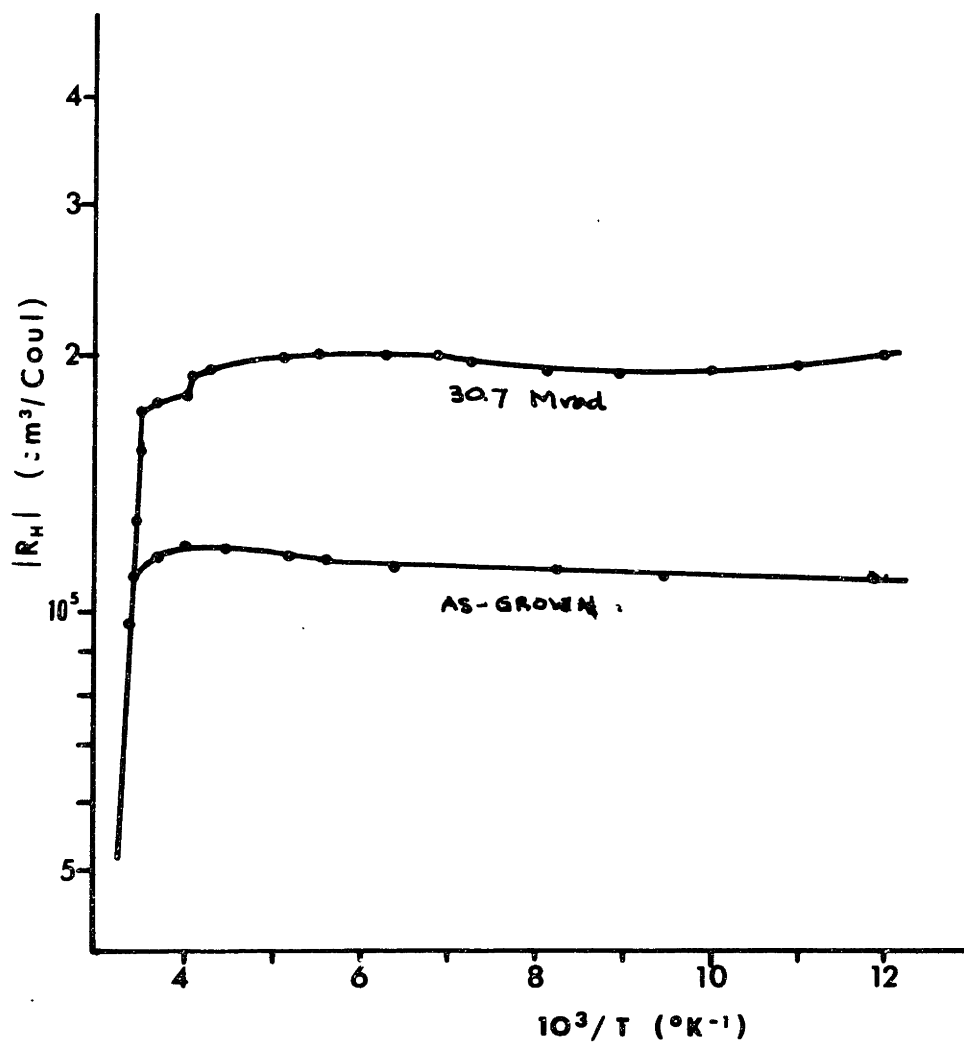
Figure 19. Irradiation   Hall Curve for Sample IIIa
            (n-type)
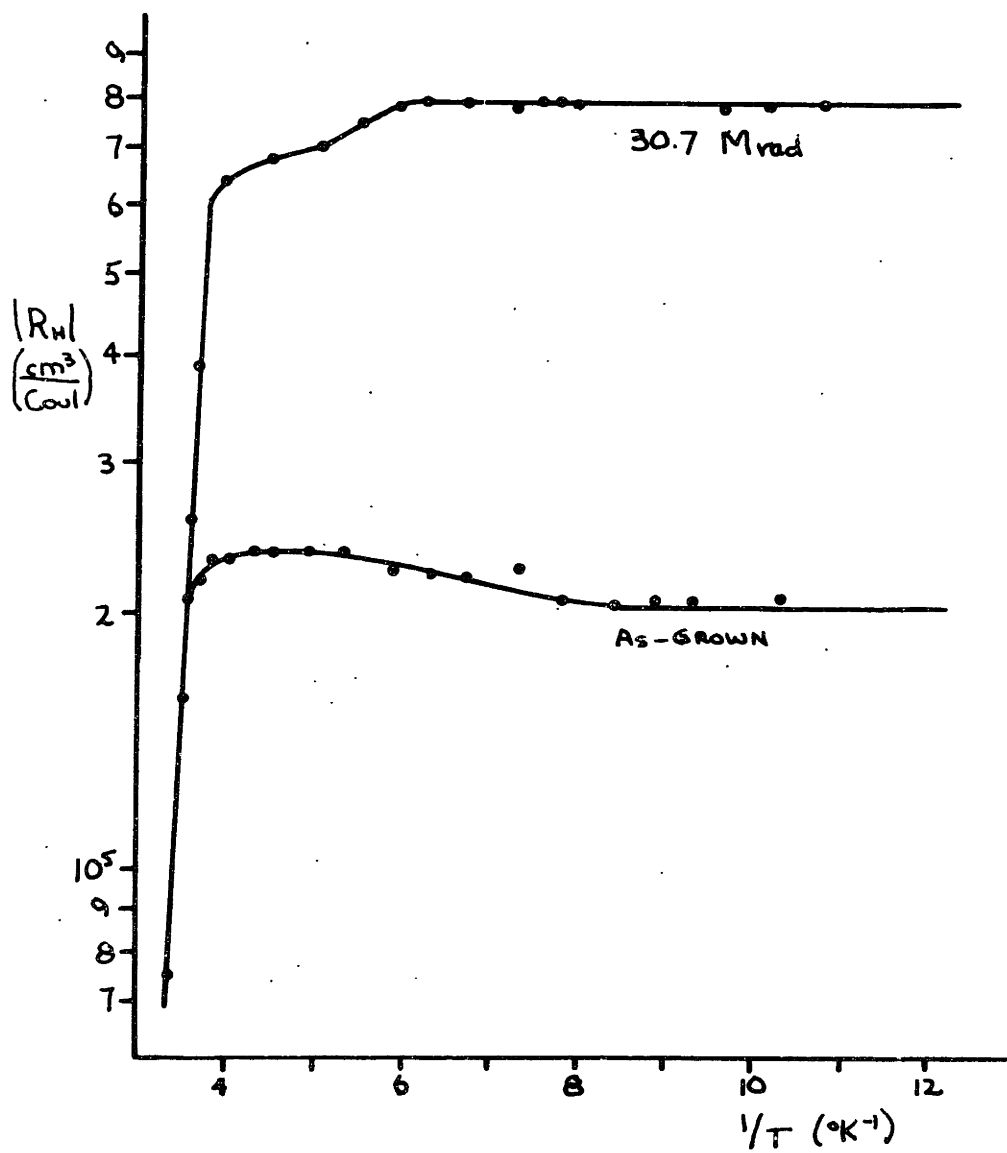
Figure 20. Irradiation Hall Curve for Sample II
(n-type)
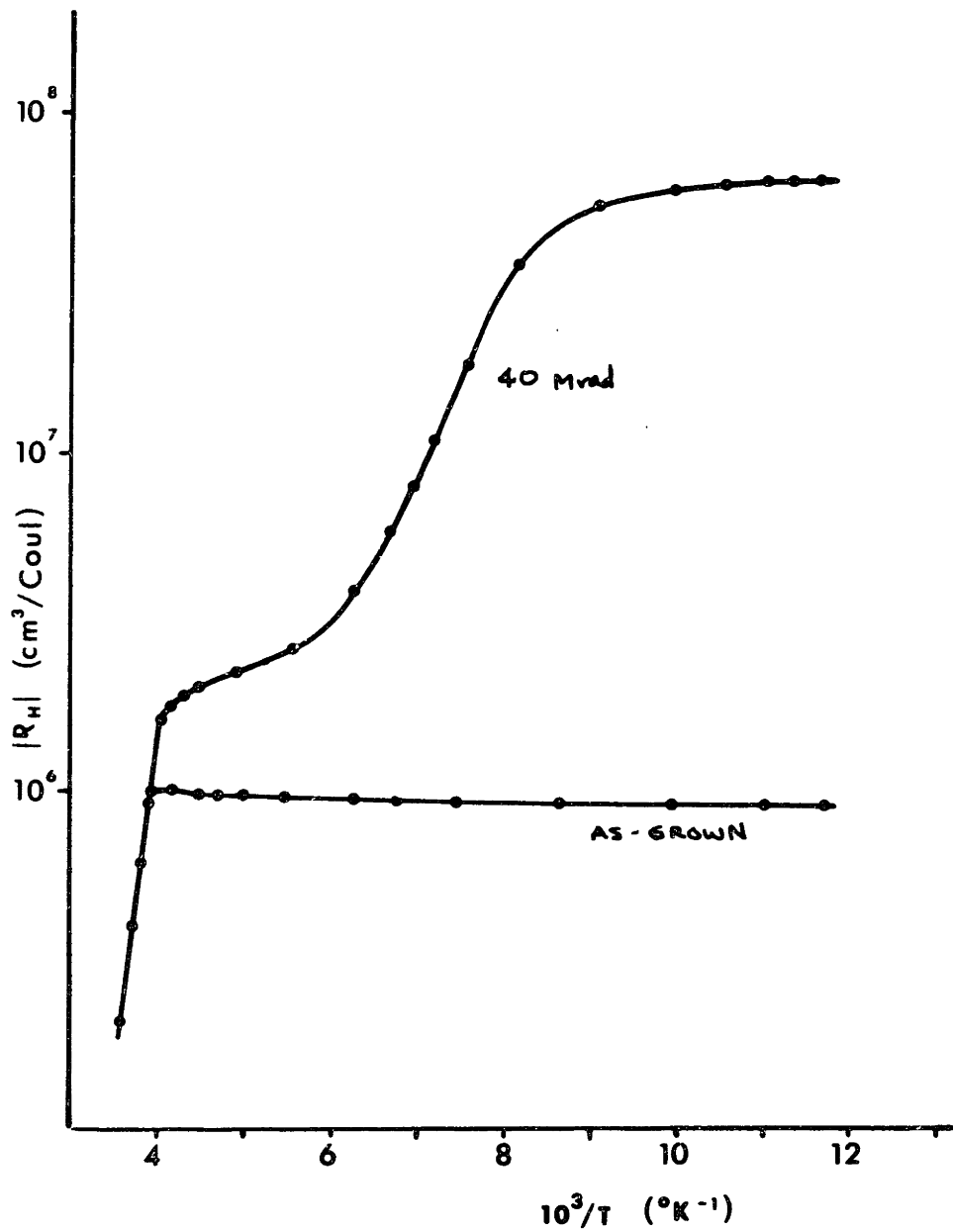
Figure 21.   Irradiation Hall Curve for Sample VI
             (n-type)
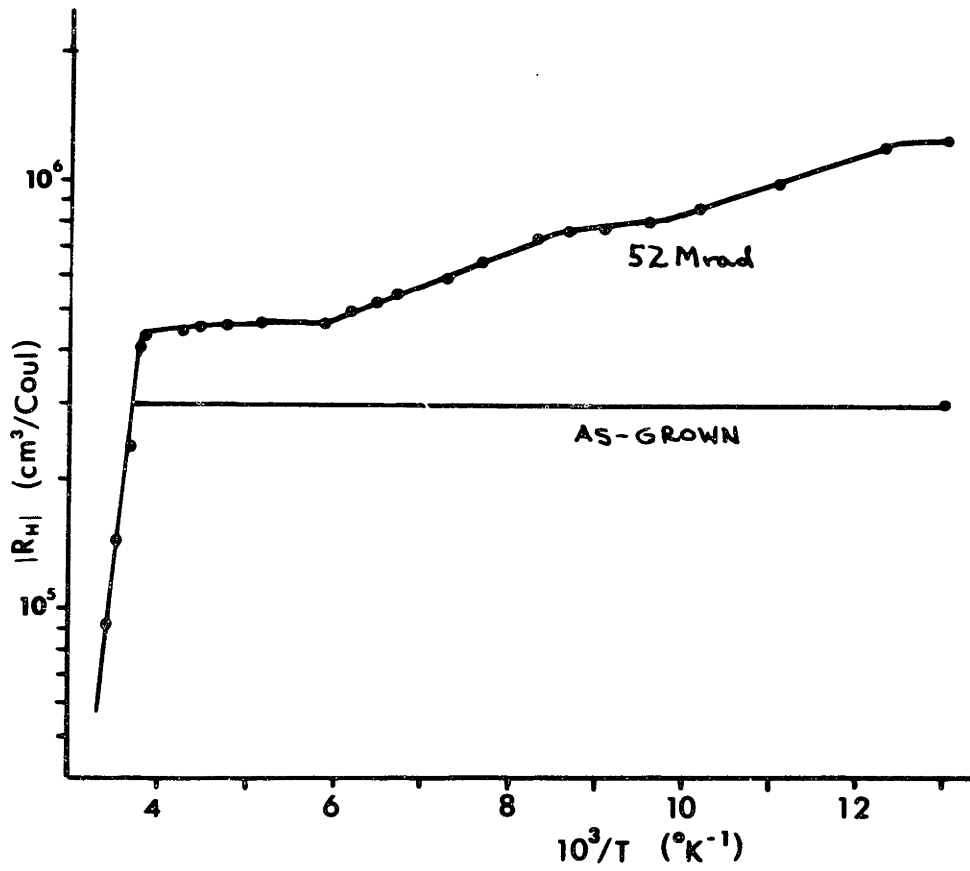
Figure 22. Irradiated Hall Curve for Sample A
(n-type)
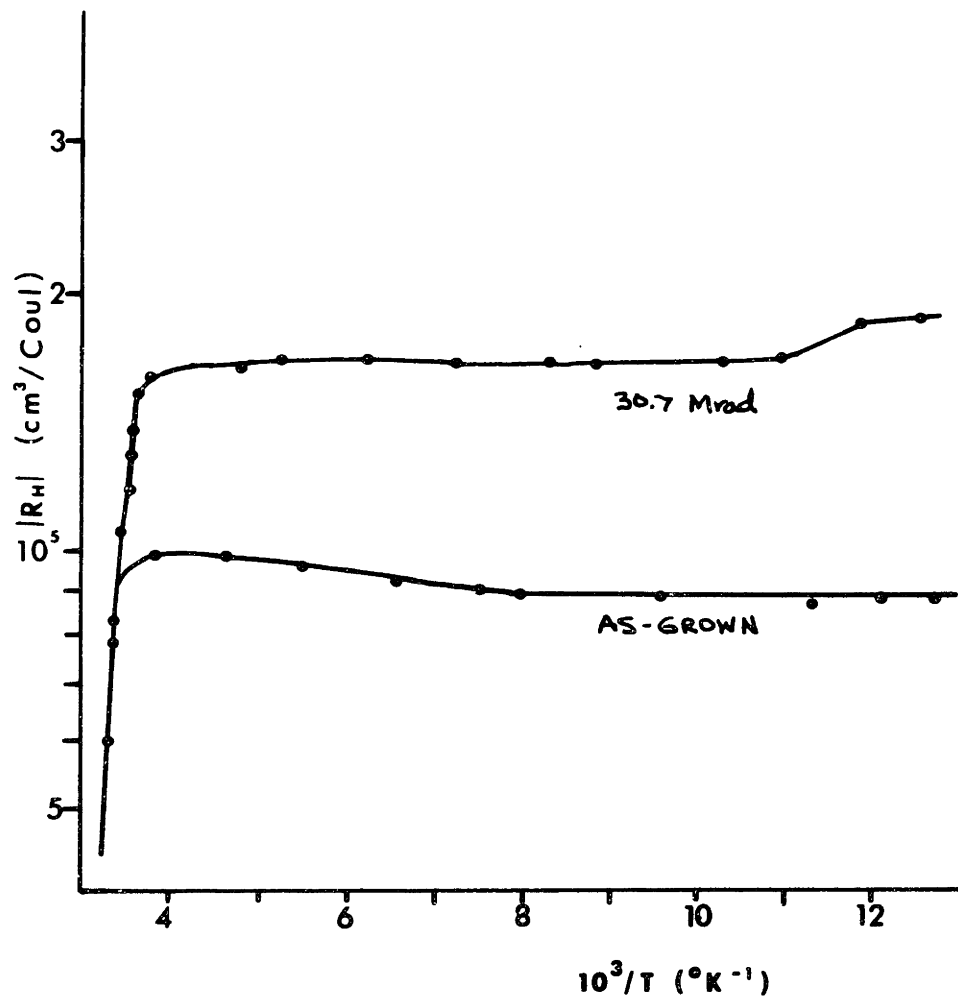
Figure 23. Irradiation Hall Curve for Sample IIIb
Heat Treated in Air
(n-type)

TABLE 2

Hall Analysis of Radiation Effects in N-Type Samples

Sample	Dose (Mrad)	N_D (cm^{-3})	N (a) (cm^{-3})	N_T/N (b)	$\frac{\Delta n}{\Delta \phi}\left(\frac{e^-}{Mrad}\right)$ (c)	E_c-E_i ($\pm$.02 eV)
IIIa	30.7	5.7x10^{13}	1.8x10^{12}	9.9	8.6x10^{11}	.19
II	29.3	2.8x10^{13}	2.4x10^{12}	8.6	7.6x10^{11}	.22
VI	40.0	6.3x10^{12}	3.1x10^{12}	2.1	1.6x10^{11}	.19
A	52.0	2.1x10^{13}	4.0x10^{12} 7.0x10^{12}	2.3	3.2x10^{11}	.20 .10
IIIb	30.7	7.0x10^{13}	6.2x10^{12}	6.0	1.2x10^{12}	.08

(a) N = concentration of defects at given ionization level

(b) N_T/N = ratio of total concentration of carriers compensated at 77°K to number of carriers compensated by states in the upper half of the gap.

(c) $\Delta n/\Delta \phi$ = concentration of carriers compensated per unit radiation dose. Referred to as carrier compensation rate or carrier removal rate.

energy positions within the energy gap corresponding to a negative and doubly negative charge state. If it is assumed that the E_c -0.20 eV level is actually a donor level related to an interstitial which has lost its electron to an unknown acceptor level in the lower half of the gap, then the high values of N_T/N would correspond to a large amount of annealing of interstitials during irradiation. The decrease of values to two would correspond to the decreasing stability of the lower acceptor levels, or vacancy annealing. This idea is particularly powerful in view of the decreasing carrier removal rate (corresponding to a net defect introduction rate).

Defect levels were also investigated in high purity p-type material. In principle, the joint evaluation of results for n and p-type material should provide a complete picture of the energy structure of radiation defects. It must be kept in mind, however, that the relaxed defect configurations in the two types of material need not be the same. The Hall effect data for p-type samples is presented in Table 3 and Figures 24 and 25.

The increase in Hall coefficient after irradiation does not necessarily imply that more donors than acceptors were introduced during the irradiation process. In fact, the appearance of an ionization slope below the initial value of the Hall constant indicate that a net increase

in acceptor concentration was effected. However, since
at least one of the acceptor levels is deep (freezes
out around 200°K), it is not electrically ionized at
77°K. The increase in the Hall constant at 77°K after
irradiation indicates though, that there are fewer ion-
ized acceptors existing in this temperature range. If
it is assumed that none of the acceptors originally in
the material have been removed, the above behavior shows
that irradiation introduces both donor and acceptor states
into p-type material.

An energy state at E_v +0.16 eV was located from the
change of the Hall coefficient with temperature in the
200°K range. This information together with the previously
discussed increase in R_H upon irradiation, leads to the
conclusion that a donor level is situated at or above
E_v +0.16 eV in the energy gap.

A level at E_v +0.16 eV has not been well established.
Cleland, et al[77] observed that such a state appeared
upon mild annealing (90 minutes at 120°C) of an antimony
doped sample which had been converted to p-type by cobalt
60 irradiation. Konopleva, et al[78] found a level at
E_v +0.165 eV to represent a primary defect in fast neutron
irradiated germanium. Streetman[17] has observed a trap-
ping level at E_v +0.16 eV in arsenic doped material.
There has been very little work on the identification
of defect levels in gamma irradiated p-type germanium.
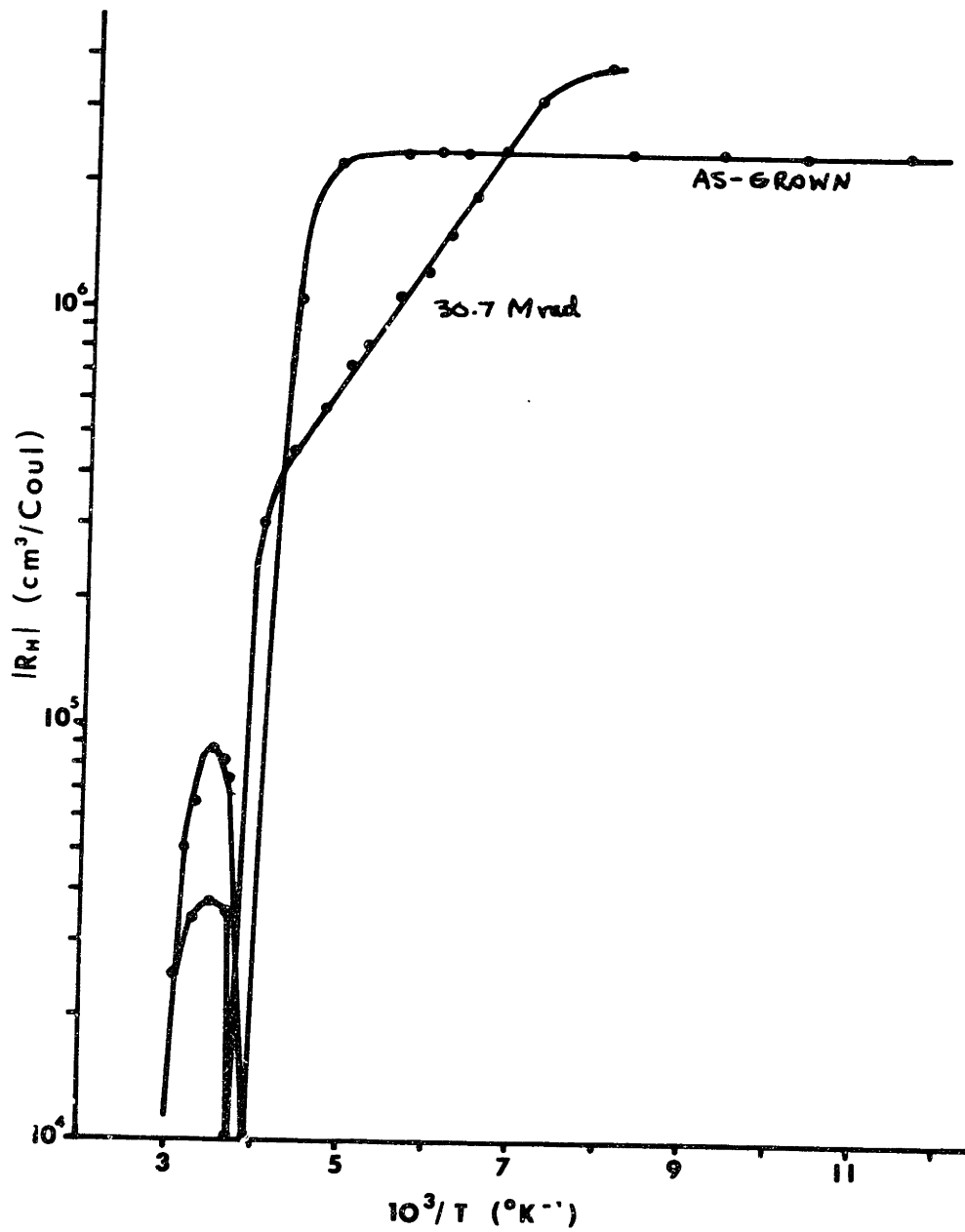
Figure 24. Radiation Hall Curves for Sample X
(p-type)
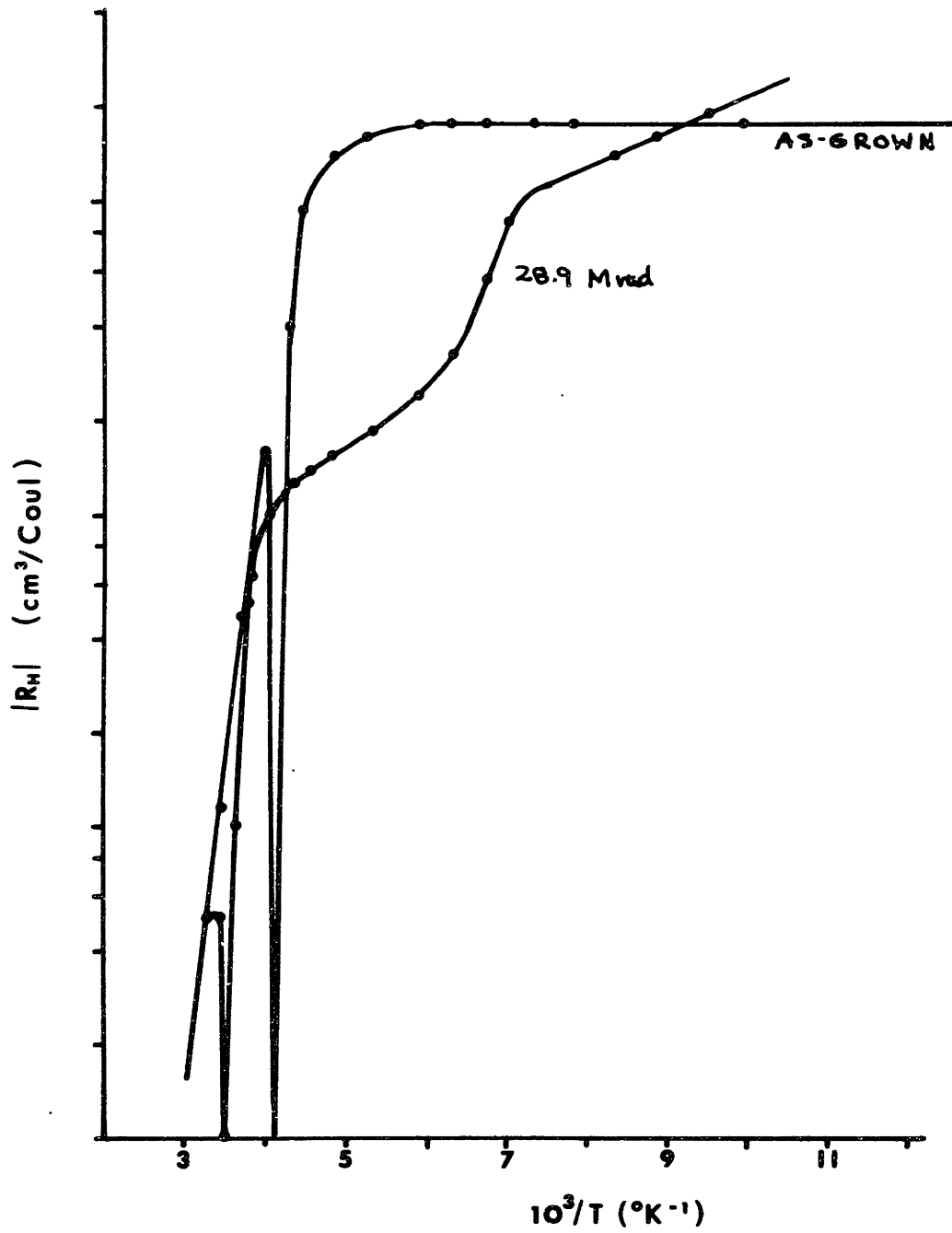
Figure 25.   Irradiation Hall Curves for Sample XII
              (p-type)

TABLE 3

Hall Analysis of Radiation Effects in P-Type Samples

Sample	Dose (Mrad)	N_A (cm^{-3})	N (cm^{-3})	NT/N	$\frac{\Delta n}{\Delta \phi}$ $\left(\frac{e^-}{Mrad}\right)$	$E_v + E_i$ ($\pm$ .02 eV)
X	30.7	2.5×10^{12}	1.4×10^{13}	.07	4.1×10^{10}	.15
XII	28.9	3.65×10^{11}	5.6×10^{12}	.02	2.1×10^{10}	.16

This is probably due to the very low carrier removal rates of these materials.

The values of N_T/N give a rough estimate of the ratio of the introduction rate of stable donor states to the E_v +0.16 eV levels. However, these values should not be followed too closely because the curves are still sloping in the low temperature range. This implies that N_T could be underestimated. The values of N and N_T/N indicate that both the donor states and the E_v +0.16 eV states become more stable with increasing initial hole concentration. Extension of these measurements to liquid helium temperatures (4°K) is necessary to acurately assess this relationship.

b. Carrier compensation (removal) rates

The variation in apparent defect stability was explored in depth by observing the defect introduction rate in a number of samples of different purity. Previous studies have noted a dependence of introduction rate on impurity concentration but this phenomenon has not been specifically studied. Pigg and Crawford mentioned in 1964[23] that the carrier removal rate was a function of antimony concentration in gamma irradiated (at 77°K) germanium samples with antimony concentrations of 1.0×10^{13} to 1.0×10^{15} per cubic centimeter. However, under the exact same experimental conditions, the carrier removal rate was reported to be independent of antimony

concentration by the same authors in 1966[23]. The dopant

concentrations in this case ranged from 5.5 x 10^{13} to

5.3 x 10^{15} per cubic centimeter. Defect introduction

rate, though, was not the prime objective of these

studies.

The behavior observed in the present work is presented

in Table 4 and Figure 26. Figure 26 graphically confirms

the idea that the carrier removal rate is a function

of initial dopant concentrations. The dependence is

approximately logarithmic in the doping range of 10^{13} -

10^{14} per cubic centimeter. It appears to saturate, however,

at either end of this range. The logarithmic dependence

can be described by the relation

$$\frac{\Delta n}{\Delta \phi} = 4.2 \times 10^{11} \ln \left[\frac{n_o}{5.4 \times 10^{12}} \right]$$

where $\Delta n / \Delta \phi$ is the carrier removal rate and n_o is the

initial electron concentration. It is particularly

pleasing that the saturation value at high concentrations

coincides with the latest values, published by Cleland,

Bass, and Crawford[5], of the "constant" removal rate

for n-type germanium irradiated with gamma rays. These

findings will be discussed in detail in section VI.

However, some preliminary observations will be noted here.

The defect introduction process may be viewed as

the instantaneous creation of both donor and acceptor

states followed by a relaxation process which involves

TABLE 4

Carrier Compensation Rates for N-Type Samples

Sample	Dose (Mrad)	N_D (cm^{-3})	$\frac{\Delta n}{\Delta \phi}\left(\frac{e-}{Mrad}\right)$	$\mu\left(\frac{cm^2}{V-sec}\right)$	$\mu'\left(\frac{cm^2}{V-sec}\right)$
IIa	30.7	2.1×10^{14}	1.6×10^{12}	23,240	23,550
IIb	29.3	1.3×10^{14}	1.4×10^{12}	-	-
IIIa	30.7	7.0×10^{13}	1.2×10^{12}	-	-
IIc	30.7	5.2×10^{13}	9.0×10^{11}	34,680	33,750
IId	29.07	3.5×10^{13}	9.6×10^{11}	30,420	28,391
IIe	29.07	3.3×10^{13}	9.0×10^{11}	32,110	29,571
IVa	29.07	3.3×10^{13}	9.4×10^{11}	32,385	34,770
IIf	29.3	3.0×10^{13}	7.6×10^{11}	-	-
IVb	30.7	2.2×10^{13}	6.3×10^{11}	46,500	35,700
Vb	29.07	9.7×10^{12}	3.0×10^{11}	-	-
GEa	29.07	5.1×10^{11}	1.1×10^{10}	-	-
GEb	29.07	4.6×10^{11}	9.1×10^{9}	-	-
GEc	28.5	3.8×10^{11}	8.2×10^{9}	31,313	20,350
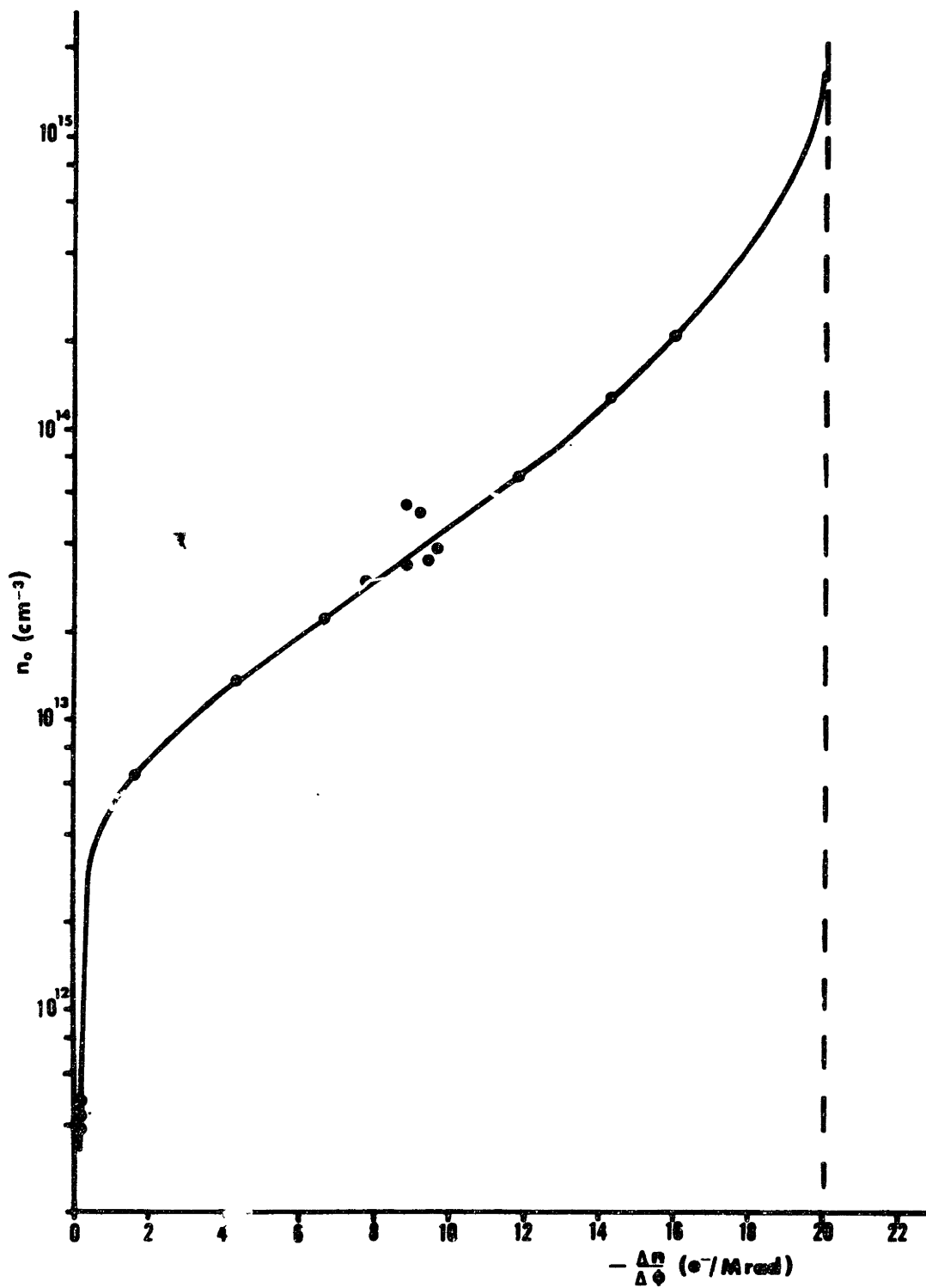
Figure 26. Carrier Compensation Rate
for As-Grown n-type Samples

modification and, sometimes, annihilation of these
states. An increase in the carrier removal rate would
indicate an increase in the stability of the acceptor
states. It could also indicate a decrease in the stability
of donor states, but this alternative will be ignored
for the present. Saturation of this effect in the
high and low purity ranges implies two possible relaxation
mechanisms:

(1) At room temperature, the Fermi level is
located at about E_c -0.34 eV for electron concentrations
of 10^{13} per cubic centimeter and about E_c -0.29 eV for
concentrations of 10^{14} per cubic centimeter. If an
ionization state of an acceptor level were located at
about E_c -0.32 eV, its occupation would vary with the
position of the Fermi level. The dependence would saturate
when the Fermi level is more than 2kT away from the E_c -0.32
eV level. Furthermore, if the site is more stable when
occupied by an electron, the behavior would be similar
to that in Figure 26.

(2) The acceptor level could also be stabilized
by association with an impurity atom. As the supply of
free impurity atoms is reduced, the number of stabilized
acceptors would decrease. Saturation would occur at
high concentrations where every acceptor introduced ca
readily find a stabilization site. Saturation at low
impurity concentrations would result when the acceptors

cannot locate stabilization sites within their "lifetime".
These alternatives will be considered in depth in section VI.

The carrier removal rate in p-type material was
studied in the same manner. The value of the Hall constant
at 77^OK corresponds to a position of the Fermi level
below E_v +0.16 eV level. Further studies at lower temp-
eratures are necessary to determine that other radiation
defect levels are positioned closer to the band. The
results are given in Table 5 and Figure 27.

Figure 27 shows that the carrier removal rate in
p-type material is, in general, much less than in n-type
material. In the high purity saturation region, however,
the introduction rate in p-type material is slightly
higher. These results confirm the tendencies expressed
in Table 3 for p-type material.

Some light could be shed on the stabilization process
by varying the structural character of the irradiated
material. Figure 28 and Table 6 show the results of
irradiating crystals that already contain radiation
defects. As one would expect from earlier discussions,
the carrier removal process tends to saturate with increasing
radiation dose. For low radiation doses (30 Mrad), the
carrier removal rate is approximately linear with the
exception of sample Va which is already in the saturation
range of Figure 26. High radiation doses, though,
indicated saturation effects before the electron concentration

TABLE 5

Carrier Compensation Rates for P-Type Samples

Sample	Dose (Mrad)	N_A (cm^{-3})	$\frac{\Delta p}{\Delta \phi} \left(\frac{h^+}{Mrad} \right)$
IX b	28.3	7.3×10^{12}	5.2×10^{10}
X	28.3	2.5×10^{12}	3.8×10^{10}
XI	28.3	2.1×10^{12}	3.2×10^{10}
XII a	28.3	7.5×10^{11}	2.0×10^{10}
XII b	2883	3.6×10^{11}	1.4×10^{10}
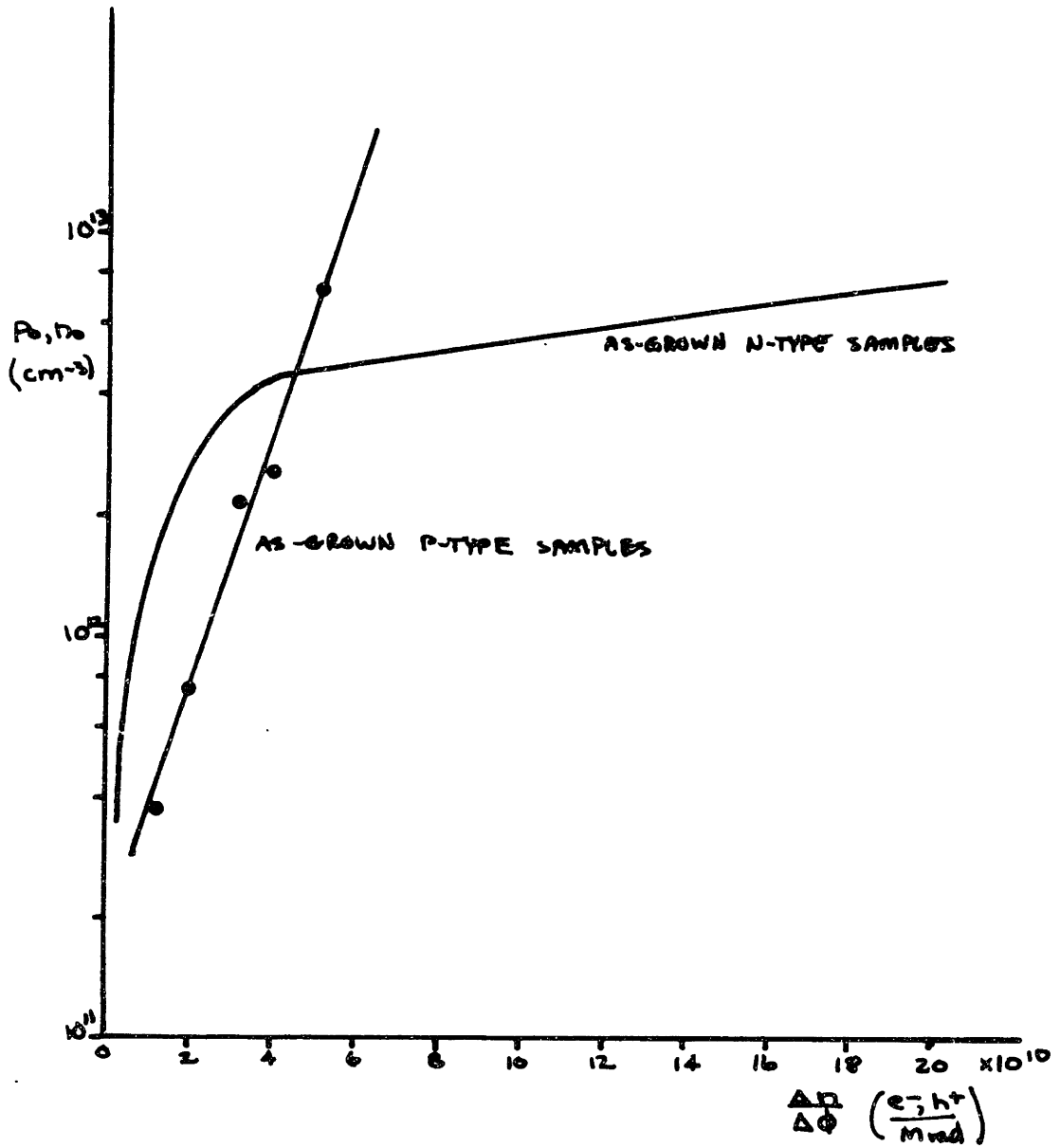
Figure 27. Carrier Compensation Rates for P-Type Samples

TABLE 6

Effects of Irradiation History on Carrier Compensation in N-Type
Material

Sample	Previous Irradiation (Mrad)	N_D (cm^{-3})	Dose (Mrad)	$\frac{\Delta n}{\Delta \phi}\left(\frac{e^-}{\text{Mrad}}\right)$
IIa	28.9	1.7×10^{14}	30	1.07×10^{12}
IIc	30.7	2.8×10^{13}	30	4.47×10^{11}
Va	28.9	1.1×10^{12}	30	1.9×10^{10}
IVc	-	2.8×10^{13}	150	1.87×10^{11}
I	-	6.3×10^{13}	140	4.3×10^{11}
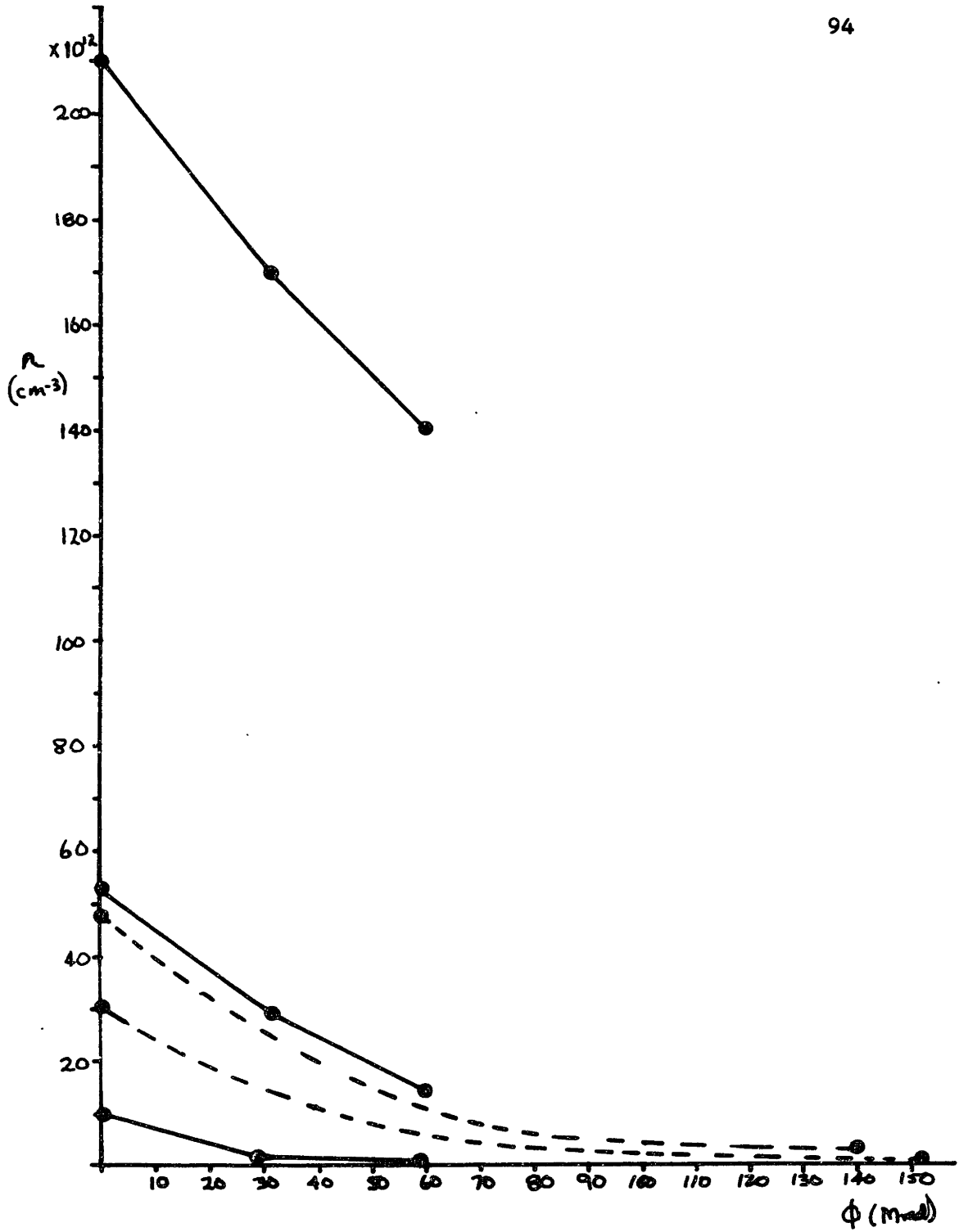
Figure 28. Effects of Irradiation History on Carrier
Compensation in N-Type Samples
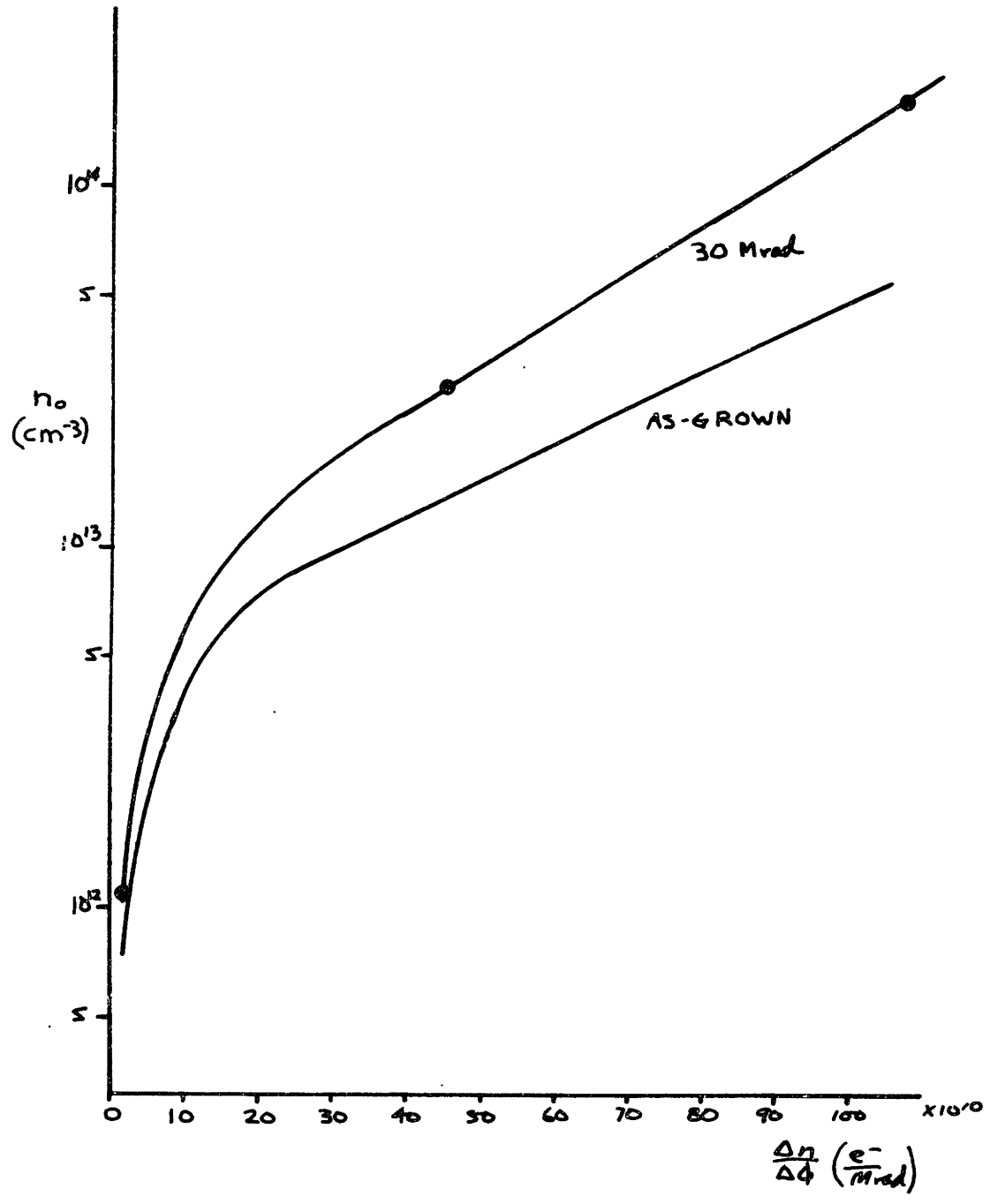
Figure 29. Contrast of Carrier Compensation Rate in
N-Type Materials with Different Radiation
Histories.

was reduced to the level (10^{13} cm^{-3}) established as
the onset of saturation by Figure 26. Figure 29 demon-
strates this reduced radiation sensitivity in materials
already containing radiation defects.

Following these results, a quenching experiment was
designed to evaluate the general effects of initial defect
concentration on the carrier removal rate. Hall effect
samples were carefully prepared and quenched in room
temperature water from a one hour heat treatment at 500°C
(according to the procedure outlined in section IV H).
Table 7 and Figure 30 give the results of this experiment.
The behavior is somewhat similar to that of the reirrad-
iated materials. There is a strong reduction of radiation
sensitivity in the logarithmic region with very minor
deviations in the high purity saturation region.

A full discussion of these results is given later
(section VI). In a general way, it appears that there
is not a unique correlation between the carrier concentration
and the stabilization of radiation acceptor defects.

2. Defect Characterization by Lifetime Analysis

The variation of minority carrier lifetime with
temperature was studied in order to supplement the
information obtained from Hall effect measurements. It
is difficult to observe energy levels near the center
of the gap with Hall measurements because the onset of
intrinsic conduction coincides with the temperature
region of ionization. The states of the levels, however,

TABLE 7

The Effects of Thermal Defects on Carrier Compensation
Behavior in N-Type Germanium

Sample	N_D (cm^{-3})	n_o after heat treatment* (cm^{-3})	Dose (Mrad)	$\dfrac{\Delta n}{\Delta \phi}\left(\dfrac{e-}{Mrad}\right)$
IIIA	1.3×10^{14}	8.7×10^{13}	28.3	4.1×10^{11}
IIIB	8.5×10^{13}	5.8×10^{13}	28.3	4.4×10^{11}
IIA	7.0×10^{13}	9.0×10^{11}	28.3	2.6×10^{10}
VIIA	1.9×10^{13}	1.6×10^{13}	28.3	3.5×10^{11}
VIA	7.5×10^{12}	1.0×10^{12}	28.3	2.9×10^{10}

98
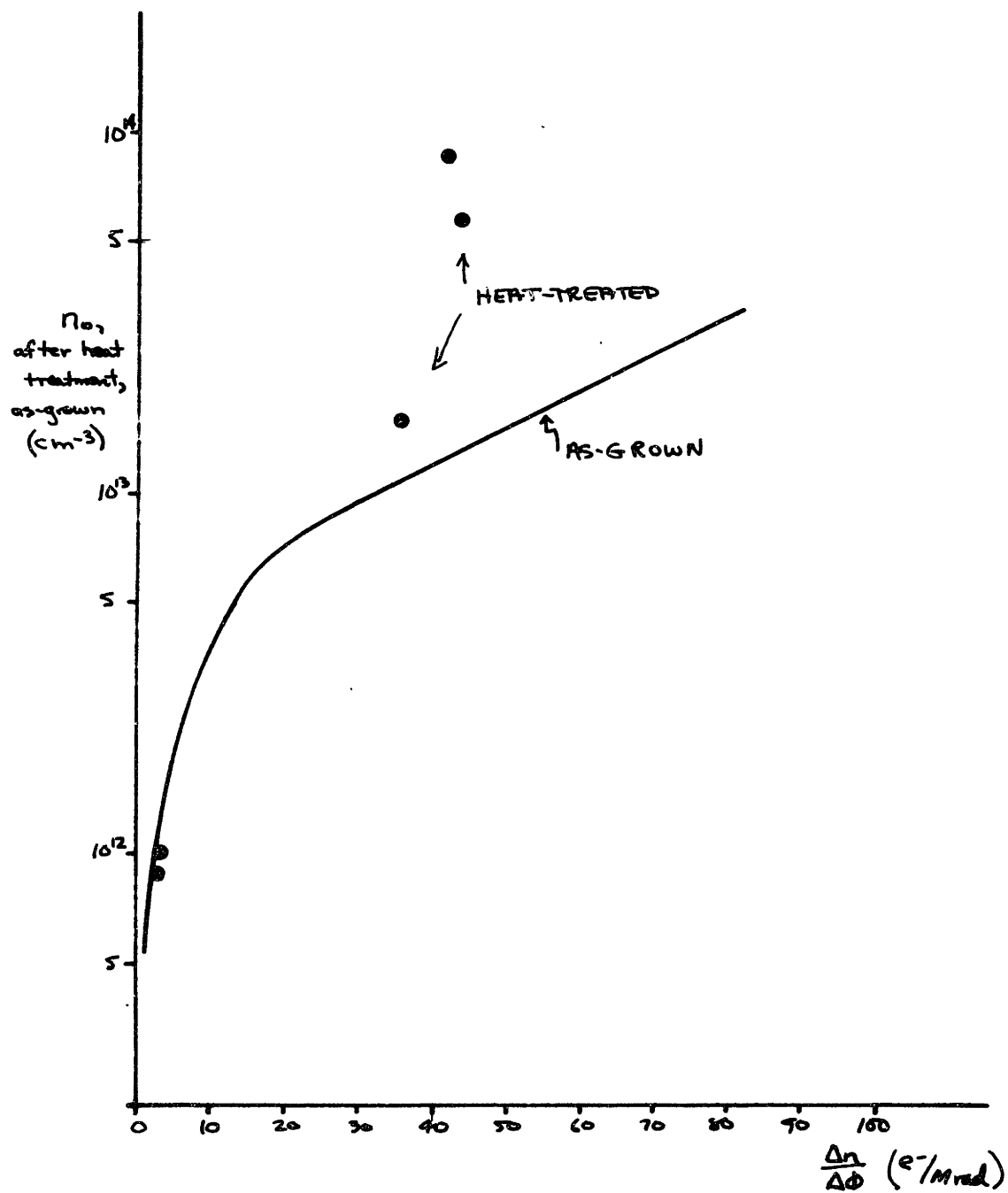
Figure 30.   Carrier Compensation Rate in Heat
             Treated Samples.

are frequently active as recombination or temporary
trapping centers for extended temperature ranges. In this
case, the energy positions may be determined with a life-
time analysis. Qualitative information about the general
electrical character of the center may be derived form
its carrier capture behavior. Details concerning the
analysis of lifetime data are given in Appendix B.

Figures 31-37 demonstrate the lifetime curves for
typical irradiated samples. Temporary trapping effects
are recognized as an increase in lifetime in the low
temperature region as the traps prevent minority carriers
from interacting with the recombination centers. It is
noted that the p-type sample shows no trapping effects.
A summary of the data extracted from the curves is given
in Table 8.

A temporary trap located at 0.26 eV above the valence
band was observed in all the n-type samples under invest-
igation. As mentioned in Appendix B, lifetime data alone
is not sufficient to determine the reference band edge
for the location of a level. In this case, the level
was placed in the lower half of the energy gap because
the Hall effect data for n-type material (discussed
earlier) did not suggest that such a level existed in the
upper half of the gap.

A recombination center was located 0.20 eV below
the conduction band in n-type material. This level is,
presumably, the same level which was identified by the
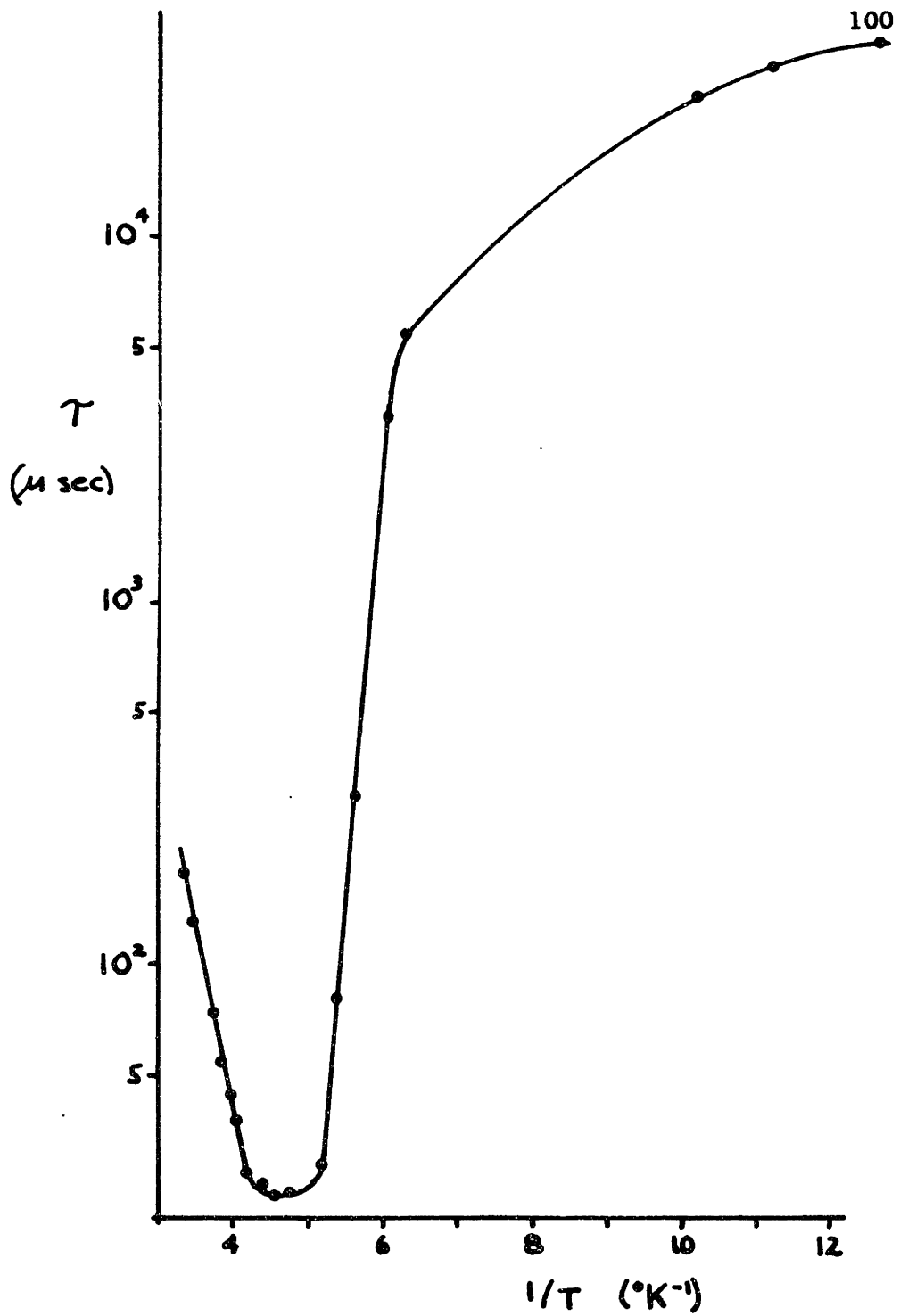
Figure 31. Sample IIC - Irradiated Lifetime Curve
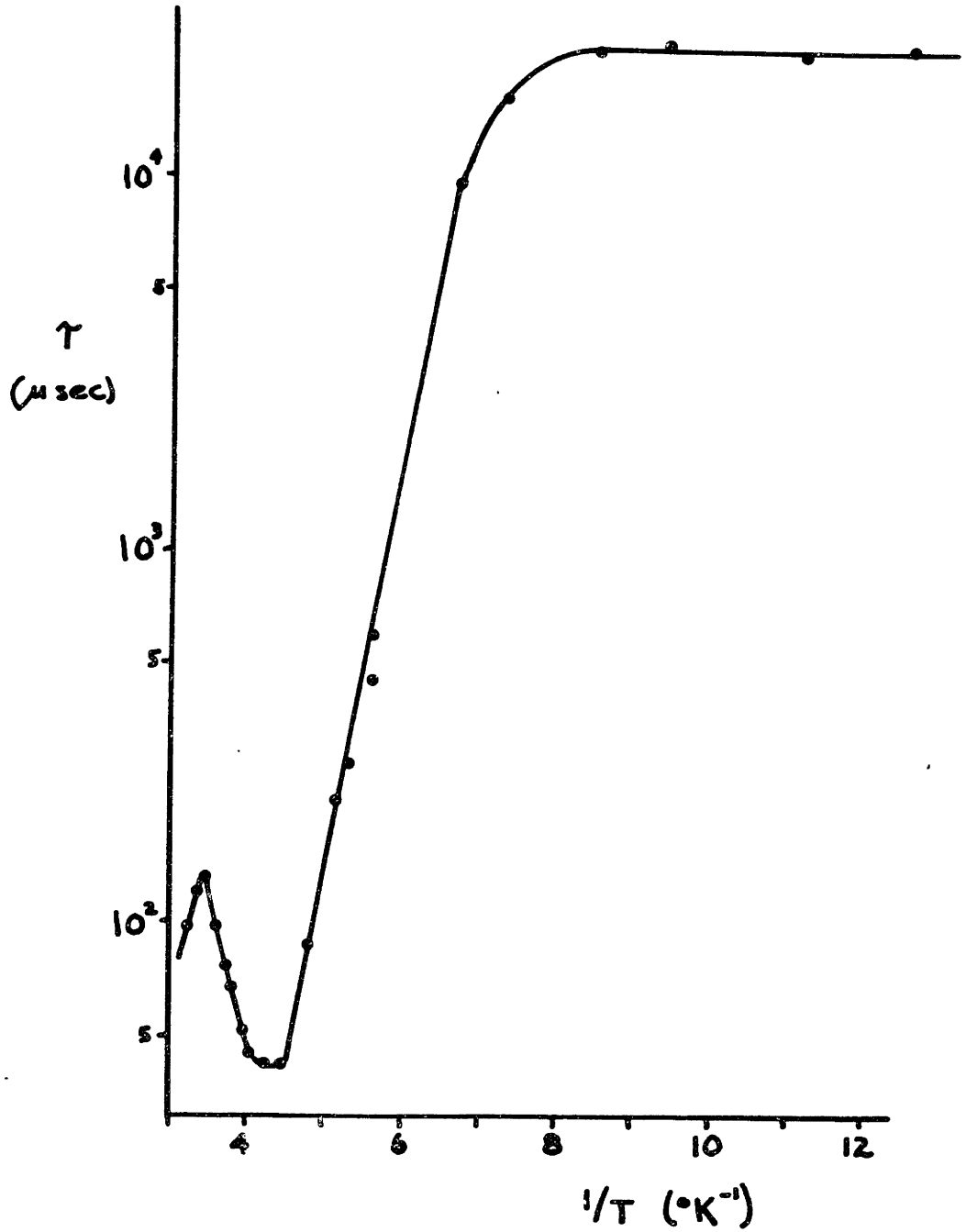
Figure 32. Sample IIE - Irradiated Lifetime Curve
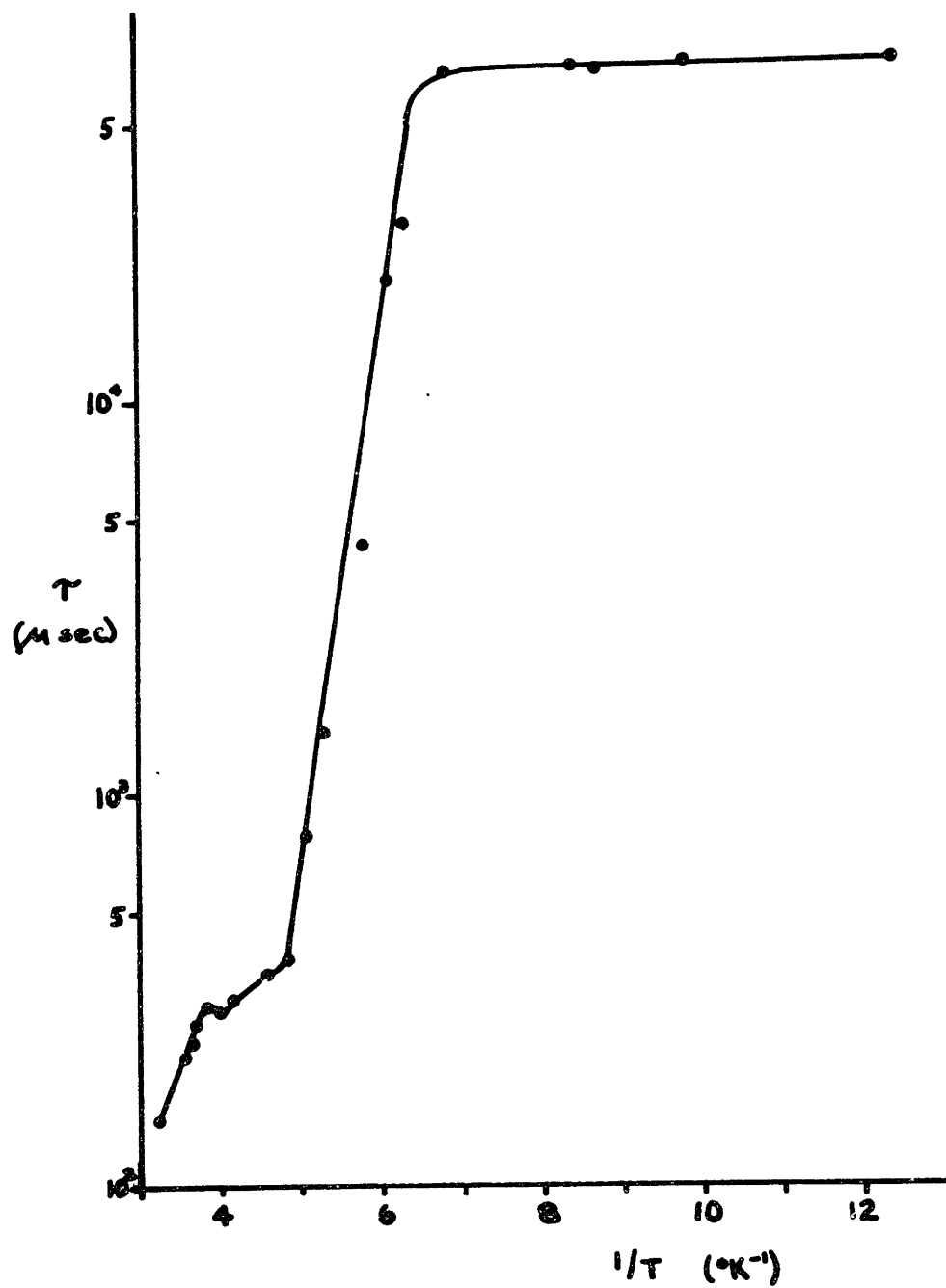
Figure 33.   Sample VA - Irradiated Lifetime Curve
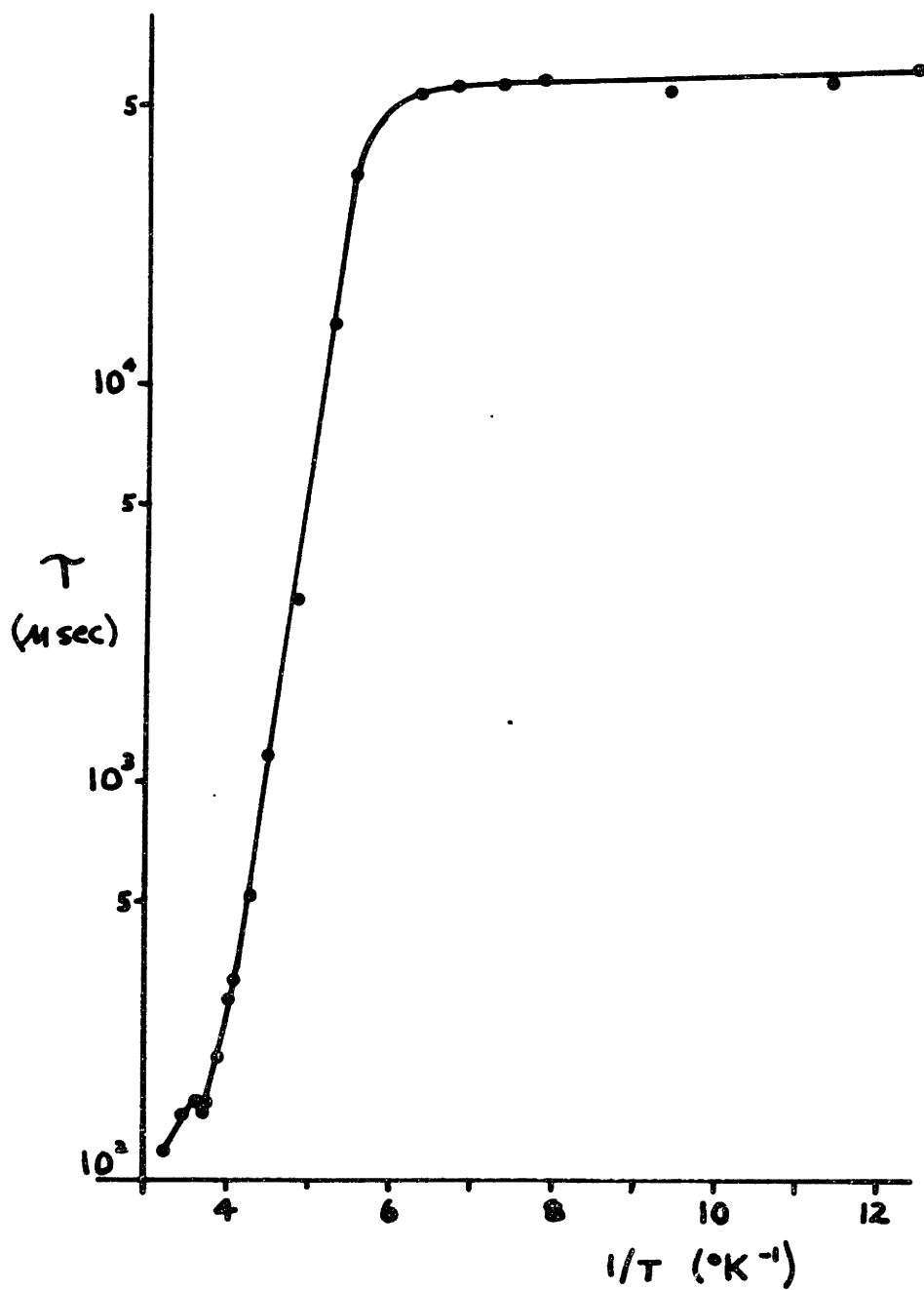
Figure 34.   Sample VB - Irradiated Lifetime Curve
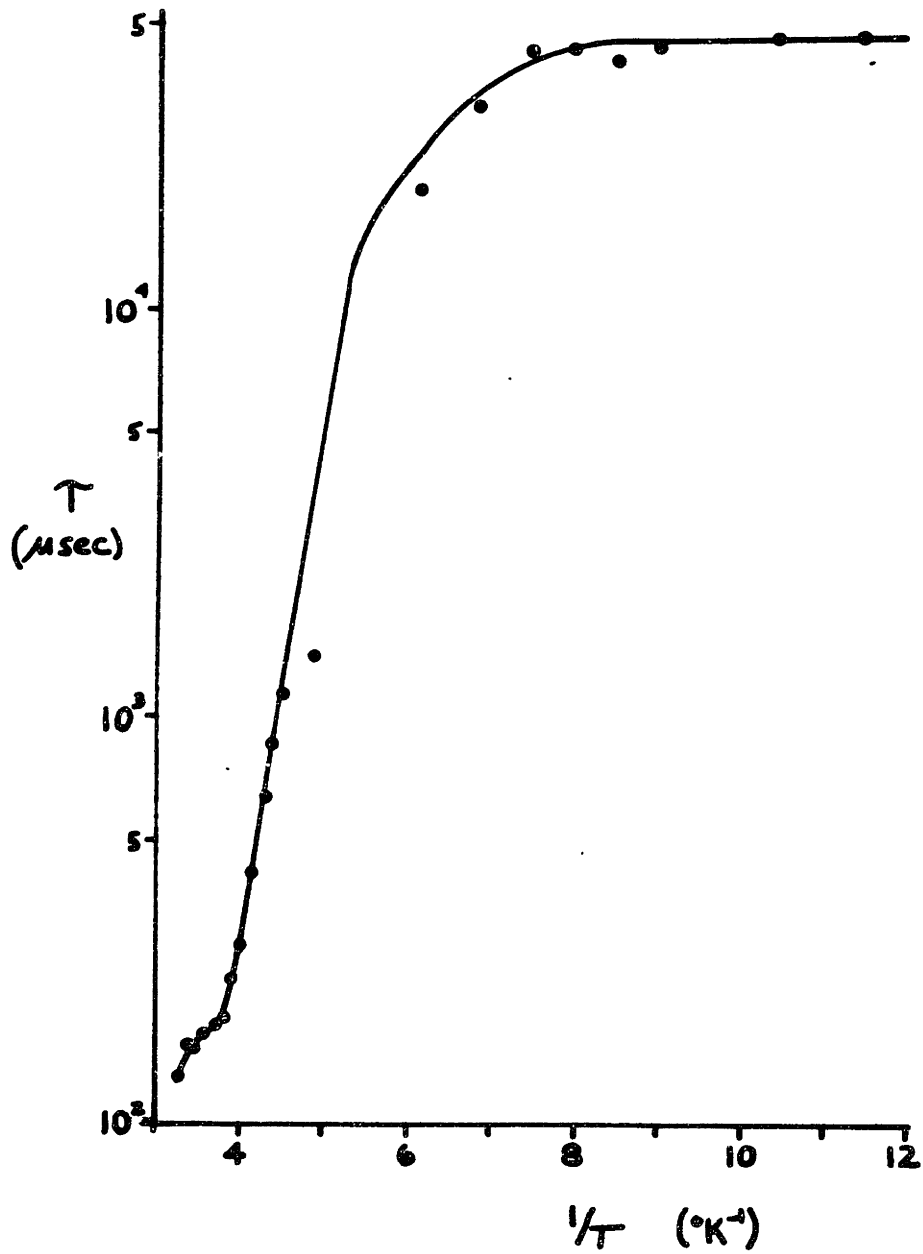
Figure 35. Sample UC - Irradiated Lifetime Curve
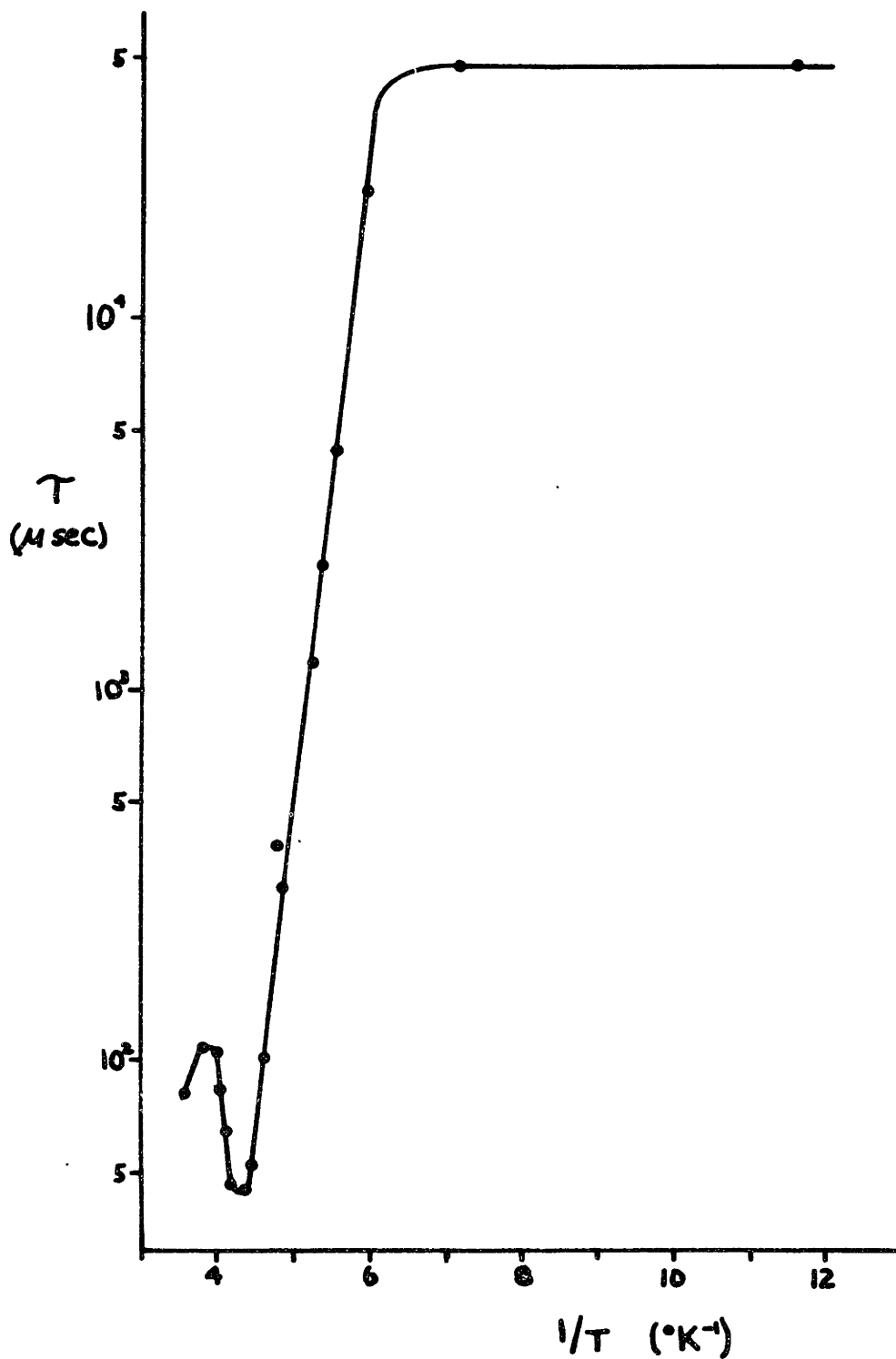
Figure 36. Sample VI - Irradiated Lifetime Curve
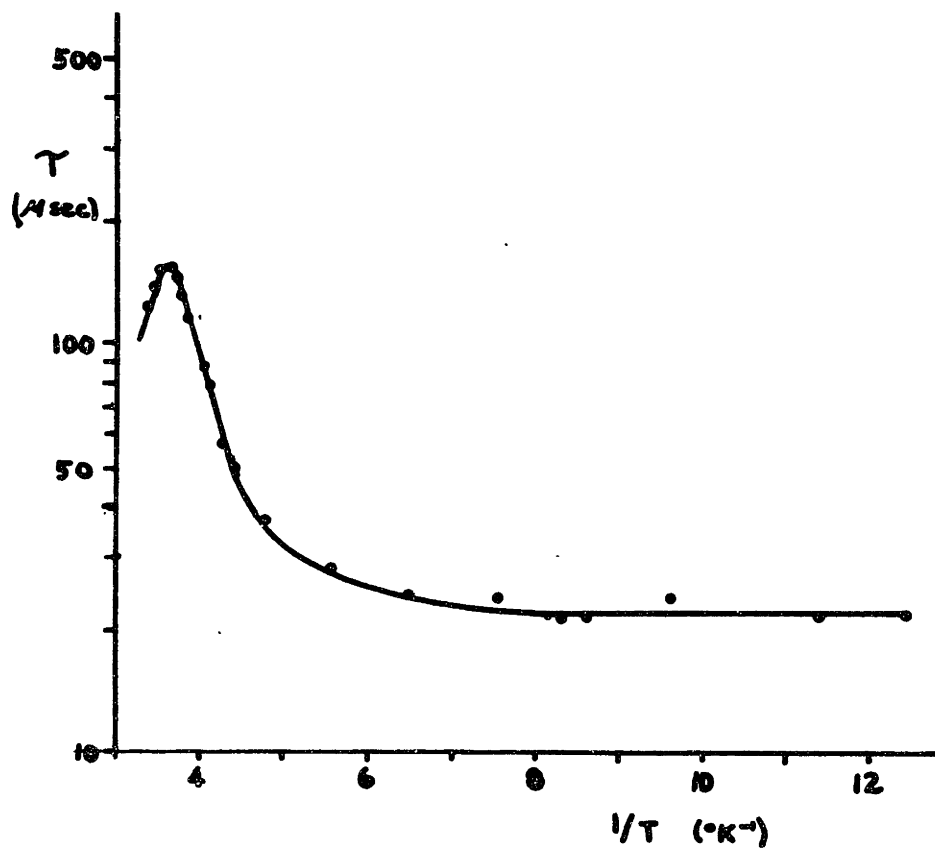
Figure 37. Sample XI - Irradiation of Lifetime Curve

TABLE 8

Summary of Lifetime Results

Sample	$n_o,(p_o)$ (cm^{-3})	Dose (Mrad)	E_T-E_v (ev)	E_R (ev)	$\frac{E_G}{2}-E_R$ (ev)	$c_n(R)$ (250°K)	$c_n(T)$ (200°K)
IIC	9×10^{13}	26.2	.26	.21	.15	-	5.3×10^{-13}
IIE	1×10^{13}	26.2	.26	.19	-	-	3.4×10^{-12}
VA	9×10^{12}	26.2	.26	-	.15	-	5.2×10^{-12}
VB	8×10^{12}	26.2	.26	-	.12	-	5.3×10^{-12}
VC	7×10^{12}	26.2	.26	-	.12	-	5.3×10^{-12}
VI	7×10^{12}	30.7	.26	.20	.15	-	1.8×10^{-12}
XI	(3×10^{12})	26.2	-	.16	.13	4.2×10^{-9}	-

E_T refers to the energy position of a temporary trap.

E_R refers to the energy position of a recombination center.

$c_n = \sigma_n \langle v \rangle$ refers to the capture coefficient of a center.

Hall measurements. This center was not evident in crystals Va, Vb, and Vd. This result is apparently due to a high concentration of traps relative to the carrier concentration. The occupation of the traps would, in that case, determine the majority carrier concentration. This phenomenon is discussed in Appendix B.

In the p-type crystal, a recombination center was located 0.16 eV above the valence band. This level also, is presumed to be the center identified in the Hall effect data.

Electron capture coefficients, C_n, are listed in Table 8 for some of the levels. These values are not to be regarded as exact, but should be of the correct order of magnitude. The meaning and derivation of this parameter is considered in Appendix B. The capture coefficient is strictly defined as the product of a capture cross section and the mean thermal velocity of a given carrier.

The electron capture coefficient for the $E_v + 0.16$ eV recombination center was determined to be 4.2×10^{-9} cm^3/sec. This corresponds to a capture cross section of 2.1×10^{-16} cm^2 at $250^\circ K$ which is the same order of magnitude as the size of an atomic site in the crystal structure (about 6×10^{-16} cm^2). This comparison suggests that the electron is captured by a **neutral** site. The increase in lifetime with increasing temperature could, then, be interpreted in terms of the occupation of these

centers with electrons from the valence band and the consequent decrease in the electron capture coefficient of the occupied centers. This portrayal agrees well with the ionization behavior observed by measurement of the Hall coefficient.

The most probable value of the electron capture coefficient for the E_v + 0.26 eV level appears to be about 5×10^{-12} cm^3/sec. This corresponds to a capture cross section of 2.8×10^{-19} cm^2 at 200°K. Since this area is considerably smaller than that of a lattice site, one would postulate that a repulsive force acts on the electron. Thus, it is suggested that the center is negatively charged with a low probability of electron capture because of Coulomb repulsion. The behavior of the center as a temporary trap can be characterized accordingly:

(a) The center possesses a double negative charge in its equilibrium state and readily captures nonequilibrium holes.

(b) After hole capture, the center has a single negative charge. The probability of electron capture is low and holes are emitted without recombination.

(c) At low temperatures, the probability of hole emission is low and recombination eventually occurs in the trap. While this line of reasoning is not based on exact quantitiative evidence, it does explain the observed behavior based on the data available.

The capture parameters of the recombination center in the n-type samples (E_c - 0.20 eV) could not be determined because of the dominance of trapping effects at low temperatures. Following along previous lines of reasoning, it is suggested that this center must either be neutral or negatively charged in order to function as a recombination center for nonequilibrium holes.

This section has demonstrated the type of additional information that can be derived for lifetime measurements. Minority carrier behavior is also an important determinant in the qualification of semiconductor material for device uses. The importance of this parameter will be discussed in section V C.

3. Mobility Analyses

An attempt was made to determine the charge state of the radiation defects by following the change in mobility with defect density. According to the Conwell-Weisskopf theory[79], the change in mobility associated with an addition of charged scattering centers to a semiconductor is given (in the impurity scattering range) by

$$\Delta \frac{1}{\mu_I} = \Delta \sum_i q_i^2 N_i \quad ,$$

where μ_I is the contribution to the mobility from charged center scattering (dominant at low temperatures), q_i is the charge on the defect, and N_i is the density of the defect. In most cases the number of defects introduced

by radiation was not large in comparison with the con-
centration of scattering centers present in the initial
material. Also, the temperature range of measurement
did not extend low enough for an accurate evaluation of
charged center scattering. However, some preliminary
observations can be made that might prove helpful for
future experiments.

Figures 38-41 show typical mobility behavior for
n- and p-type crystals. Electron mobility is generally
unchanged by irradiation in relatively impure n-type
crystals. In fact, a slight increase is sometimes
detected. While this increase is near the range of
experimental error, it could be significant. In higher
purity material, there appears to be a strong tendency
for the mobility to decrease. The p-type material
was of relatively high purity and shows a correspondingly
large decrease in hole mobility. Table 4 gives further
supporting evidence of this dependence. The implications
of this behavior will be discussed in section VI.
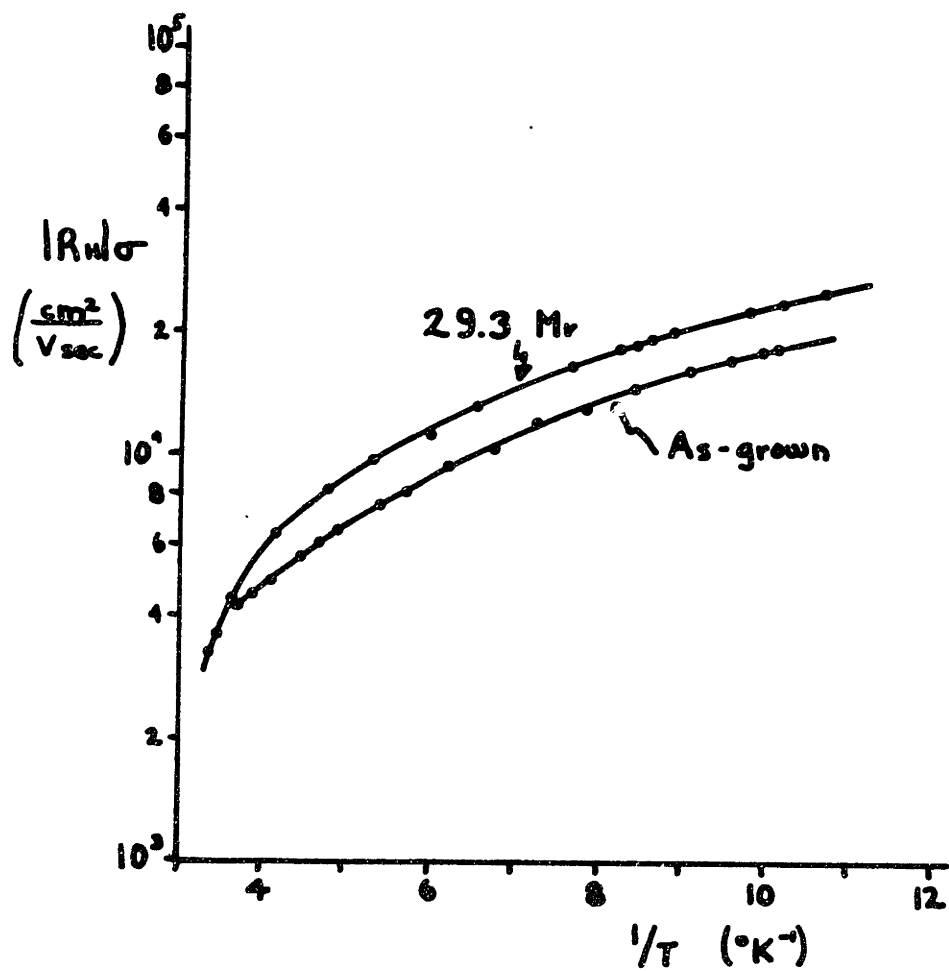
Figure 38. Effects of Radiation on Mobility
Sample II
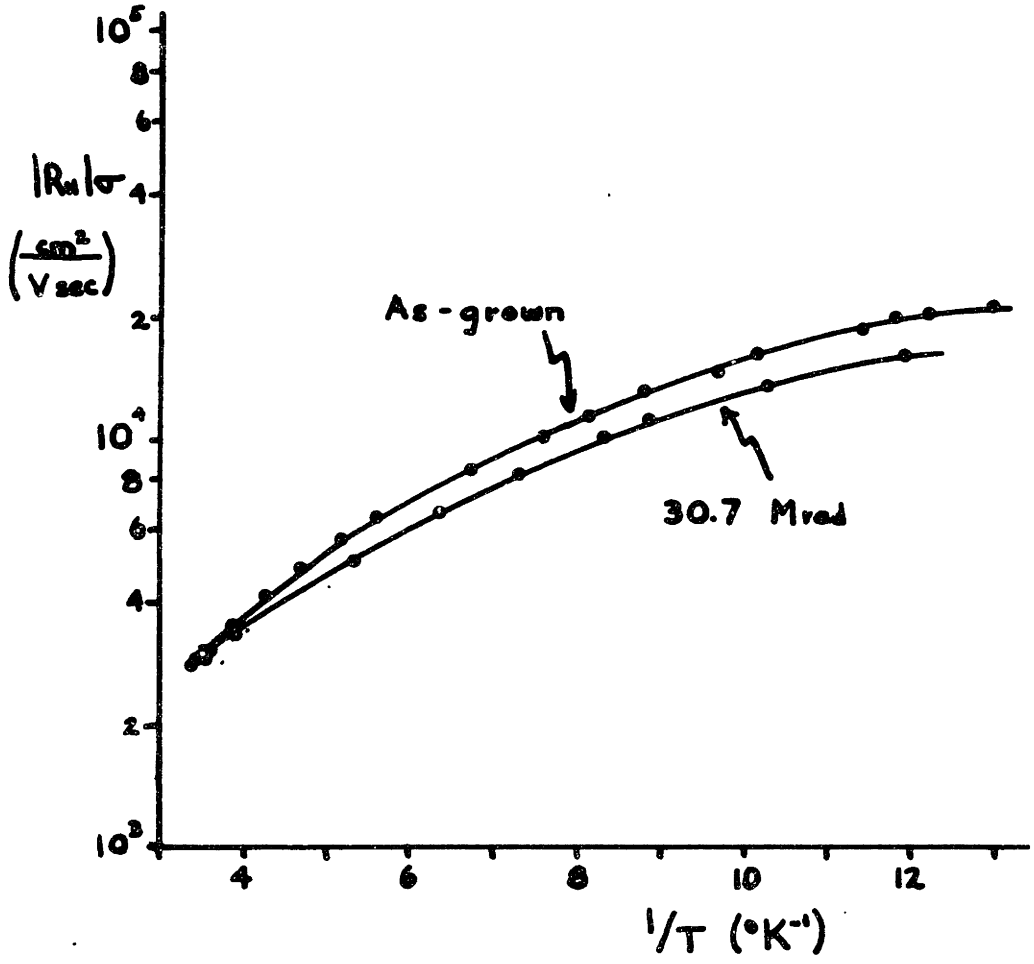
Figure 39.   Effects of Radiation on Mobility
             Sample IIIa
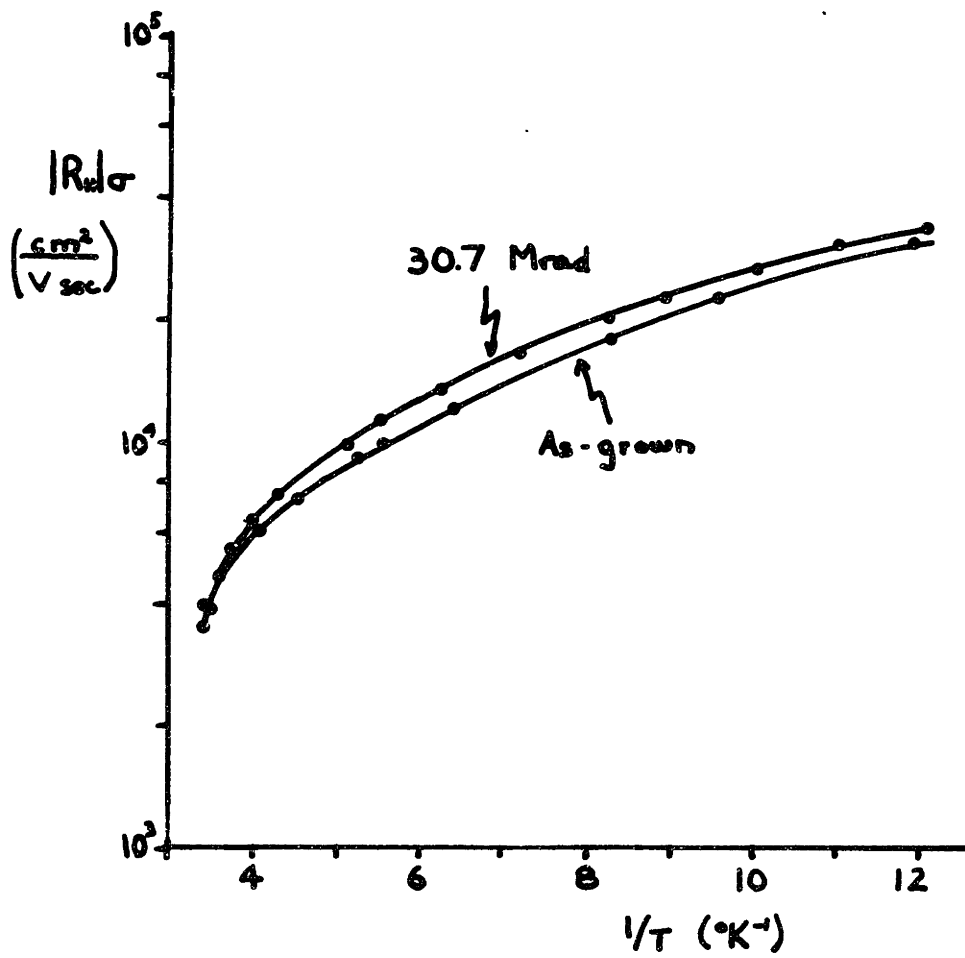
Figure 40. Effects of Radiation on Mobility
Sample IIIb
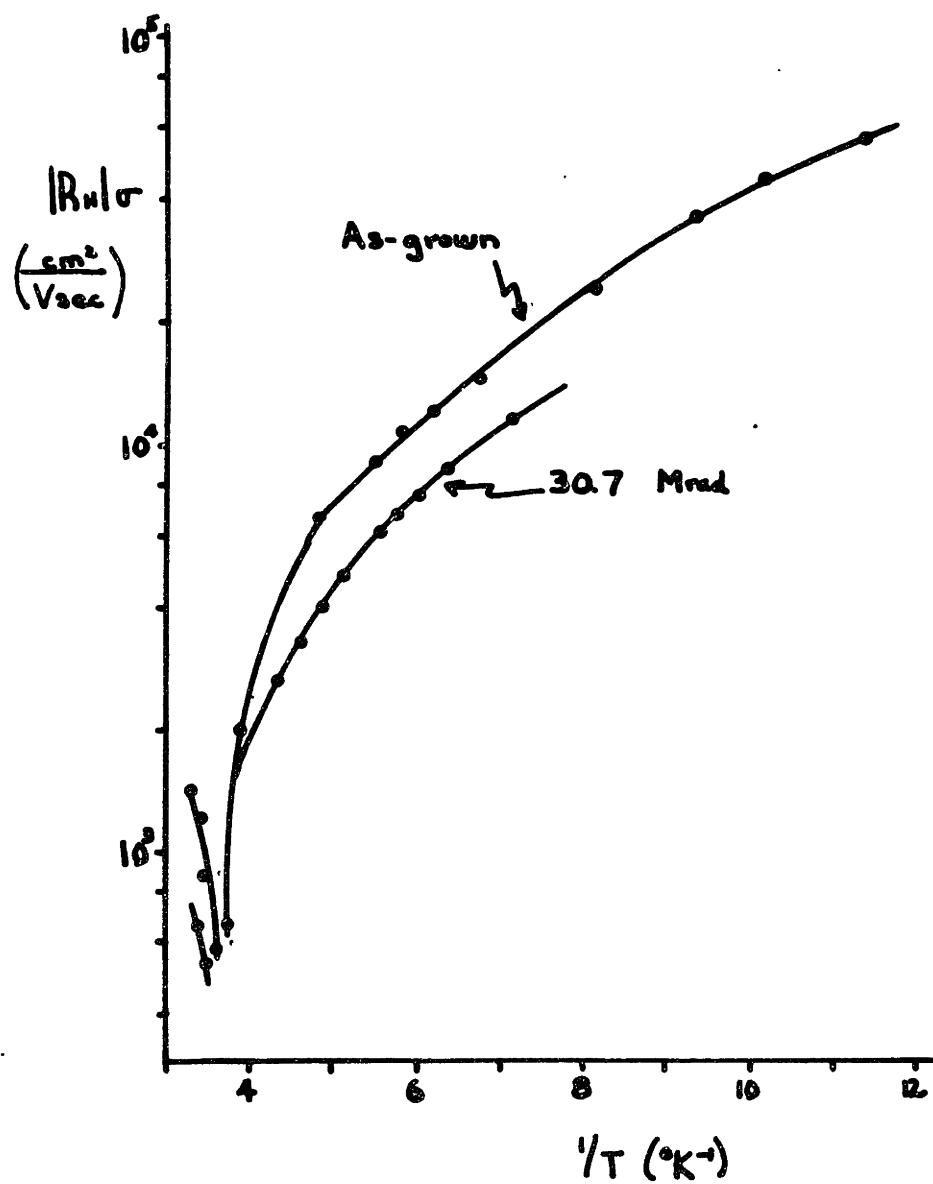
Figure 41. Effects of Radiation on Mobility
        Sample X

C.   Detector Construction and Performance

A series of p-i-n radiation detector devices were constructed as a direct application of the radiation compensation process. The performance of these devices reflects the quality of the starting material. The principles of the detector operation are outlined in Appendix C.

The characterization of the germanium base material used in the detectors is given in section V A (table 1). Two main problems were evident in the construction of the devices. Nonuniform junctions frequently led to low breakdown voltages and high leakage currents; and, surface leakage channels frequently resulted in high currents under back bias. The adoption of the procedures outlined in section IV G served to reduce both of these problems. The work leading to the development of this procedure and the performance of the finished device will be discussed in this section.

The final procedure was developed after the construction of 24 detector structures. It must be pointed out, however, that the techniques of execution were found to be almost as important as the procedure.

Nonuniform junctions produced overall erratic results. For the n-type contacts, the lithium diffused junction gave the most overall reproducible results. Gold-antimony alloyed junctions were also tried, but

junction formation was not consistent. Gold and antimony were evaporated simultaneously on the crystal surface and subsequently alloyed by heat treatment at 350°C. Spalling of the evaporated metal was frequently evident during the alloy treatment. It is plausible that antimony may have been rejected by the gold-germanium eutectic. Further experiments with low antimony contents were not performed, but they seem advisable.

The lithium contact appeared to be both stable and consistent. It is estimated that lithium atoms diffused to a depth of about 1 millimeter during the five minute heat treatment at 425°C. The main problem encountered in this process was the precipitation of lithium to an electrically inactive state. This effect was retarded by fast cooling of the sample to room temperature after heat treatment. Precipitation was evident by the presence of large pits on the contact surface. After lapping to a smooth surface, it was found that, with the fast cooling technique, enough lithium remained in solution to give a uniform surface resistivity of about 2 ohm-centimeters.

Since the base material for these radiation compensated detectors is n-type, the critical contact is the p-type junction. It is from this contact that the depletion will expand to the n-type contact. The gold evaporated and nickel plated contacts were found to be

best in terms of homogeneity, but the gallium-indium
alloyed contact gave the most consistent results.

The evaporated gold junction acts as a surface
barrier contact. The physical principles underlying
the operation of this junction are not well formulated.
It os believed, however, that an oxide layer between the
semiconductor and the gold determines the properties of
this junction. Results in this study were found to vary
from excellent rectification to ohmic behavior. This
behavior is probably derived from a lack of reproduc-
ibility in surface conditions before evaporation. The
gold layer was also subject to peeling during construction
procedures.

The nickel contact was consistently rectifying, but
frequently resulted in high leakage currents. This effect
is probably related to initial surface preparation or
impurities in the plating solution.

The gallium-indium alloyed contact gave consistently
good results. The main problem was the wetting of the
germanium surface with the liquid gallium-indium metal.
If the contact was not intimate, the metal would coagulate
into small spheres which resulted in a nonuniform junction.
This behavior was corrected by careful etching of the
surface before application of the metal.

Surface breakdown and leakage effects were, by far,
the dominant problems in detector construction. These

effects are believed to be associated with the conditions under which the depletion region spreads from the p-type contact. The behavior of the surface is believed to be related to states which arise from the structure of an adsorbed oxide layer. These states are presumed to determine the conductivity type of the surface and, hence, the surface leakage characteristics.

If the surface is n-type, a p-n junction is formed at the intersection of the surface and the p-type contact. Since the surface is relatively more n-type than the compensated bulk material, a relatively thin depletion region exists at the surface junction while in the bulk, the depletion region extends further. As the reverse bias is increased, very high fields are created at the thin surface junction. These fields lead to eventual electrical breakdown for the structure. This breakdown occurs at actual bias voltages much lower than would be expected for these structures.

Conversely, a p-type surface forms a poor reversed bias junction with the bulk. This junction results in the copious injection of minority carriers into the bulk. These carriers lead to high leakage currents.

The ideal surface should be, of course, intrinsic. However, one must, in reality, choose between n- and p-type. Since a high bias is necessary for the device function (short collection times), a p-type surface

should be preferred. Furthermore, a lightly p-type condition is most desireable for uniform spreading of the bulk depletion region and minimum leakage currents.

It is expected that the application of a mild oxidizing treatment to an etched surface should introduce states with a high electron affinity, thus making the surface p-type. Experimentally, it has been shown[107] that a mild oxidizing treatment will result in a p-type surface, but heavy oxidation tends to convert the surface conductivity to n-type.

In these experiments, the crystal surfaces were first given a long etching in CP4 making the surface presumably smooth to an atomic scale. It is believed that this etching removed all surface strains and other constituents that might lead to a high density of surface states. The etching reaction was quenched with methyl alcohol in order to minimize any irregular oxidation effects that might be associated with a water quench. The surfaces were then given a light oxidizing treatment in 6 parts (70%) HNO_3 and 1 part (48%)HF for 10 seconds. This treatment presumably leaves the surface lightly p-type. Rinsing in methyl alcohol followed the short etching. Surface leakage characteristics improved greatly as a result of this treatment. Before it was adopted one structure in ten possessed adequate leakage current characteristics. Following the adoption of this treatment

approximately seven tests in ten were acceptable.

The results of performance tests on the finished devices are given in Table 9 and Figure 42-45. Energy resolution was measured as the width at half maximum height of the 662 keV photopeak of the cesium 137 spectrum.

The best results were obtained using the gallium-indium alloyed p-type contact. All n-type junctions were of the lithium-diffused type. The unifying trends which are evident in these results are summarized as follows:

(1) The best resolution was obtained with crystals I and IV. Both of these crystals exhibited a high degree of homogeneity in the analyses of section V A.

(2) Crystal V showed relatively poor energy resolution. This structure was given a relatively high dose of radiation. The position of the peak shows a considerable displacement to lower energies relative to the other peaks measured. The shape of the peak, in addition, shows a broadening to higher energies indicating large carrier losses. The extension of the peak in the low energy region (to the range of Compton interaction) suggests a large variance in the carrier losses.

(3) The resolution of crystal GE is fair. The leakage current and capacitance for this structure were the best of any tested. The dislocation density in this crystal was the highest of all tested (13,000 cm^{-2}). The broadening of the peak to the right and extension

TABLE 9

Summary of Detector Performance

Crystal	I	IV	V	GE
Dimensions (mm)	4x4x3	4x4x3	1.5x4x3	6x6x3
Dose (Mrad)	30.3	30.3	107	28.5
p contact	Ga-In	Ga-In	Ga-In	Ni
i_r at 360v (amperes)	1.6×10^{-9}	3.5×10^{-10}	2×10^{-9}	2×10^{-10}
measured capacitance at - 360v (pf)	12.7	12.5	16.4	11.5
contact face	{111}	{111}	{111}	{100}
resolution	11.9 eV	10.5 keV	>61 keV	39 keV
	1.8%	1.6%	>9.2%	5.9%
peak channel	344	348	324	335
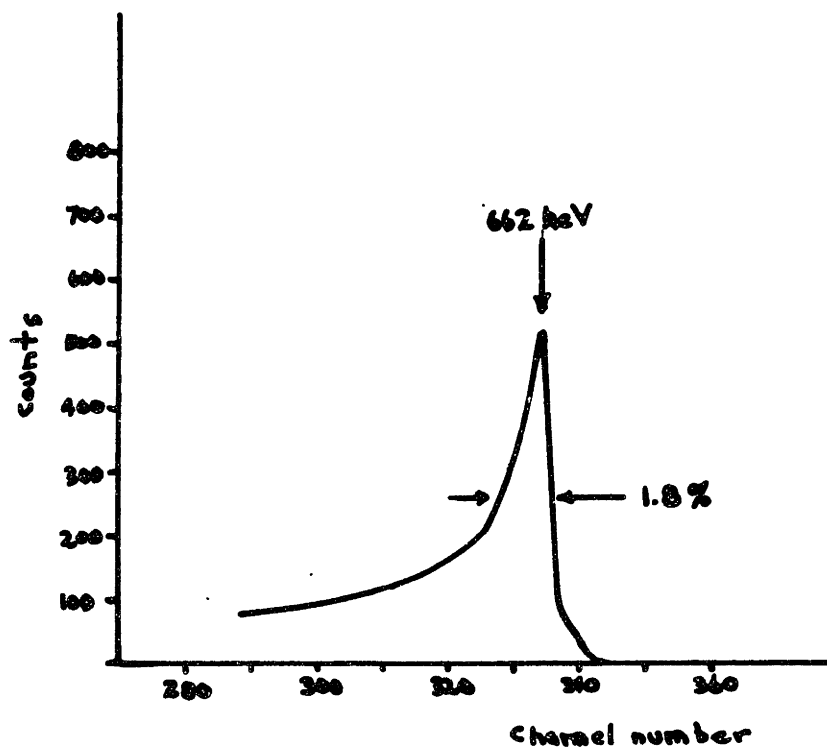
Figure 42.   Cesium 137 Spectrum Obtained from Crystal I
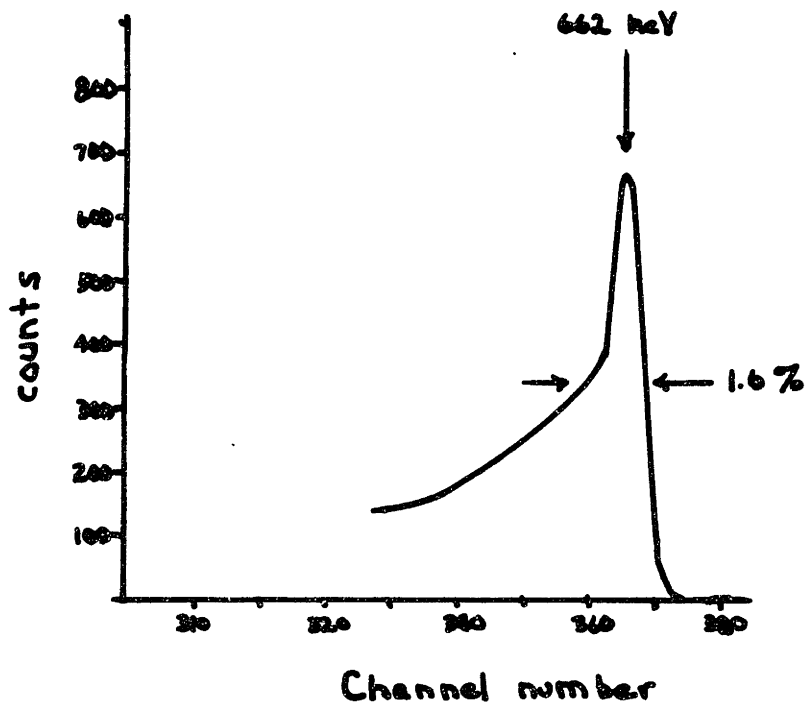
Figure 43.   Cesium 137 Spectrum Obtained from Crystal IV
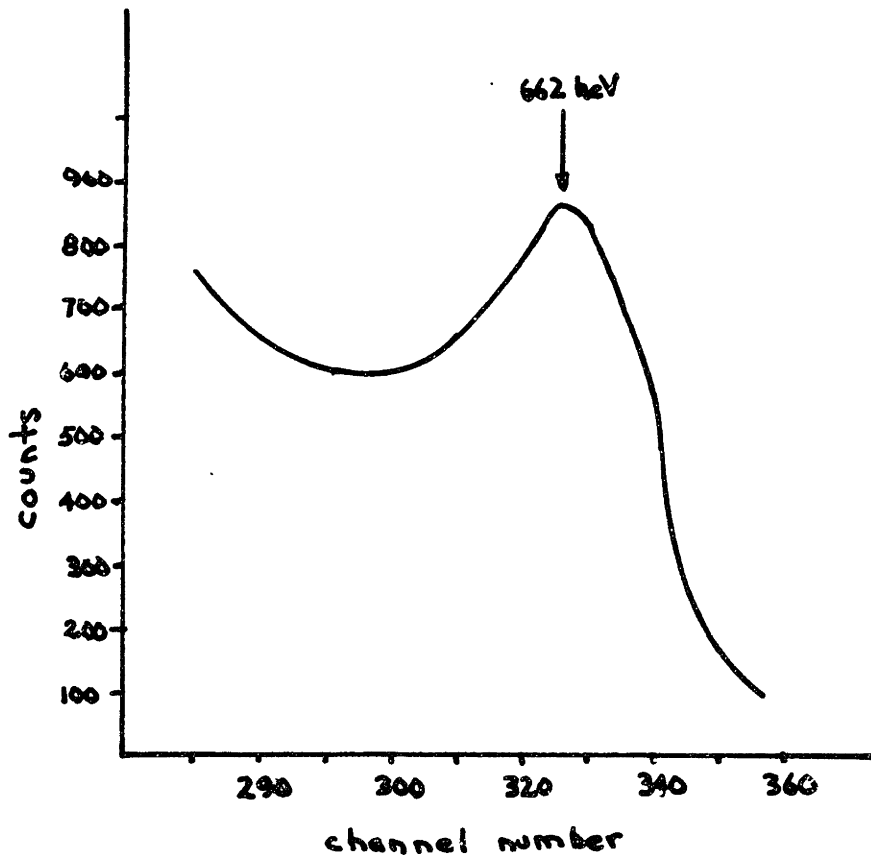
Figure 44. Cesium 137 Spectrum Obtained from Crystal V
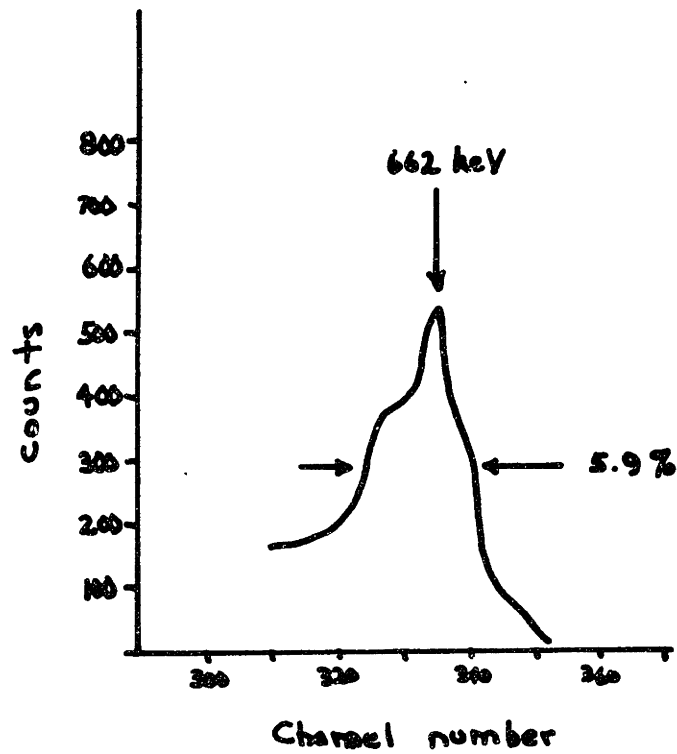
Figure 45. Cesium 137 Spectrum Obtained from Crystal GE

to the left indicate high carrier losses. Crystal II, also with a high dislocation density (12,000 cm^{-2} near the edge) was tested during early stages of device development and showed a spectrum similar to crystal V indicating high losses.

(4) In general, smaller detectorsstructures provided better resolution and more reliable performance than larger ones. This effect is probably related to the $\underline{inhomogeneity}$ of the donor concentration in the base material. Gamma radiation introduces defects homogeneously. The resulting compensation is $\underline{inhomogeneous}$ and leads to nonuniform fields within the device and,hence, variation of the collection times.

Whereas no definitive conclusions can be drawn from this preliminary study of radiation detection devices, certain observations can be made based on the behavior of the device tested. In general, the method of compensation by radiation defects appears to be effective in these devices. The energy resolution of the $\underline{best}$ lithium-drifted germanium detectors is .5 percent for the cesium 137 spectrum. The result, here, of 1.6 percent is comparatively good in view of the early stage of development and the characteristic problems of the lithium detectors. Results from the Soviet Union [108] quote a 1 to 2 percent resolution with the radiation compensated devices for the cesium 137 spectrum.

Because the radiation compensated detector is relatively easy to prepare (compared with the lithium-drift process) it is suggested that they are an ideal tool for the study of the role of materials parameters in the general device performance. The following are some observations based on this study which may be helpful in guiding future experiments.

There appears to be a realtion between signal losses and the dislocation density of the base material. The losses are apparently due to recombination or trapping at vacant orbitals along the dislocation line.

Similar losses were noted in structures given high doses of radiation. These losses are presumed to be directly related to the trapping phenomena observed at the E_v + 0.26 eV level, for low temperatures, in the lifetime studies of section V B.

No satisfactory detectors were constructed using alloyed contacts on {100} surfaces. The regrowth processes on the {111} planes tend to form a flat (facet effect) junction, wheras regrowth on the {100} plane may be irregular.

An oxidizing treatment of the surface after etching appears to lead to smaller values of leakage current and higher values of breakdown voltages for an n-type base material. This effect was discussed earlier.

The radiation compensated devices underwent no decrease in resolution upon storage for several weeks at room

temperature.   In this respect, they are far more desireable than the less stable lithium-drifted devices.   It is believed that these detectors can currently compete with the lithium-drifted devices for many detection applications. This preliminary study has uncovered no obstacle to the eventual universal use of these devices as high resolution spectrometers.

VI. DISCUSSION

A. Carrier Compensation Rate in Pure Germanium

Despite the intensive study of radiation effects in semiconductor materials, a complete formulation of the process of defect stabilization has yet to be developed. For the case of germanium, it has been found that the observed carrier compensation (removal) rates are more than an order of magnitude less than predicted by theory. (A theoretical value for $\Delta n/\Delta\phi$ has been calculated to be approximately 8×10^{13} electrons/Mrad)[5]. If this behavior is to be understood, some mechanism of defect relaxation and annihilation must be introduced. In this work, several parameters for this relaxation process are indicated. In this section, these parameters are defined and their role in the relaxation process is explored.

The results of section V B may be summarized as follows:

(a) A defect level was observed at $E_c - 0.20$ eV in n-type material. It was determined to be in either a neutral or positive charge state at room temperature. The introduction rate of this level showed no apparent dependence on the initial carrier concentration. However, more data is needed for a definate conclusion.

(b) A defect level at $E_v + 0.26$ eV was observed in n-type material. It was determined to be in a double

negative charge state at room temperature.

(c) The introduction rate of levels at or below
midgap was found to increase with increasing initial
donor concentration.

(d) In p-type material a defect level was observed
at E_v + 0.16 eV. It was determined to be in a singly
negative charge state at room temperature. The intro-
duction rate of this level increased with the increase
of the initial hole concentration.

(e) The carrier compensation (removal) rate was
reduced more by irradiation than by an equivalent decrease
in the initial carrier concentration. Thermal defects
produced similar results. The compensation rate was
also found to approach a constant value at very low or
very high values of the initial carrier concentration.

The objective of this discussion is to justify the
carrier compensation behavior in terms of the observed
facts. Based on an earlier discussion of crystal purity
(section V A), it is assumed that the initial carrier
concentration is exactly equal to the initial dopant
concentration. The net concentration of electrons
removed by irradiation in n-type material is assumed to
be directly related to the net number of stable vacancies
introduced. The acceptor properties of the vacancy are
discussed in Appendix E.

Electron paramagnetic resonance experiments performed

on irradiated silicon indicate that a large number of different defect configurations exist[28]. In general, these seem to be associated with vacancies, vacancy aggregates, and vacancy-impurity complexes. Similar studies in germanium have not, as yet, proved definitive because the resonance signal tends to possess an excessive line width. However, in view of the similarity between silicon and germanium, it is probable that analogous configurations exist in germanium.

The reduction of the compensation rate in n-type germanium with decreasing electron concentration of the initial material agrees with the intuitive reasoning that a vacancy should be more stable in a negative charge state. In an equilibrium situation, the number of neutral vacancies which are stable is controlled thermodynamically by the energy of formation and the temperature. In germanium this relationship is expressed as

$$[V_o] = A \exp\left[- \frac{2.0 \text{ eV}}{kT}\right] \text{ cm}^{-3} \tag{1}$$

where $[V_o]$ is the equilibrium concentration of neutral vacancies and 2.0 eV is the energy of formation of an isolated vacancy in the lattice. At room temperature this concentration is insignificant.

If negatively charged vacancies also exist, then the total number of vacancies is given by

$$\left[V_T\right] = \left[V_o\right] + \left[V^-\right] + \left[V^=\right] + \cdots \qquad (2)$$

Thus, the <u>total</u> concentration of vacancies is in excess of V_o . The concentration of a particular charge state is found using Fermi-Dirac statistics.

$$\left[V^{-z}\right] = \frac{V_T}{1 + g_i \exp\left[\frac{E_z - E_F}{kT}\right]} \qquad (3)$$

where E_z is the energy position of the electron residing at the z charged vacancy relative to the conduction band. It is shown in Appendix E that the vacancy will not ionize beyond the doubly negative charge state.

According to the treatment of multicharged centers by Shockley and Last[82], the vacancies will tend to possess a charge indicated by the vacancy ionization level nearest, but below, the Fermi level. If the level observed at E_v + 0.26 eV is assumed to be related to a vacancy in the double negative charge state, then the concentration of this species is given by equation (3).

If the energy gap of germanium is taken as 0.67 eV at room temperature[83], then practically all of the radiation introduced vacancies will become negatively charged until the Fermi level approaches the energy position of the E_v + 0.26eV level. Therefore, the variation of the carrier compensation rate with initial electron concentration <u>cannot</u> be simply explained by a change in the charge stabilization of the vacancies. As this con-

clusion is based on the assumption that the E_v + 0.26 eV level corresponds to a double negatively charged vacancy as pointed out above. In view of the limited number of possible defect configurations with a double negative charge, the assumption appears to be a good one.

An alternative stabilization process is based on the association of the negatively charged vacancies with positively charged imperfections. The positively charged entities may be germanium interstitials, substitutional donors, or interstitial donors.

Reiss, et al [80] have shown that such interactions can be described by the application of ion pairing theory to the semiconductor system. This approach is based on an analogy between a liquid electrolyte and ions in the elemental dielectric. The principles of this theory are outlined in Appendix F.

B. A Model for Defect Stabilization

The as-grown germanium crystal may be regarded as a uniform dielectric medium containing a concentration, N_D, of immobile charged ions. Irradiation introduces positive and negative ions into the system in the form of interstitials and vacancies, respectively. The interactions among these ions are described in terms of an interaction energy, ΔH_{AB}. This term represents short range effects arising from the localized strain fields

surrounding the defect and long range interactions through Coulombic forces. When two ions are separated by a distance, r, less the capture radius, r_c, the pair is bound. This pairing reaction may result in either annihilation or complex formation.

Waite[84] has treated the case of short range interactions in electron irradiated germanium. By considering the resulting annihilation kinetics and related experimental results for germanium, he showed that 70 percent of the interstitials returned to the vacancy from which they were dislodged (correlated recovery). He did not, however, consider the possibility of long range vacancy motion at room temperature. The complex defect structues which have been identified in silicon indicate that long range interactions must be considered. The identification of an oxygen-vacancy complex in irradiated germanium below liquid nitrogen temperatures[24] further strengthens this suggestion. In the following discussion, no direct assumption will be made concerning the mobility of these defects. It is assumed, however, that the semiconductor system, which has been displaced from equilibrium by the introduction of radiation defects, will _tend_ to approach an equilibrium state at room temperature. In view of recent findings which are discussed in section II A, it appears that this assumption must be made.

Of the vacancy-interstitial pairs introduced during

irradiation, a certain fraction are onitially separated
by a distance less than r_c. These pairs will eventually
recombine according to the specific kinetics involved.
The low temperature annealing behavior outlined in section
II A suggests that the thermal energy available at room
temperature is sufficient to overcome any barrier to
annihilation that might exist. It is assumed, therefore,
that this mutual annihilation will occur inaattime short
compared to uncorrelated interactions.

Free interstitials and vacancies now migrate to
sinks and stabilization sites. Some of the possible
reactions are:

(a) $[I] + [V] \longrightarrow$ uncorrelated annihilation

(b) $[I] + [N_D] \rightarrow [N_{D_I}]$ (intersticialcy mechanism)

(c) $[I] + [\text{vacancy cluster}] \longrightarrow$ annihilation

(d) $[I] + [\text{dislocation}] \longrightarrow$ annihilation

(e) $[V] + [N_D] \rightarrow [N_D V]$

(f) $[V] + [\text{interstitial cluster}] \rightarrow$ annihilation

(g) $[V] + [\text{dislocation}] \longrightarrow$ annihilation

The data indicates greater vacancy stabilization
in materials with higher donor concentrations, N_D.
It appears that reaction (e) is consistent with this
behavior. Reaction (c) is suggested as the primary
process for interstitial annihilation in dislocation free
material. The existence of vacancy clusters in such
material has been discussed earlier (section II B).

According to reaction (e) the donor concentration at equilibrium is given by

$$[N_D] = \frac{[N_D V]}{K_e [V]} \qquad (4)$$

where K_e is the equilibrium constant for this reaction. Initially,

$$[N_D] = n_o$$

$$[V_R] = \text{const.} \phi = \text{concentration of free vacancies produced by radiation}$$

where ϕ is the integral flux or dose of radiation employed. If x is the fraction of donors which pair with vacancies, then equation (4) may be written as

$$n_o(1-x) = \frac{xn_o}{K_e ([V_R] - xn_o)} \qquad . \qquad (5)$$

The carrier compensation results are represented graphically by a plot of n_o vs. $\Delta n/\Delta \phi$. If the dominant process for carrier removal is the stabilization of vacancy acceptors at donor sites, then the number of carriers removed, Δn, is directly proportional to the number of complexes which are formed, xN_D. Also, the radiation dose, $\Delta \phi$, is directly proportional to the number of vacancies produced in the material. (The concentration of vacancies initially present in the material may be assumed to be negligible. This relationship may be expressed as

$$\frac{\Delta n}{\Delta \phi} = K_1 \frac{x[N_D]}{[V_R]} \qquad (6)$$

Therefore, the variable $\Delta n/\Delta\phi$ may, be replaced by an equivalent term, $X = x[N_D]/[V_R]$.

Equation (5) may be written in terms of n_o and X as follows

$$n_o(1-x) = \frac{1}{K_e} \frac{X}{(1-X)} \qquad (7)$$

The carrier compensation data presented in section V B can be adapted to the form of equation (7) by adjusting the function of the ordinate from n_o to $n_o(1-x)$. The fit of the experimental data with the theoretical expression given by equation (7) is shown in Figure 46.

The open circles represent the experimental values for $n_o(1-x)$ for the data given in Table 4 and Figure 26 based on associate involving a single negatively charged vacancy (one electron removed for each complex). The solid circles represent experimental values of $n_o(1-x)$ for the same samples on the basis of a double negatively charged vacancy associate (two electrons removed for each complex). The X's represent the fit for the samples given a 60 Mrad total dose, originally shown in Figures 28 and 29.

The following conclusions are indicated by the nature of the fit of the experimental data with equation (7):

(a) The observed carrier compensation behavior can apparently be described in terms of defect stabilization by the association of a double negatively charged vacancy with an impurity atom.

(b) The anomalous results concerning the low radiation sensitivity of samples containing radiation defects can be explained by this model.

Figure 47 shows a composite of the carrier removal data in the earlier form. It is expected that as the initial defect concentration increases the curves should be pushed up to higher values of n_o ($\frac{X}{1-X}$ is multiplied by the factor $\frac{1}{1-x}$ which increases with initial defect concentration). This behavior is evident. The shape of the curves may not be entirely accurate though because the points on a given curve do not correspond to exactly the same x. The figure does indicate, however, the relative effectiveness of each process in introducing lattice defects.

The best fit in Figure 46 yields the results

$$K_e = 2.5 \times 10^{-14} \text{ cm}^3$$
$$= 1.07 \times 10^9 \text{ atom fraction}$$

and $K_1 = 2.0 \times 10^{12}$ cm^{-3}/Mrad.

The equilibrium constant, K_e, may be expressed by

$$K_e = Z \exp - \frac{\Delta H}{kT}$$

where Z is the number of possible ways a pair can form, as discussed in Appendix F.

In addition

$$\Delta H = - \frac{z_1 \, z_2 \, q^2}{\epsilon \, r_p} \qquad ,$$
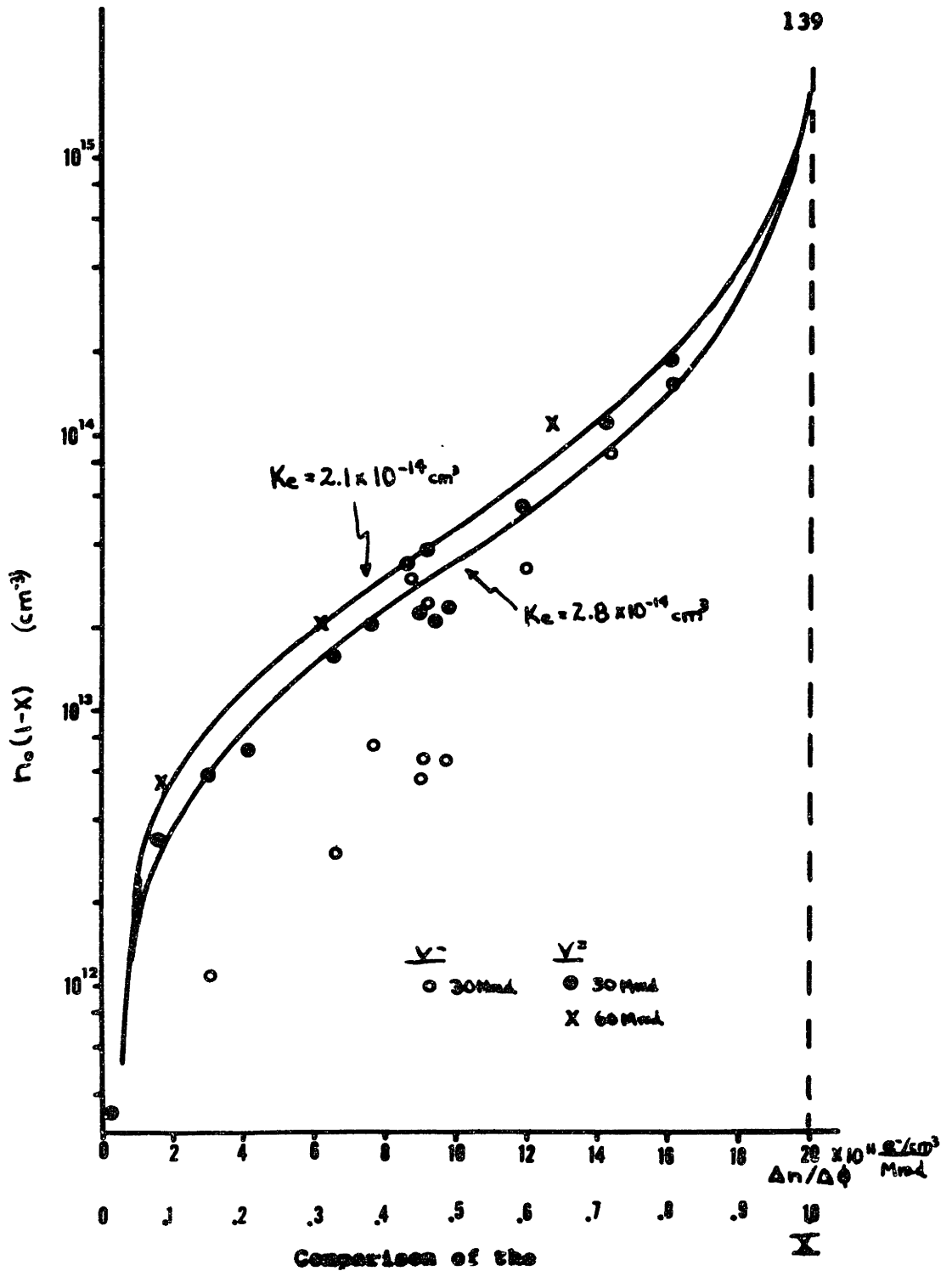
Figure 46. Experimental Data to Equation (7)

where z_1 and z_2 are the numerical charges on the ions, ϵ is the dielectric constant of germanium, and r_p is the pairing distance (see Appendix F). Table 10 gives the solutions for ΔH and r derived from K_e for a number of different pairing configurations.

It is expected that the strong electrostatic forces between the doubly charged vacancy and the singly charged donor would tend to pull the two entities closely together, locally distorting the lattice in the region of the pair. A similar lithium-gallium complex, between two singly charged species, was found to have a pair separation of 2.05 Å [80] as compared with the normal lattice separation of 2.44 Å. Following along this line of reasoning it is concluded that the pairs form between third-nearest neighbors. Pairing between nearest neighbors represents an expanssion of the lattice. Pairing between second-nearest neighbors yields only a slight contraction. The 30 percent contraction for third-nearest neighbors appears to be more reasonable.

This pairing configuration is also favorable in view of the open nature of the diamond cubic structure. The impurity and vacancy are located at opposite corners of a large octahedral void (see Figure 48). Consequently, there is ample space for contraction in order to compensate the imbalance of the electrostatic forces. In addition it might be expected that the vacancy is somewhat enlarged
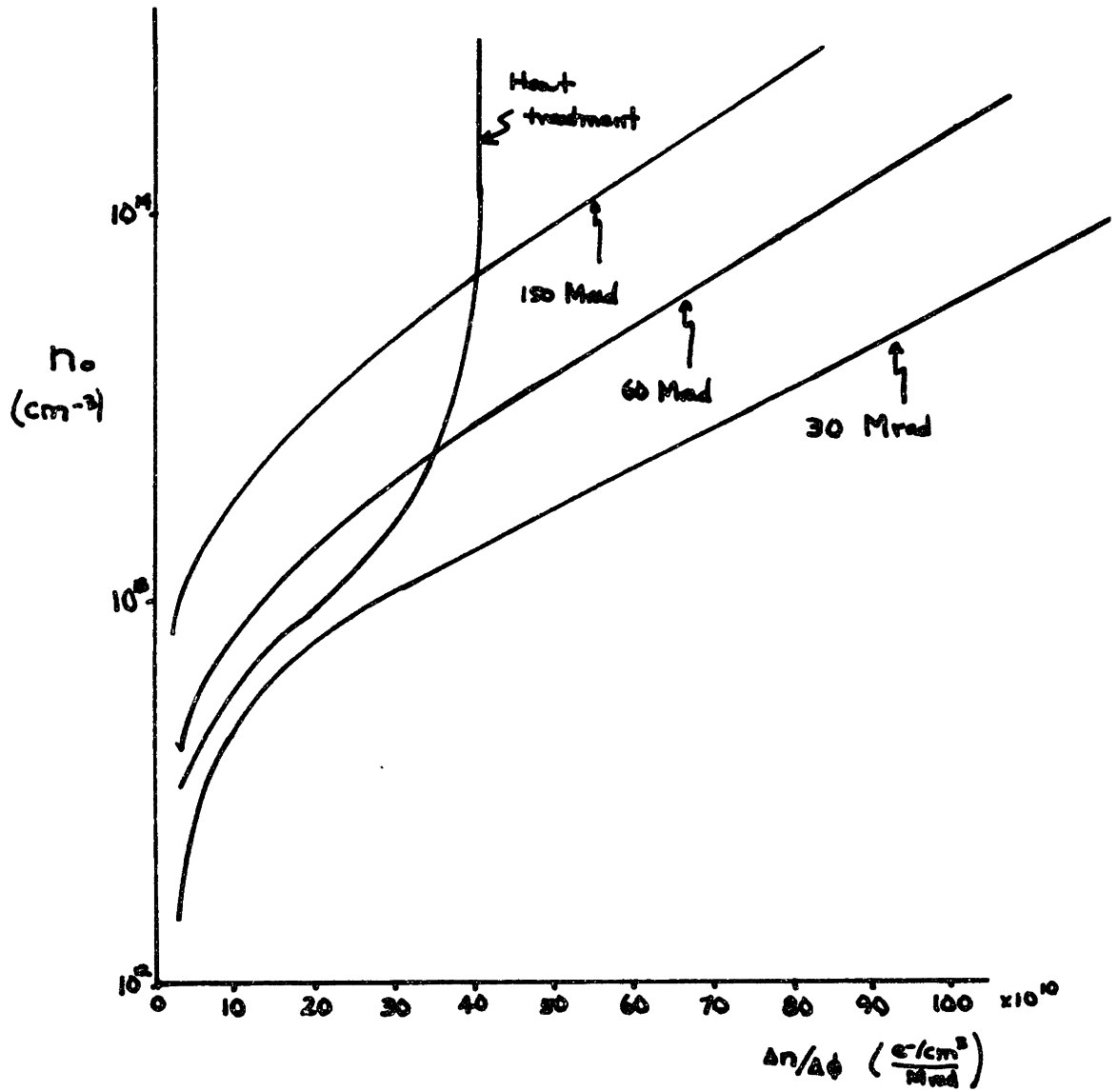
Figure 47. Comparison of the Influence of Different
            Defect Concentrations on $\Delta n/\Delta \phi$

TABLE 10

Theoretical Configurations of the Vacancy-Donor Complex

$K_e = 2.5 \times 10^{14} \text{ cm}^3 = 1.07 \times 10^9$ atom fraction

Configuration	Coordination Z	ΔH eV	pairing distance Å	lattice distance Å
1st nearest neighbor	4	-.48	3.78	2.44
2nd nearest neighbor	12	-.45	3.9	4.00
3rd nearest neighbor	8	-.462	3.8	5.66
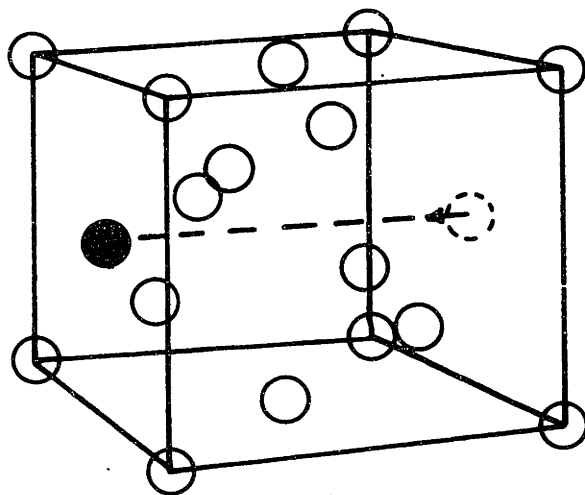
Figure 48. Probable Vacancy Donor Complex Configuration in the Germanium Structure

by its double negative character. Thus, the third-nearest
neighbor position is apparently ideal for the accommodation
of these effects. The interaction energy, ΔH, would,
thus, be -.46 eV and the pair separation, 3.8 $\overset{o}{A}$.

The capture radius, r_c, or maximum interaction
distance for the pair is taken as the ion separation
distance at which $\Delta H = 2kT$, as discussed in Appendix
F. For the interaction of a double negatively charged
center with a single positively charged center in germanium,
this radius is

$$r_c = 70 \text{ angstroms.}$$

This value is rather small in view of the low densities
of "ions" in the material. It must be, therefore, suggested
that vacancies possess an intrinsically high mobility
of an equilibrium state is to be achieved. This idea
is in accordance with the recent findings[24] discussed
earlier.

If the carrier removal is assumed to be entirely
due to stabilization of vacancies, then

$$\Delta n = 2 \cdot [N_D]$$

as each pair removes two electrons. This leads to the
expression

$$V_R = \frac{K_1 \Delta \phi}{2}$$

using $\quad K_1 = 2 \times 10^{12} cm^{-3}/Mrad,$

$$V_R = 1 \times 10^{12} \text{ vacancies/cm}^3/\text{Mrad}$$

$$= 1.15 \times 10^{-3} \text{ vacancies/cm}^3/\text{gamma photon}$$

Cleland, et al[5] have made calculations of the expected defect introduction rate based on the atomic displacement cross sections for various gamma ray energies in germanium. They derived that the total defect introduction rate, R_T, for cobalt 60 gamma rays corresponds to

$$R_T = 2.3 \times 10^{-3} \text{ defects/cm}^3/\text{photon}$$

This is in excellent agreement with the present data. In the present discussion, V_R represents the net number of vacancies which escape correlated annihilation. Thus, the difference between V_R and R_T can be interpreted to mean that

$$\frac{R_T - V_R}{R_T} = \text{fraction of defects undergoing correlated recovery}$$

$$= .50$$

This value can be contrasted to Waite's analysis[84] which predicted 70 percent correlated recovery in the absence of long range forces. This comparison suggests that Coulombic forces play a minor role in retarding correlated recovery as might be expected from the small value of r_c.

It is interesting that Cleland, et al[5] also observed that the values of R_T tended to approach the experimental values for the carrier removal rate as the

gamma photon energy increased. This behavior can be explained
within the present model. As the gamma ray energy is
increased, the average separation between the vacancy
and interstitial components of a pair would tend to
increase. Thus, the probability of correlated annihilation
is decreased and V_R represents a higher fraction of the
total damage.

The close fit of these calculations with the experi-
mental data provides a strong body of evidence that the
interactions of point defects in germanium are governed
almost entirely by equilibrium considerations!. This
conclusion suggests that the interacting species must be
mobile in order to achieve the equilibrium state!

The ability of this ion pairing model to answer
the many questions that have typified the study of radiation
defects is indeed striking. These results also serve
to reinforce the basic assumption of this work, that
materials must be accurately characterized, initially,
if radiation effects are to be understood.

C. Implications of the Model

This discussion has shown that the behavior of radiation
defects in germanium can be described in terms of the
tendency of the irradiated system to approach an equilibrium
state. It was observed that appooximately 50 percent
of the radiation produced defects undergo correlated

This is the most complete text of the
thesis available. The following page(s)
were not included in the copy of the
thesis deposited in the Institute Archives
by the author:

Pg. 147

recovery. Of the remaining defect concentration, the interstitials are probably annihilated at vacancy clusters within the material and the vacancies associate with positive charges in the material according to the chemical equilibrium of the process.

The vacancy and impurity most probably associate in a configuration of third-nearest neighbors at a distance of 3.8 angstroms. A high vacancy mobility must be postulated in order to justify this behavior.

The suggestion of vacancy mobility at room temperature and below is found with increasing frequency in recent studies of point defects in germanium and silicon. It appears that, soon, the quantity of new evidence of vacancy mobility will equal that of the early work from quenching and self-diffusion studies establishing the vacancy immobility. This question will certainly be the subject of much research in the future. It is suggested here that a key might be found by a correlation of the increasing size of the vacancy as it accepts a double negative charge with its mobility.

The model further suggests that impure materials remain more stable defects than do high purity materials. Accordingly, compensation by radiation defects would be more readily achieved in n-type counter-doped materials, which have both high resistivity and high donor concentrations, than in more pure high resistivity material containing only a low concentration of donors. Such a study appears to be a logical continuation of the

ideas presented here.

VII. SUMMARY AND CONCLUSIONS

The electronic behavior of radiation defects in
high purity germanium was studied in order to evaluate
the role of irradiation in the mechanism of carrier
compensation. In particular, the role of impurities
as defect stabilizing agents was suggested. It was
assumed from the start that accurate characterization
of the initial materials used would be necessary in
order to understand the subsequent defect behavior.

A technique was developed for the growth of highly
perfect, high purity germanium single crystals by the
Czochralski method. Antimony doped n-type crystals were
grown with impurity concentrations as low as 6×10^{12}
per cubic centimeters. Undoped p-type crystals were
prepared with concentrations as low as 2×10^{11} per cubic
centimeter. The dislocation densities in these crystals
were kept below the level of 1000 per square centimeter by
"necking down" the seed diameter to about one millimeter
before growth (Dash method). Most crystals exhibited
the well known tendency to contain a highest impurity
content in the center of their cross section. Dislocation
densities were frequently observed to increase at the
outer edge of the crystal cross section. The factors
contributing to such inhomogeneities were discussed.

It was determined the cobalt 60 gamma irradiation introduce compensation levels predominately at E_c - 0.20eV and E_v + 0.26 eV (and possibly a shallow level near the valence band edge) in n-type material. The E_v + 0.26 eV state was found to possess a double negative charge and is possibly related to a vacancy. In general, states below the middle of the band gap were observed to become more stable as the concentration of donors in the material increased.

The net electron compensation rate, in n-type material exhibited a strong dependence on the initial donor concentration in the range of 10^{12} - 10^{15} donors per cubic centimeter. Samples containing a large initial defect concentration appeared to have a reduced sensitivity to radiation effects. A model was developed to explain this behavior based on the stabilization of vacancies by association with donor impurities in the lattice. Interpretation of the experimental results on the basis of this model indicates that 50 percent of the vacancies introduced by radiation undergo correlated annhilation. The remaining vacancies associate with donor impurities in the lattice according to the constraints of chemical equilibrium. The experimental data suggests that the vacancies have double charge and are positioned as the third-nearest neighbor of the substitutional donor at a distance of 3.8 angstroms. The binding energy of this

complex was found to be 0.46 eV. Vacancy mobility at room temperature must be assumed in order to justify this model.

The idea of defect-impurity complex formation tends to explain previous observations concerning the net defect introduction rate as well as the present results. It is surprising that the results can be interpreted in terms of chemical equilibrium in view of the popular conceptions of the immobility of vacancies and substitutional impurities in the germanium lattice. As a result, the conclusion must be drawn, in accordance with recent findings in oter laboratories (discussed in section II A), that the vacancy is mobile at room temperature.

P-I-N radiation detection devices were constructed as an application of the radiation compensation process. The compensation of the material was effective and stable at room temperature. The role of materials parameters in device construction and performance was discussed, but no major obstacle to the eventual use of those devices as high resolution spectrometers was found.

VIII. SUGGESTIONS FOR FURTHER WORK

Further experimental work is necessary in order to definitely confirm the model for defect stabilization presented here. Some implications of the model that should be investigated are:

(a) The carrier compensation rate should increase with increasing donor concentration. This effect should be studied in counter-doped materials and samples doped with neutral impurities such as tin and silicon.

(b) The vacancy is assumed to be mobile at room temperature. The effect of charge state on the pairing behavior of the vacancy could be studied in counter-doped materials by varying the Fermi level with the donor concentration constant.

In general, further work is suggested to provide a definitive correlation between the defect states in the band gap and the defect configurations in the lattice.

The performance of the radiation compensated detectors is promising. It is recommended that the results of this work be applied to future studies. These include (a) counter-doping to increase the effeciency of the radiation compensation process, (b) investigation of the effects of dislocations of device performance, (c) study of factors contributing to cross sectional inhomogeneities in crystal growth.

IX. APPENDICES

A. Hall Effect Measurement and Analysis

Hall effect measurements were made to determine the energy positions and concentrations of radiation defects in germanium.

1. Hall effect measurement

Excellent discussions of the techniques involved in the measurement of the Hall effect are given by Lindberg[85] and Putley[86]. The important aspects of the measurement are summarized here.

The Hall effect occurs when a material carrying a current is subjected to a magnetic field perpendicular to the direction of current flow. (Figure 49). A Lorentz force acts on the moving carriers deflecting them according to their charge and velocity. An electronic field is established within the materials as a result of this nonuniform charge distribution. The Hall coefficient is expressed in terms of this voltage according to

$$R_H = \frac{V_H\, t}{BI} = \frac{\text{volts} \cdot \text{centimeter}}{\text{gauss} \cdot \text{ampere}} \times 10^{8} = \frac{cm^3}{\text{Coul.}} \quad (1)$$
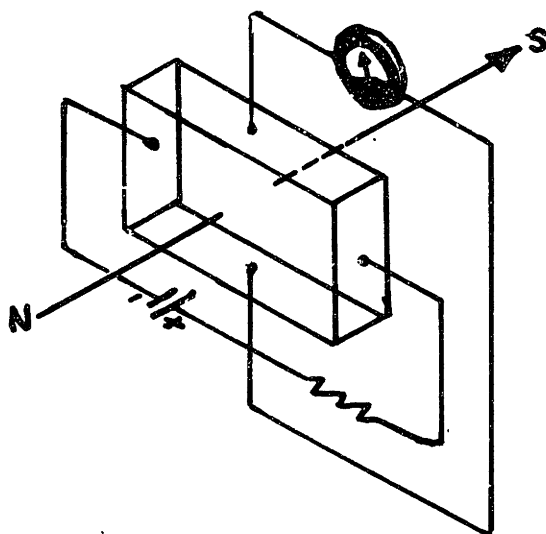
Figure 49. The Hall Effect

where V_H is the Hall voltage, t is the sample thickness, B is the magnetic field, and I is the sample current.

When electrons are present as the majority carrier, the Hall coefficient is related to the electron concentration by

$$R_H = \frac{1}{ne} = \frac{6.25 \times 10^{18}}{n(cm^{-3})} = \frac{cm^3}{Coul.} \qquad (2)$$

where n is the elctron concentration and e is the charge on an electron.

The conductivity is given by

$$\sigma = ne \, \mu_e \qquad (3)$$

where μ_e is the electron mobility. Thus, the mobility may be determined from Hall and conductivity measurements according to

$$\mu_e = R_H \sigma \qquad (4)$$

In practice, four measurements are necessary to determine the value of the Hall coefficient accurately. They involve reversal of the sample current and applied magnetic filed directions.

Since it is difficult to align the Hall voltage probes in equipotential positions, a finite "IR" voltage drop is added to the measured voltage. Reversal of the magnetic field reverses the sign of the Hall voltage while the "IR" drop stays fixed. Thus, the true Hall

voltage is given by

$$V_H = \frac{(V_H + V_{IR})_B - (-V_H + V_{IR})_{-B}}{2} \qquad (5)$$

If there is a temperature gradient along the sample, the Hall voltage will be modified by transverse voltages resulting from the Nerst, Righi-Leduc, and Ettingshausen effects*. The Nerst and Righi-Leduc effects depend only on the temperature gradients and the direction of the magnetic field. Reversing the sample current will reverse the Hall voltage while these thermoelectric voltages remain fixed. The Ettingshausen voltage is dependent on both the current and the magnetic field directions, as is the Hall voltage. It, therefore, cannot be isolated. The net measured Hall voltage, in this case, is given by

$$V_H + V_E = \frac{(V_H + V_E + V_N + V_R)_I - (-V_H - V_E + V_N + V_R)_{-I}}{2} \qquad (6)$$

However, the Ettingshausen voltage is usually negligible compared to the Hall voltage. It is evident, though, that the desired practice would be to minimize all temperature gradients by controlling the sample temperature isothermally.

The absolute accuracy, is, then, dependent on only the homogeneity of the material and the accuracy of the measurement of the sample dimensions.

The final consideration is sample preparation.
Sample dimensions should correspond to about the ratio
10:2:1 for length: width: thickness so that current flow
is free of end effects in the region of the Hall contacts.
In this way, the current electrodes will not tend to
short out the Hall field.

Ohmic contacts must be used to transmit the current
through the sample since the relations given in the
equations (1) and (2) are based on the validity of ohms
law. Rectification, of course, is a form of non-ohmic
behavior. Rectifying contacts may also introduce errors
through local Peltier heating, stray potentials, and
stray conduction paths.

The voltage probe contacts need not be ohmic if
measurements are made with a potentiometer or high im-
pedance electrometer. In this case, no current flows
in the measuring circuit so that the Hall voltage drop
across the sample is detected.

The limit of accuracy in Hall effect measurement
is estimated to be about ± 3 percent.

2. <u>Derivation of energy positions from Hall effect analysis</u>

The determination of defect energy positions from
log Hall coefficient vs. inverse temperature curves is
not straight forward in a system involving complex defect
structures and multiple energy levels. The simple
exponential dependence found in single level systems

(e.g. one impurity in a semiconductor) must be modified because the total carrier concentration, reflected by the Hall coefficient, represents not just the occupation of one level, but a summation of the contributions form many levels.

In this work, two methods of analysis have been developed. One is based on the slope of the log Hall coefficient vs. inverse temperature curve, and the other is derived from the position of the Fermi level when the defect level is apparently one-half full. The first method is presumed to be accurate. The second was used mainly as a check on the results. These methods of analysis were derived mainly from a consideration of discussions given by Shockley and Last[82] and Ketovskii, Mashovets, and Ryvkin[87]:

Analysis Using the Slope of log R_H vs. $1/T$

Figure 50 represents an imaginary n-type system of k defect energy levels. (The analysis of a p-type system is identical). The uppermost level is occupied by N electrons/cm^3 at $0°K$. N_1, N_2, ...N_{12} represent the concentrations of each level. An expression for the number of electrons in the conduction band, n, may be written as a summation of the electrons excited from each level.
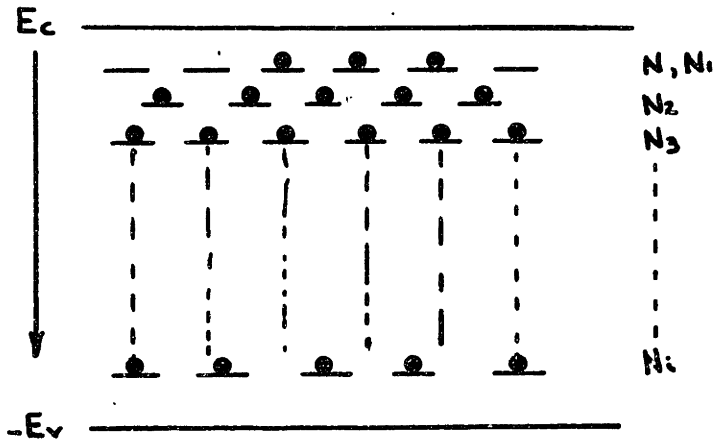
Figure 50. The Occupation of N_i Levels at $0^\circ K$.

electrons in CB $|_{T°K}$ = electrons in level 1 $|_{0°K}$

— electrons in level 1 $|_{T°K}$

$+ \sum_i$ electrons excited from level $i |_{T°K}$

$$n = N - \frac{N_1}{1 + g_1 \exp\left[\frac{E_1 - E_F}{kT}\right]} + \sum_{i=2}^{k} \frac{N_i}{1 + \frac{1}{g_i}\exp\left[\frac{E_F - E_i}{kT}\right]} \qquad (1)$$

where Fermi-Dirac statistics are employed with g_i the

degeneracy factor and E_i the energy position of the ith

level. E_F is the Fermi energy, k is Boltzman's

constant, and T is the absolute temperature. It should be

noted that N is not usually equal to N_1 because of the

normal presence of compensating acceptor levels.

The value of n is also given by

$$n \simeq N_c \exp\frac{E_F}{kT} \qquad (2)$$

where $N_c = 2(2\pi m_n^* k h^{-2})^{3/2} T^{3/2} =$ the density of states in the

conduction band. Thus, equation (1) may be written

$$n = N - \frac{N_1}{1 + \frac{g_1 N_c \exp[E_1/kT]}{n}} + \sum_{i=2}^{k} \frac{N_i}{1 + \frac{1}{g_i}\frac{n}{N_c \exp[E_i/kT]}} \qquad (3)$$

Further simplifying, let

$$F_i = g_i N_c \exp\left[E_i/kT\right]. \qquad (4)$$

Thus,

$$n = N - \frac{N_1}{1 + \frac{F_1}{n}} + \sum_{i=2}^{k} \frac{N_i}{1 + \frac{n}{F_i}} \qquad (5)$$

The following assumptions are applicable to this

system:

(a) $|E_{i+1} - E_i| \gg kT$, so that each level empties and fills separately.

(b) The defects which introduce these states are present in a relatively low density. Therefore, interactions at the same level, such as impurity banding, can be neglected.

(c) Electrons are excited only to the conduction band, not to higher levels. (Reasonable at equilibrium).

By employing assumption (a), the excitation from each level may be considered separately.

Occupation by N_1

By assumption (a), it is assumed that, in this temperature range, all states but those at level 1 are frozen and do not contribute to n. Equation (5) simplifies to

$$n = N - \frac{N_1}{1 + \frac{F_1}{n}} \quad . \tag{6}$$

For the early stages of ionization when $n \to 0$, equation (6) reduces to

$$n = \frac{F_1 N}{N_1 - N} = \text{const.} \; T^{3/2} \exp\left[E_1 / kT \right] . \tag{7}$$

E_1 is, thus, given by

$$E_1 = k \; \frac{d \ln(n)}{d \, 1/T} \; + \; \tfrac{3}{2} kT \qquad \Big|_{T_1 \, \pm \, 2kT}$$

$$= -k \; \frac{d \ln R_H}{d \, 1/T} \; + \; \tfrac{3}{2} kT \qquad \Big|_{T_1 \, \pm \, 2kT} \tag{8}$$

Occupation of N_i

By assumption (a), in the temperature range $T_i \pm 2kT$, all states above level i are empty and all states below are filled. Therefore, equation (5) reduces to

$$n = N + \sum_{j=2}^{i-1} N_j + \frac{N_i}{1 + \frac{n}{F_i}} \quad . \tag{9}$$

Solving for n,

$$n^2 + n\left[F_i - \left(N + \sum_{j=2}^{i-1} N_j\right)\right] - F_i\left[\left(N + \sum_{j=2}^{i-1} N_j\right) + N_i\right] . \tag{10}$$

By the quadratic formula,

$$n = \frac{\left[\left(N + \sum_{j=2}^{i-1} N_j\right) - F_i\right]}{2} \pm \frac{1}{2}\left\{\left[F_i - \left(N + \sum_{j=2}^{i-1} N_j\right)\right]^2 \right.$$
$$\left. + 4 F_i\left[\left(N + \sum_{j=2}^{i-1} N_j\right) + N_i\right]\right\}^{\frac{1}{2}} \tag{11}$$

Equation (11) is greatly simplified at the point

$$\left(N + \sum_{j=2}^{i-1} N_j\right) = F_i \tag{12}$$

which defines T_i . Here,

$$n = \left\{F_i\left[\left(N + \sum_{j=2}^{i-1} N_j\right) + N_i\right]\right\}^{\frac{1}{2}}$$
$$= \left\{\left(N + \sum_{j=2}^{i-1} N_j\right)\left[\left(N + \sum_{j=2}^{i-1} N_j\right) + N_i\right]\right\}^{\frac{1}{2}} \tag{13}$$

The change in n with $1/T$ in the region of T_i is derived from equation (11).

$$\left.\frac{d \ln(n)}{d \, 1/T}\right|_{T_i} = \left.\frac{dn/n}{d \, 1/T}\right|_{T_i}$$
$$= -\frac{1}{2}\left\{\frac{1}{n}\frac{d F_i}{d \, 1/T}\right\} \pm \left\{\frac{1}{n}\left[\left(N + \sum_{j=2}^{i-1} N_j\right) + N_i\right]^{\frac{1}{2}}\frac{d F_i^{\frac{1}{2}}}{d \, 1/T}\right\}$$
$$= -\frac{1}{2}\left\{\left[\frac{E_i}{k} - \frac{3}{2}T_i\right]\frac{F_i}{n}\right\} \pm$$
$$\left\{\left[\frac{E_i}{2k} - \frac{3}{4}T_i\right]\left[\frac{1}{n}\right]\left[F_i\right]^{\frac{1}{2}}\left[\left(N + \sum_{j=2}^{i-1} N_j\right) + N_i\right]^{\frac{1}{2}}\right\}$$

$$\frac{d \ln (n)}{d\, 1/T}\bigg|_{T_i} = -\frac{1}{2}\left(\frac{E_i}{k} - \frac{3}{2}T_i\right)\left[1 - \frac{N + \sum_{j=2}^{i-1} N_j}{\left\{(N + \sum_{j=2}^{i-1} N_j)\left[(N + \sum_{j=2}^{i-1} N_j) + N_i\right]\right\}^{1/2}}\right] \quad (14)$$

The energy position of level i is, thus, given by

$$E_i = 2k\,\frac{d \ln R_H}{d\, 1/T}\bigg|_{T_i}\left[1 - \frac{N + \sum_{j=2}^{i-1} N_j}{\left\{(N + \sum_{j=2}^{i-1} N_j)\left[(N + \sum_{j=2}^{i-1} N_j) + N_i\right]\right\}^{1/2}}\right] + \frac{3}{2}kT_i \quad (15)$$

When level i contains a relatively high concentration
of states so that $N_i \gg N + \sum_{j=2}^{i-1} N_j$, equation (15)
reduces to

$$E_i = 2k\,\frac{d \ln R_H}{d\, 1/T}\bigg|_{T_i} + \frac{3}{2}kT_i \quad . \qquad (16)$$

While equation (15) may appear cumbersome, values
of E_i can be calculated fairly easily and accurately from
it. A second method was used as a general check on
values obtained from equation (15). This analysis is
based on equation (2).

Analysis by the Position of the Fermi Level

It is known that when the Fermi level is coincident
with a defect level, the probability of occupation of
states at that level is one-half. The temperature and
electron concentration where level i appears to be one-
half filled can be obtained from the $\ln R_H$ vs. $1/T$ curve.
By fitting these values into equation (2) the value of
E_F can be determined.

$$E_F = \varepsilon_i = kT \ln \left[\frac{N + \sum_{j=1}^{i-1} N_j + N_i/2}{N_c} \right], \qquad (17)$$

where

$$N_{c_{Ge}} = 2 \times 10^{15} \ T^{3/2} \ cm^{-3},$$

and

$$N_{\sigma_{Ge}} = 1.05 \times 10^{15} \ T^{3/2} \ cm^{-3}.$$

This method, while being the simplest, is probably not the most accurate because of the critical dependence on the choice of N_i.

---

*   In the Nerst effect a potential gradient appears in the y-direction if a thermal current flows in the x-direction and a magnetic field is applied in the z-direction.

The Righi-Leduc effect produces a temperature gradient in the y-direction when a thermal current flows in the x-direction, and a magnetic field is applied in the z-direction.

In the Ettingshausen effect, a permanently maintained temperature gradient will appear if an electron current is subjected to a magnetic field perpendicular to its direction of current flow.

B. Lifetime Measurement and Analysis

1. Measurement Techniques

The measurement of minority carrier lifetime character-
izes the return of the semiconductor system to equilibrium
from a slightly perturbed condition. In this work, the
perturbation was effected by the injection of excess holes
and electrons by a short pulse of light. The disappearance
(recombination) of these carriers was monitored by the
change in the elctrical conductivity of the sample.

An excellent discussion of the measurement of life-
time by photoconductive decay was published in the I.R.E.
Proceddings in 1961[88]. Various techniques and analyses
have been discussed by Haynes and Shockley[89], Navon,
et al[90], Many[91], Mc Kelvey and Longini[92], Haynes
and Hornbeck[93], Smith[94], and Blackmore and Nomura[95].

The most important consideration in a bulk lifetime
measurement is the avoidance of surface effects. Since
recombination cenetrs exist on the surface in high concen-
trations (surface states), the measured lifetime can be
misleading. As a result, steps must be taken to assure
that most of the recombination takes place in the bulk
of the material.

The first step is to minimize the surface area. This
is satisfactorily accomplished by prolonged etching in a
chemical polishing solution such as CP4. Displacement
quenching at the termination of etching will give the

thinnest oxide layer on the surface.

It is not desireable to employ radiation that is strongly absorbrd by the semiconductor. In that case, most of the excitation, and therefore recombination, would occur in the surface region. The energies which are highly absorbed correspond to those above the value of the energy gap (which readily create electron-hole pairs). Penetrating radiation was obtained in the present experiments by placing a thin piece of germanium between the light source and the sample. Qualitatively, radiation that is not absorbed by a one millimeter germanium filter should not be absorbed within one millimeter of the surface of the sample. The energies transmitted are less than or equal to E_G. Since E_G varies with temperature, it is necessary that the filter be at the sample temperature in order to insure energies high enough for excitation. Because only a very narrow range of energies (those exactly at E_G) take part in excitation, a low injection level can be maintained. This situation considerably simplifies analysis as is discussed later.

The sample size should be large so that carriers excited in the bulk will recombine before they can diffuse to the surface. This effect can be further ehhanced by masking the sample edges from the light so that excitation occurs more than a diffusion length away from the surface. This also minimizes any possible photovoltaic effects at

the contacts.

It is necessary that the contacts to the samples be ohmic. Otherwise, injection at the contact will provide an uncertain source of minority carriers which would invalidate the measurement.

The electronic field in the sample should be small so that minority carriers are not swept out of the sample before they recombine. The effects of sweep-out can, however, be calculated and subtracted from the decay curve in a similar fashion to Navon, et al[90].

The decay constant of the photoconductive signal can be determined by plotting the signal curve on the semi-log paper (ln V vs t). The top of the curve does not usually conform to an exponential decay. This behavior is assumed to be the result of the faster modes of surface recombination. As a result, only the lower one-fifth of the decay is measured (assuming that faster modes affect very few carriers and have died out).

If minority carriers are captured by temporary traps, the lower part of the decay possesses a long tail. This process corresponds to the relatively slow emptying of traps which delays the recombination process. If this tail has a magnitude larger than about 5 percent of the excitation signal, the decay curve cannot be fitted to an exponential. However, if the emptying of the traps is linear, the final tail is exponential. This "trapping

time" is related to the character of the temporary traps and is discussed in detail later.

This discussion has mentioned briefly the important experimental considerations in making lifetime measurements. For a detailed examination of the subject, the references noted earlier are recommended.

2. Principles of Analysis

The limiting consideration in a recombination process is the evolution of energy. The difference in energy between an electron and a hole is equal to the height of the energy gap. Upon their recombination, this amount of energy must be liberated. In an indirect gap material, such as germanium, a change in momentum as well as energy is required.

Shockley and Read[96] proposed a model for this process based on recombination through localized states in the energy gap. The statistics developed in this model have proved to be an accurate description of the recombination phenomenon when a single local level is responsible. In the case of irradiated materials, however, there are indications that more than one recombination level may be active and that temporary trapping states also exist which limit the recombination process. With a number of unknown processes available, it is difficult to develop a single structure of statistics that will accurately describe the situation. Most attempts[89-93] in this area

have been extensions of the original Shockley-Read theory.

In the author's opinion, the value of a lifetime measurement becomes severly limited when the number of assumptions made in analysis is greater than the number of known variables in the system. The concept of lifetime is necessary, however, for a complete description of the electronic behavior of a semiconductor. In this work lifetime-temperature profiles are measured in an effort to supplement Hall effect data in the characterization of the material.

A semi-qualitative consideration of the recombination process is developed here which is used in the analysis of the lifetime data. This approach is intended more to set bounds for interpretation than to provide rigorous representations of the process.

Recombination through local centers

Two steps are considered to be involved in the recombination process: capture and recombination.

The capture process is described by a capture coefficient, c. The rate of capture, R_i, of a carrier, i, is proportional to the density of that carrier and the number of free capture centers. Thus, the capture process can be simply represented by

$$R_i = c_i \, n_i \, t_j \tag{1}$$

where n_i is the concentration of carrier i, and t_j is the net number of capture centers which are empty. Since, in

this work, we deal mainly with n-type material, further development will be in terms of electrons as the majority carrier and holes as the minority carrier. Thus, the rate of capture for holes is given by

$$R_p = c_p \, p \, t_n \tag{2}$$

where p is the concentration of holes and t_n is the concentration of centers which are filled with electrons (do not already contain holes).

The recombination process is described by statistics which relate the capture probability and the energy position of the center to the rate of recombination. Since the system is one of electrons and holes, Fermi-Dirac statistics have been invoked to describe it. It is assumed that the carriers in each band are always in thermal equilibrium among themselves, even though the two bands may not be in equilibrium. The basic limitation to the recombination rate is derived from the availability of carriers to enter the centers.

Provided that the equilibrium electron concentration, n, is much greater than the recombination center concentration, it may be assumed that hole capture does not effect the population of the center. Thus, if T_c is the total number of centers, the number of centers occupied by electrons is given by

$$t_n = \frac{T_c}{1+\exp \dfrac{E_T-E_F}{kT}}$$

$$\doteq T_c \exp-\left[\frac{E_T-E_F}{kT}\right] \qquad \text{for } \left|\frac{E_T-E_F}{kT}\right| \ll 1 \qquad (3)$$

where E_T is the energy between the level of the center and the conduction band, and E_F is the Fermi level relative to the conduction band.

The thermal emission of captured holes can compete with the recombination process. These transitions are thermally activated by microscopic fluctuations of the solid. The rate of hole emission to the valence band may be expressed in terms of the number of centers containing holes and an emission coefficient, e_p, which represents a rate of emission per hole, or the inverse of the time that the hole would be in the center if recombination did not take place.

Thermal equilibrium may be invoked here to determine the value of e_p because it is an intrinsic property of the center only. In this case, the capture rate and emission rate of the center are equal.

$$e_p(T_c-t_n) = c_p \, p \, t_n \qquad (4)$$

$$t_n = \frac{T_c}{1+ \dfrac{e_p \, p}{e_p}} \qquad (5)$$

Comparing with equation (3),

$$e_p = c_p P \exp - \left[\frac{E_T - E_F}{kT} \right] . \tag{6}$$

At equilibrium,

$$p = N_v \exp \left[\frac{E_v - E_F}{kT} \right] , \tag{7}$$

where N_v is the density of states in the valence band and E_v is the energy position of the valence band relative to the conduction band.

Thus,

$$e_p = c_p N_v \exp \left[\frac{E_v - E_T}{kT} \right] . \tag{8}$$

Application

The application of these principles to the present work is now treated through a series of general examples shown in Figures 51-53. Consideration is given, mainly, to hole-limited kinetics. The case for electrons can be formulated by reversing the roles of holes and electrons. The limits of this approach will be discussed at the end.

Lifetime is the average amount of time that a non-equilibrium carrier can exist before recombination and corresponds to the inverse of the recombination rate for a single carrier.

The lifetime expression developed by Shockley and Read[96] for recombination through a single localized center is given below for reference.

$$\gamma = \frac{1}{c_p T_c} \frac{n_0 + N_c \exp\left[\frac{E_T}{kT}\right] + \Delta n}{n_0 + p_0 + \Delta n} + \frac{1}{c_n T_c} \frac{p_0 + N_v \exp\left[\frac{E_v - E_T}{kT}\right] + \Delta p}{n_0 + p_0 + \Delta n} \qquad (9)$$

where n_0 and p_0 are the equilibrium concentrations of holes and electrons, and $\Delta n = \Delta p$ is the deviation from equilibrium.

For the experiments done in this work, the injection level (Δn) was always very low in comparison with at least one term in each of the sums. Thus, for the present use, the equation may be written as

$$\gamma = \frac{1}{c_p T_c} \frac{n_0 + N_c \exp\left[\frac{E_T}{kT}\right]}{n_0 + p_0} + \frac{1}{c_n T_c} \frac{p_0 + N_v \exp\left[\frac{E_v - E_T}{kT}\right]}{n_0 + p_0} \qquad (10)$$
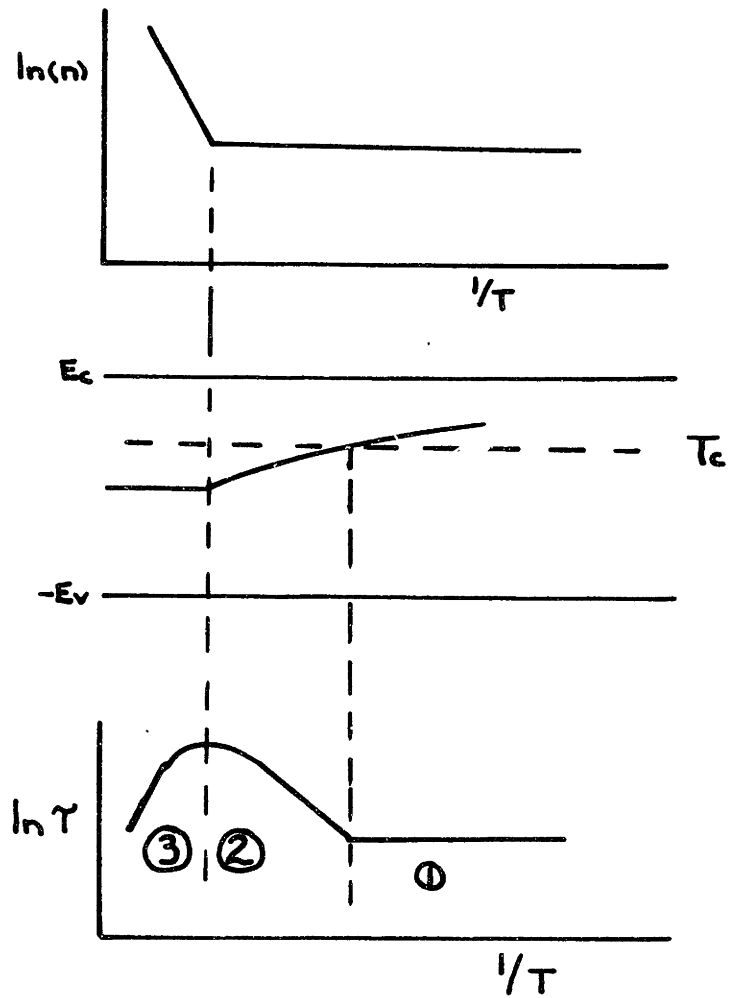
Figure 51. Lifetime Analysis
            Case I
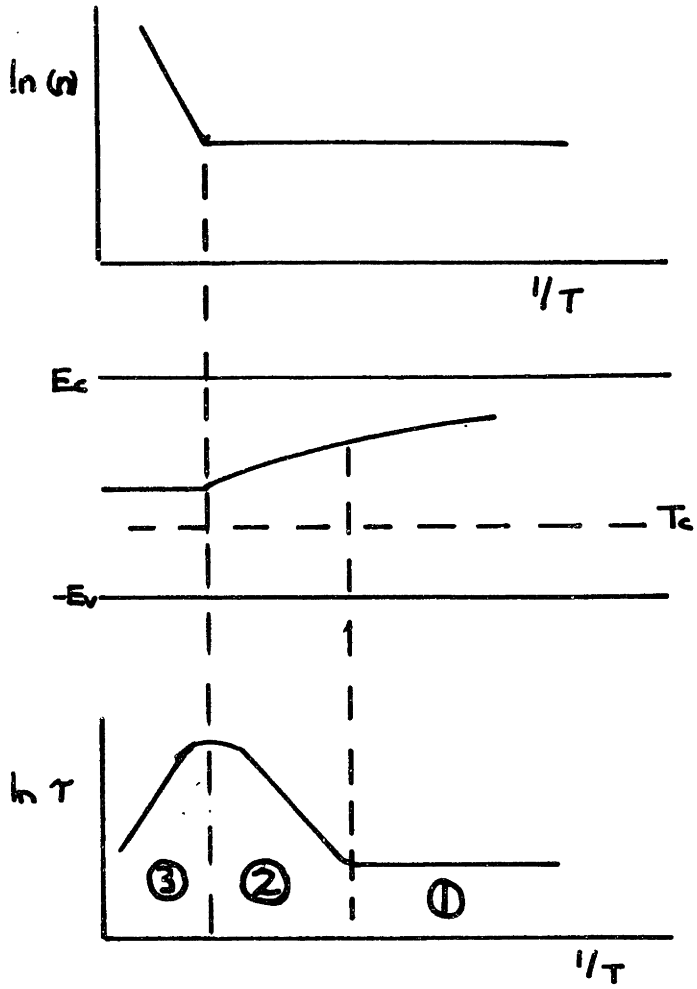
Figure 52.   Lifetime Analysis
             Case II
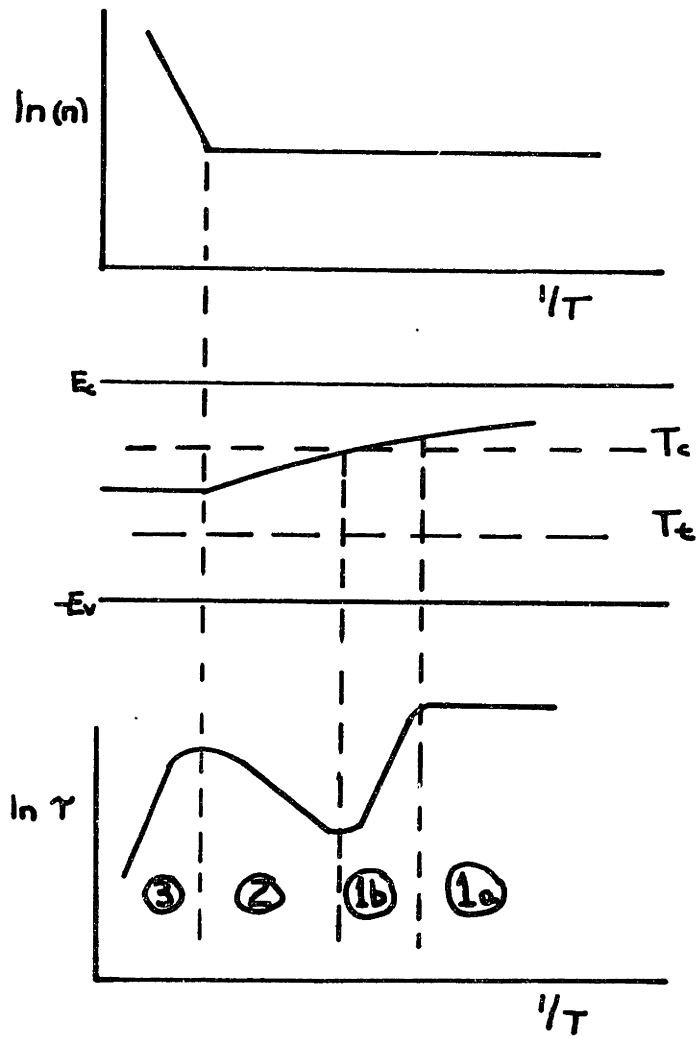
Figure 53. Lifetime Analysis
Case III

If one considers region 1 of cases I and II, it is
noted that the Fermi level lies more than a few kT closer
to the conduction band than the center. From equation
(3), practically all of the centers are filled with electrons.
If a hole is captured, recombination takes place immediately.
This is because of the relatively high concentration of
electrons in the conduction band, the near unity prob-
ability of the filling of these states by electrons, and
the relatively slow rate of hole emission at this low
temperature. Therefore, the rate of recombination is
identical with the rate of hole capture, and the life-
time is given by

$$\tau_1 = \frac{1}{c_p T_c} \quad .$$

(11)

This result can also be derived from equation (10) by
noting that $n_o \gg p_o$, and $\left[\frac{E_T}{kT}\right] \ll -1$, $\left[\frac{E_v - E_T}{kT}\right] \ll -1$
and that c_n is reasonably high.

In region 1 of case III, the behavior is vastly
different. There exists a second center, T_t , which also
has a finite capture cross section, c_p, for holes. However,
the capture cross section of electrons for this center
is extremely small so that after hole capture the next
event is emission to the valence band. This type of center
is known as a temporary trap. After emission, the hole
is captured by the recombination center and immediately
annihilated. Therefore, the lifetime is determined by
the mean time that the hole resides in the temporary

trap. This was derived in equation (8).

In region la, the temperature is so low that electron capture occurs before hole emission. The lifetime, therefore, is expressed by terms of the capture rate of electrons.

$$\tau_{la} = \frac{p}{C_n} = \frac{p}{C_n \, n_o \, T_t} \tag{12}$$

In this case $T_t = p$ because the only holes existing which have not recombined are in the temporary traps. Thus,

$$\tau_{la} = \frac{1}{C_n \, n_o} \tag{13}$$

It is this ultimate capture of the electron that is noted in the photoconductive decay.

In region lb, hole emission becomes important even though it is a slow process at this temperature. Thus, the lifetime is expressed as

$$\tau_{lb} = \frac{1}{e_p} = \frac{1}{C_p \, N_v \, exp\left[\frac{E_v - E_T}{kT}\right]} \tag{14}$$

The slope of the curve in this region gives the energy position of the temporary trap, according to

$$\frac{d \ln \tau}{d \, 1/T} = \frac{3}{2} T - \frac{E_v - E_T}{k T} \tag{15}$$

where $N_v = 2(2 \pi m_p^* k h^{-2})^{3/2} T^{3/2}$.

The effects of temporary trapping have been expressed in a somewhat more quantitative fashion by Wertheim[98], Curtis, et al[14], and Streetman[109], but the final results are exactly the same.

Region 2 of cases I, II, and III appear to be similar,

but they represent different situations. In case III,
the temperature is high enough to make the temporary trap,
T, ineffective. The emission rate of holes from the traps
is very high, so that, effectively, all of the nonequilibrium
holes interact directly with the recombination centers.

In cases I and III, the recombination center is
located in the upper half of the energy gap. Region 2,
in these figures, is the part where the Fermi level is
between the center and midgap. The centers are no longer
completely occupied. The number of electrons in the
conduction band is still very high in comparison with the
number of centers so that the recombination of holes
remains a rapid process(the capture cross section for
electrons for a recombination center is reasonably large by
definition). However, the capture of holes is now limited
by the concentration of centers containing electrons
according to equation (2). By equation (3), this occupation
was shown to vary exponentially with the movement of the
Fermi level. Therefore, the expression for the lifetime
takes the form

$$\tau_2 = \frac{1}{c_p\, t_n} = \frac{1}{c_p\, T_c} \exp\left[\frac{E_T - E_c}{kT}\right] . \qquad \left[\frac{E_T - E_F}{kT}\right] \ll 1 \qquad (16)$$

It is known that

$$n_o = N_c \exp\left[\frac{E_F}{kT}\right] = \text{constant in region 2} \qquad (17a)$$

$$N_c = 2(2\pi m_n^* k\, h^{-2})^{3/2}\, T^{3/2} = \text{density of states} \atop \text{in the conduction band} \qquad (17b)$$

Thus, the lifetime can be expressed as

$$\tau_2 = \frac{1}{c_p \tau_c n_0} \cdot 2(2\pi m_n^* k h^{-2})^{3/2} T^{3/2} \exp\left[\frac{E_T}{kT}\right]$$

$$= \text{constant} \cdot T^{3/2} \exp\left[\frac{E_T}{kT}\right] \tag{18}$$

The energy position of the recombination center can be derived from the slope of the curve in this region according to

$$\frac{d \ln \tau}{d \; 1/T} = -\frac{3}{2} T + \frac{E_T}{k} \; .$$

This relation may also be derived from equation (10) by noting that $N_c \exp E_T/kT$ is greater than n_0 when the Fermi level is below the center.

In region 2 of Figure 52, the recombination center is located in the lower half of the energy gap and the Fermi level is far above in the upper half of the gap. The centers are completely filled with electrons so that the hole capture rate is maximum. Since the centers are in the lower half of the gap, however, the thermal emission of holes to the valence band becomes important as $\exp \frac{E_V - E_T}{kT}$ is finite. The rate limiting process is the net occupation of the recombination centers by holes. This is exactly the reverse of region 2 in cases I and III where the occupation by electrons is limiting. By analogy, the lifetime may be expressed as

$$\tau_2 = \frac{1}{c_n \tau_c n_0} \cdot 2(2\pi m_n^* k h^{-2})^{3/2} T^{3/2} \exp\left[\frac{E_V - E_T}{kT}\right] \tag{20}$$

The energy position of the centers is found according to

$$\frac{d \ln \tau}{d \, 1/T} = -\frac{3}{2} T + \frac{E_v - E_T}{k} \tag{21}$$

This result is obtained from equation (10) when it is considered that $\exp\left[\frac{E_v - E_T}{kT}\right]$ is large compared with $\exp\left[E_F/kT\right]$ and $\exp\left[E_T/kT\right]$.

In region 3, the lifetime decreases in all three cases with the onset of intrinsic conduction. This can be understood along the following lines. The Fermi level is pinned at midgap, a fixed distance from the trap level. The equilibrium concentration of holes, p_o, is now finite and equal to $\bar{n}_o$. This has the effect of doubling the re-combination rate or halving the lifetime. Both n_o and p_o are increasing with the temperature, further decreasing the lifetime. The expression for the lifetime may be written as simply one-half of the lifetime in region 2 subject to intrinsic conditions.

In region 3,

$$n_o = p_o = n_i = \sqrt{N_c N_\sigma} \, \exp\left[\frac{E_G}{2kT}\right] . \tag{22}$$

For cases I and III, from equation (18),

$$\tau_3 = \frac{1}{2} \tau_2 = \frac{1}{2 c_p \tau_c} \sqrt{\frac{N_c}{N_\sigma}} \, \exp\left[\frac{E_T - E_G/2}{kT}\right]$$

$$= \frac{1}{2 c_p \tau_c} \left(\frac{m_n^*}{m_p^*}\right)^{3/4} \exp\left[\frac{E_T - E_G/2}{kT}\right] . \tag{23}$$

The slope of the curve in this region gives the position of the center relative to the middle of the energy gap.

$$\frac{d \ln \Upsilon}{d \, 1/T} = \frac{E_T - E_G/2}{k} \tag{24}$$

For case II, from equation (20),

$$\Upsilon_3 = \pm \, T_2 = \frac{1}{2 c_n T_c} \sqrt{\frac{N_v}{N_c}} \, \exp\left[\frac{E_G/2 - E_T}{kT}\right]$$

$$= \frac{1}{2 c_n T_c} \left(\frac{m_p^*}{m_n^*}\right)^{3/4} \exp\left[\frac{E_G/2 - E_T}{kT}\right]. \tag{25}$$

The position of the center is found by

$$\frac{d \ln \Upsilon}{d \, 1/T} = \frac{E_G/2 - E_T}{k} \tag{26}$$

Again, there is an ambiguity concerning which half of the gap contains the center.

In the preceeding discussion three basic assumptions are made. One, the equilibrium electron concentration, n_o, in the exhaustion range is much greater than the trap concentration. If this were not so, n_o would change with the occupation of the traps. One may extrapolate from the approach that has been developed, that a relatively high density of traps would have the effect of masking the increase of lifetime in region 2. The increase in electron occupation of the traps, t_n, would be balanced by a decrease in n_o, and the lifetime would tend to remain constant.

The second assumption was that of low injection which could not be violated under the experimental conditions.

The third assumption was that the capture coefficient does not vary with temperature. This is the weakest point of the analysis, but should amount to only a minor correction, if any at all. The increase of the average thermal velocity of carriers has a $T^{\frac{1}{2}}$ dependence which corresponds to about 0.01 eV.

A number of general conclusions can be drawn from the preceeding analysis and are listed below.

1. All other things being equal, the closer a center is to a band edge, the higher will be the lifetime. Thus, if two similar centers are present in the same material, the deeper one would be expected to dominate the recombination behavior in region 2.

2. If a number of different centers are present in low concentrations, the recombination rates for each would add to the given total for the system. The effective lifetime is, therefore, given by

$$\frac{1}{\tau} = \sum_i \frac{1}{\tau_i} \tag{27}$$

3. If the number of recombination centers is much higher than the concentration of temporary traps and their capture cross section for holes are similar, recombination would dominate the lifetime behavior. Very little trapping effect would be noted. Thus, a qualitative idea of the relative concentration of traps can be derived from the fraction of the photoconductive decay that is dominated by trapping effects.

4. A number of checks can be employed to test the matching of the system with the required conditions.

(a) The sum of the activation energies derived from regions 2 and 3 of the curve should equal $\frac{1}{2} E_G$.

(b) The maximum in region 2 should correspond to the onset of intrinsic conductivity.

(c) The extrapolated junction between regions 1 and 2 correspond to the temperature T_o, where the Fermi level coincides with the trap level. Thus, the energy position of the recombination center should be given by

$$E_T = kT_o \ln \left[\frac{N_c}{n_o} \right] .$$

(28)

C. Principles of P-I-N Radiation Detector Operation
and Materials Requirements

The operation of the P-I-N detection structure is
directly analogous to the function of a gaseous ionization
chamber. The incident radiation interacts with a detection
medium to produce charged particles (by an ionization
process) which are collected at boundary electrodes
under an applied field. In the germanium detector, the
covalently bonded semiconductor lattice is the detection
medium. Electrons and holes are released during ionization
and constitute the signal through which radiation is detected.
This process is illustrated in Figure 54.

The process by which radiation is absorbed by the
semiconductor lattice leads to a signal which is directly
proportional to the energy of the incident radiation.
One or more secondary electrons are produced by Compton
and photoelectric interactions of the primary radiation
with the bound electrons. An ionization cascade is,
thus, initiated which continues until no electron has
enough energy to produce further impact ionization. This
cascade effect implies that the number of electron-hole
pairs produced depends only and directly on the energy
of the incident radiation (independent of its type). This
linear relationship between signal amplitude and energy
deposited in the detection medium is the basis of the

device function.

In order to collect all of the ionization charge without losses a strong electric field must be maintained within the sensitive volume of the detector. If this sensitive volume is not free of thermally generated carriers, then current flow will be induced by the applied field. These carriers are a source of noise as they interfere with the counting of the ionization charge. For best device performance this leakage current should be in the range of 10^{-10} amperes. Consequently, the sensitive volume of the detector must be highly compensated (fewer than 10^{10} free carriers per cubic centimeter). Reversed biased p-n junctions are employed as electrodes in order to minimize carrier introduction at the contacts.

Surfaces also provide a generation source for carriers. In order to minimize this effect, steps must be taken to provide a compensated surface condition.

The detector resolution is determined by the statistical spread in the quantity of charge collected for an ionization event. This spread results from the variation in the ionization charge and losses during charge collection.

The variation in ionization charge for identical events is a pure statistical effect. The mean square fluctuation is given by $(FN)^{\frac{1}{2}}$ where N is the average number of electron-hole pairs produced and F is the
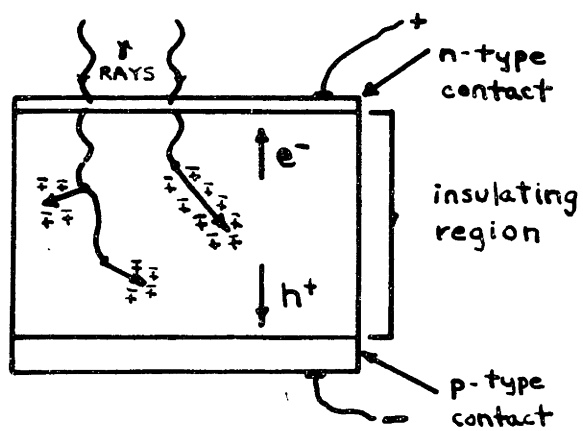
Figure 54.   Typical Germanium Radiation Detector

Fano factor. For germanium F is .3, and the average
ebergy required to produce an electron-hole pair (with
high energy radiation) is 2.9 eV. Thus, this statistical
variation results in a .77 keV broadening for the 662
keV photon of cesium 137.

Carrier losses mainly result from recombination
or temporary trapping processes. Recombination effects
occur only at the ionization site. Along the ionization
track there is a large density of electrons and holes
and a high probability of recombination, provided that
recombination centers exist in this region. Conversely,
when the carrier is traveling to an electrode, there
is a very low density of carriers in the depleted region,
and, consequently, a very low probability of recombination.
The smaller quantity charge collected, as a result of
recombination, gives a false reduced value for the in-
cident energy.

If recombination centers are located homogeneously
throughout the sensitive volume, then there will be
relatively little additional spread in the detection
resolution. In fact, the device can be calibrated
on the basis of this reduced collection efficiency and
will function well as a detector. The more frequently
occuring situation is that these centers are preferr-
entially distributed. Thus, the net ionization product
is dependent on where the event took place. This behavior

results in spreading of the resolution toward lower energies.
Recombination effects are generally associated only
with heavy particle interactions because of the extremely
high electron-hole densities which result.

Trapping effects may occur when a carrier is captured
by a center for a period longer than the collection time
of the device (about one microsecond). These losses
are usually inhomogeneous because the moving carrier
is able to sample a large volume of material, only parts
of which may contain traps. This inhomogeneity results
in a large amount of broadening in the average signal.

The effects of carrier losses on resolution may be
summarized as follows. If charge losses are homogeneous
over the volume of the counter, no loss in resolution
will occur. As the inhomogeneity increases, ther is
an increase in the occurence of signal amplitudes rep-
resenting reduced energy values. There also occurs a
smaller broadening of the spectral peak in the direction
of higher energies. This broadening is associated with
the statistical probability of total collection for
some ionization pulses.

From the above discussion, the following requirements
can be established for an ideal detector material.

1) The average energy to produce an electron-hole pair should be as small as possible. As this energy increases associated thermal losses tend, also, to increase. In addition, a larger ionization charge results in a lower fractional statistical variation in the signal. This requirement implies that a small energy gap is desirable.

2) The material should have few free carriers at the device operating temperature. Germanium devices must be operated at 77^oK because the thermal generation rate is high at room temperature. If the detector is to operate at room temperature, a large energy gap is necessary to lower the thermal generation rate. High purity material is, also, necessary or generation from local states in the gap will contribute to the free carrier density.

3) The density of trapping and recombination centers should be low in order to minimize carrier loss effects. If these centers are present, it is desirable that they be dispersed homogeneously.

4) the carrier collection time should be short compared with carrier lifetimes and trapping capture times. Therefore, high carrier mobilities are desired in a material that can support high electric fields. In this respect, surface breakdown effects must also be able to be controlled.

5) The material must have a high cross section for interaction with incident radiation. This consideration is mainly related to gamma ray detection. A low interaction effeciency will result in low signal to background ratio as well as inaccurate counting. The cross section for photoelectric interaction in a material is proportional to Z^5 where Z is the elemental atomic number. Therefore, a high atomic number is required.

From these considerations germanium is an ideal material with exception of the low temperature required for operation. Indium antimonide would be a further advancement in view of its higher atomic number and lower band gap (0.17 eV). The temperatures of operation, however, would have to be below liquid nitrogen. At the present time, cadmium telluride is the most promising new material. It has both a high energy gap (1.4 eV) and a high average atomic number.

D. Electroless Nickel Plating Procedures

Rectifying junctions were fabricated by nickel plating on germanium for use as p-type contacts on the detector devices studied in this work. The plating procedure is described here.

The plating solution was of the following chemicals in distilled and deionized water:

30 g/l	$NiCl_2 \cdot 6H_2O$
50 g/l	$NaH_2PO_2 \cdot H_2O$
65 g/l	$(NH_4)_2HC_6H_5O_7$
50 g/l	NH_4Cl

The solution was filtered twice after preparation.

For plating, the solution is heated to $90^{\circ}C$ and NH_4OH is added to produce a blue color (pH = 8). The etched sample is then placed in the solution for about 5 minutes. When the temperature of the sample reaches $90^{\circ}C$, nickel will plate on the surface at a rate of .2 - .3 mil/hour.

After plating the sample is rinsed in water. The surface resistance, as measured with a VOM, should be one or two ohms. The junction is then protected and nickel may be removed from other parts of the structure by etching for 1 minute in CP4.

E. The Acceptor Properties of a Vacancy in Germanium

The germanium structure has been characterized as
a covalently bonded, diamond cubic structure. The covalent
bonds are of the sp^3 hybrid character and extend radially
from the center of the atom to the four corners of a
tetrahedron. Similarly, each atom at the corner of the
tetrahedron directs one bond toward the center atom.
Cohesion results from the overlap of these bonds to
form a single, electron pair state.

When an atom is removed from the center of a tet-
rahedron, four "dangling bonds" extend inward from the
corners. Each "dangling bond" represents an unpaired
electron. These electrons can adjust to the new conditions
in three possible ways:

(1) Each electron can associate with an atom
in a corner of the tetrahedron ("defect atom").

(2) All four electrons can orbit equivalently
throughout the tetrahedron.

(3) Quasi-covalent "defect bonds" can be formed
with a corner atom sharing its unpaired electron
with the two nearest defect atoms.

The exact wave function describing the vacancy state
must include a probability for each of the three occurr-
ences.

A great deal of insight into the nature of the

vacancy state can be derived from intuitive reasoning. Since a defect atom has only three of its four valence electrons involved directly in covalent lattice bonds, it is in a more "free" state than is a normal lattice atom. The formation of a solid is based on the premise that atoms in the solid state have a lower potential energy than free atoms. It may, therefore, be inferred that the defect atom must be at a slightly higher potential than the normal bulk atom. Defect bonds, then, whatever their form, should give rise to energy states higher in energy than the top of the valence band.

It is evident that the defect bonds cannot completely recreate the normal overlapping of a double orbital bond. Thus, a vacancy corresponds to a comparatively unsatisfied situation. It is, therefore, conceivable that the vacancy site, eventhough it is neutral, could possess an electron affinity (similar to the octet tendency of the germanium atom).

Coulson and Kearsley[101] have treated this approach with a molecular orbital description. It was assumed that three of the four valence electrons of a defect atom are completely unaffected, being involved in localized covalent bonds with the second nearest neighbors to the vacancy. Four electrons, then, one from each corner defect atom, are confined to the vacancy site. These electrons are subject to the interactions of the

tetrahedral field of the vacancy and a weak field due to the rest of the lattice. An expression for the system wave function of this "defect molecule" was derived from suitable combinations of the four sp^3 orbitals which project inward from the tetrahedron corners.

Two basic models have been developed concerning the energy levels introduced into the band gap by vacancy defects. The first was proposed by James and Lark-Horovitz [7]. They suggested that localized defect energy states result from an upward distortion of the energy bands in the vicinity of a vacancy. It was predicted that two electrons could be captured at a vacancy site before the resulting coulombic repulsion would push the energy position of the defect state out of the band gap. A hydrogenic energy relation was employed to compute that the energy positions of these two electrons would be at 0.05 eV and 0.20 eV above the valence band in germanium.

The second model was proposed by Blount [8]. He formulated a tight binding description of the vacancy using sp^3 orbitals for the electrons. All electron orbitals are orthogenal but the pairs which are directed at each other by nearest neighbors. Symmetric and anti-symmetric combinations of these wave functions, which represent the bonding and antibonding states of the crystal, are expressed. The energy difference between these two states is labeled Δ .

In the vacancy, the defect orbitals are essentially atomic orbitals located at the midpoint of the bonding-antibonding separation at $\Delta/2$. If the reasonable assumption is made that these orbitals have little or no linear overlap with each other, the defect electrons would be expected to revert to the more s-like character of the free germanium atom. This change in character effectively smears the electron distribution over the entire vacancy region. Furthermore, the energy position of these electrons is reduced by an amount, δ, equal to the energy originally incorporated for the $s^2p^2 \rightarrow sp^3$ hybridization of the atomic orbitals. Thus, two electron states are introduced with energy positions at $E_c - \Delta/2 - \delta$ and $E_v + \Delta/2 - \delta$. These positions correspond to a donor and an acceptor level respectively. In germanium, both levels lie in the lower half of the band gap.

Each model is useful in a particular range of application. The Blount model has no provision for double negatively charged vacancies, but the James and Lark-Horovitz model cannot easily account for the existence of positively charged vacancies. The defect energy structure resulting from both models, however, implies that the vacancy should act as an acceptor in n-type and lightly doped p-type materials. (See Figure 55) These models are not exact descriptions of the vacancy state, but they are useful in understanding the general nature of the defect.

Figure 55. Comparison of the James, Lark-Horovitz
and Blount Energy Positions

F. Ion Pairing Theory and Semiconductors

The phenomenon of ion pairing has been invoked to describe the interactions of point defects in semiconductor materials. This application is based on the analogy between ions in a semiconductor dielectric and an aqueus electrolyte. This Appendix will outline the development of ion pairing theory and discuss its application to the germanium lattice.

The original model for ion pairing was developed by Debye and Huckel in 1923[102], formulating the well known Debye length (which characterizes the radius of a cloud of charges around an ion of opposite sign). The theory was given a rigorous statistical treatment by Bjerrum in 1926[103] which was extended by Fuoss in 1935[104] and further modified by Reiss in 1956[105]. The application of this theory will be discussed for a general system in the following paragraphs.

Consider the ion pair $(AB)_r$, where r is the distance between the paired ions. For simplicity, let A be immoble and B be able to move. Furthermore, let A and B have equal valences (if $V_A = 2$ and $V_B = 1$ then a triplet, not a pair configuration will evolve from a configuration two B atoms around one A). A pair is considered to be formed between A' and B' when B' is the nearest ion to A', regardless of the value of r. Thus, calculation

of the concentration of $(AB)_r$ reduces to an expression

of the probability of finding (1) B' as the nearest

neighbor to A', and (2) B' located anywhere on a spherical

shell of radius r, cenetred at A'.

These probabilities can be evaluated by taking into

account the interactions between ions. The difference

in potential energy between A' and B' is, in effect, the

interaction energy between the two. It is expressed by

$$\Delta H = z^2 q^2 / \epsilon r \tag{1}$$

where z = numerical charge of ions, q = electronic charge,

and ϵ = dielectric constant of the medium. Applying

Boltzmann statistics, the average number of B ions around

A, within a sphere of radius b is given by

$$n(r) = N \int_\alpha^b 4\pi r^2 \exp\left[-\Delta H / kT\right] dr \tag{2}$$

where α = distance of closest approach, and N = macro-

scopic density of B ions.

Let $q(r)dr$ be the probability that B' is the nearest

neighbor to A' at a distance r away (or the fraction of

$(AB)_r$). Thus, $q(r)dr$ may be expressed as the product of

two independent probabilities that

(1) The volume $\frac{4}{3}\pi r^3$ enclosed by the shell of radius

r will be devoid of imperfections(ions); this is expressed

as

$$1 - \int_\alpha^r q(x) \, dx \tag{3}$$

i.e., the probability that there will be no other nearest

neighbor to A at a radius less than r.

(2) A B ion will be present in the shell $4\pi r^2 dr$;

this is expressed as

$$4 \pi r^2 \, n(r) \, dr \qquad (4)$$

where $n(r)$ is as expressed in (2).

Thus, $q(r) \, dr$ is expressed as

$$q(r) \, dr = \left(1 - \int_a^r q(x) \, dx\right) \cdot 4 \pi r^2 \, n(r) \, dr \qquad (5)$$

The expression may be simplified by noticing that as r approaches a, $q(r)$ should approach $n(r)$ so that

$$q(r) \, dr = \left(1 - \int_a^a \diagup{q(r)}^{0} \, dr\right) 4 \pi r^2 \, n(r) \, dr \qquad (6)$$

$$\int_a^r q(r) \, d(r) = \int_a^r 4 \pi r^2 \, n(r) \, dr \, .$$

Since the integral will be small as r approaches a, we may approximate $(1 - Int)$ by $exp(-Int)$. Thus, the final expression has the form

$$q(r) = 4 \pi r^2 \, n(r) \, \exp\left[-4 \pi \int_a^r x^2 \, n(x) \, dx\right] \qquad (7)$$

This expression was derived, however, on the basis of a dielectric continuim (aqeous solution), not a discrete lattice. It may be adapted, though, along the general methods of Prener[106] to a lattice model, resulting in

$$\alpha_i = A N z_i \exp\left(\frac{z^2 q^2}{\epsilon r_i kT}\right) \exp\left(-N \sum_{j=1}^{j=i} z_j\right) \qquad (8)$$

where α_i is the fraction of ion pairs with a separation r_i, z_i is the number of B sites available at a distance r_i from A', and A is a normalization constant determined by $\sum_i \alpha_i = 1$.

The change to a discrete system is not a bad approximation, if the semiconductor represents an extremely dilute system (atom fraction less than about 10^{-9}) so that interaction distances are much greater than the lattice constant.

By examining the function $q(r)$, one can obtain the schematic form of the distribution of B around A'. The distribution is shown in Figure 56.

Point u is coincident with the distance of closest approach. Point v occurs approximately when $\Delta H = 2RT$. Point w occurs at about the same distance that the Deybe-Huckel model would predict for free ions, not subject to pairing. Thus, two separate groups may exist: pairs and free ions.

Pairs, therefore, may be considered as a new species. The concentration of this "pairing product" may be considered with a mass action approach.

$$A^+ + B^- \rightleftharpoons (A^+ B^-) + H_{AB} \qquad (9)$$
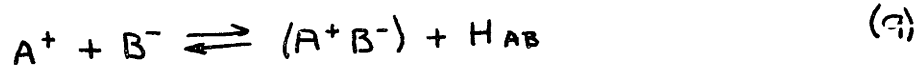
$$\frac{[A^+ B^-]}{[A^+][B^-]} = K = K_o \exp(-\Delta H / RT) .$$
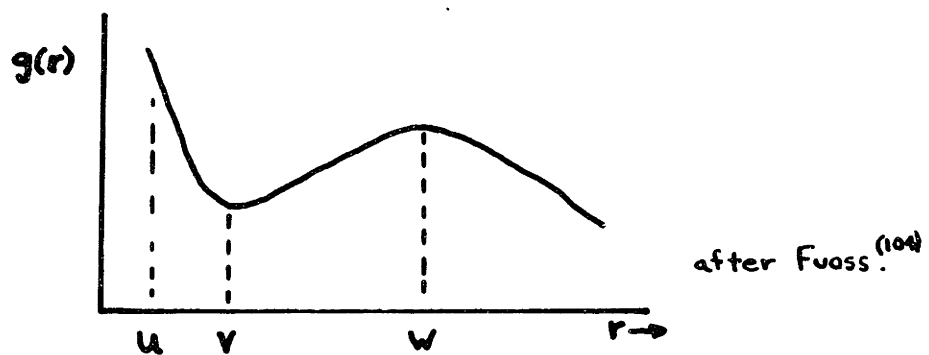
Figure 56.   Ion Pair Distribution Function

The value of K_o may be determined by noting that it is essentially a free energy expression:

$$K = \exp(-\Delta G / kT)$$

$$\Delta G = \Delta H - T\Delta S$$

$$K = \exp(\Delta S / k) \exp(-\Delta H / kT) \tag{10}$$

ΔS, in this case, is predominately a configurational or entropy of mixing term. It results form the necessary ordering of the ions in the pairing process and is expressed by

$$\Delta S = k \ln Z \tag{11}$$

where Z is the number of ways a pair may be formed, or the number of sites that can be occupied by B the smallest distance from A.

Thus,

$$K = \frac{[(A^+ B^-)]}{[A^+][B^-]} = Z \exp(-\Delta H / kT) . \tag{12}$$

If pairs were formed in germanium at the shortest distance, r, then the value of Z would be four which is both the subsitutional and interstitial coordination of a lattice site in the diamond cubic structure. The nearest neighbor distance, which would correspond to r, is 2.44×10^{-8} centimeters. It is possible, however,

that localized lattice distortions may lead to modification of this value for r.

This appendix has briefly developed the theory of ion pairing and its application to the germanium solid state system. It is suggested in the body of this work than an approach such as this may be helpful in understanding the stability of point defects in the germanium lattice.

Note on the use of the law of mass action

Until it was established that pairs and free ions could be treated as separate entities, the law of mass action could not be involved. It can now be assumed that both the associates and ions are distributed at random, $K=K(T)$, and that K is not a function of concentration.

X. BIBLIOGRAPHY

1. F. Seitz and J.S. Koehler, Solid State Physics $\underline{2}$, 305 (1956).

2. W.L. Brown and W.M. Augustyniak, J. Appl. Phys. $\underline{30}$, 1300 (1959).

3. J.J. Loferski and P. Rappaport, J. Appl. Phys. $\underline{30}$, 1296 (1959).

4. O.S. Oen and D.K. Holmes, J. Appl. Phys. $\underline{30}$, 1289 (1959).

5. J.W. Cleland, R.F. Bass, and J.H. Crawford, Jr., Radiation Damage in Semiconductors (Dunod, Paris 1965) p. 401.

6. R.H. Silsbee, J. Appl. Phys. $\underline{28}$, 1246 (1957).

7. H.M. James and K. Lark-Horovtiz, Z. Phys. Chem. $\underline{198}$, 107 (1951).

8. E.I. Blount, Phys. Rev. $\underline{113}$, 995 (1959); J. Appl. Phys. $\underline{30}$, 1218 (1959).

9. H.Y. Fan and K. Lark-Horovitz, Report of Conference on Defects in Crystalline Solids, Bristol, 1954 (Phys. Soc., London) p. 232.

10. J.H. Crawford, Jr., J.W. Cleland, K. Lark-Horovitz, and J.C. Pigg, Phys. Rev. $\underline{85}$, 730 (1952).

11. J.H. Crawford, Jr. and J.W. Cleland, J. Appl. Phys. $\underline{30}$, 1204 (1959).

12. S. Ishino, F. Nakazawa, R. Hasiguiti, J. Phys. Chem. Solids $\underline{24}$, 1033 (1963); $\underline{26}$, 1895 (1965).

13. N.A. Vitovskii, T.V. Mashovets, S.M. Ryvkin, V.P. Sondaevskii, Soviet Phys. - Solid State $\underline{3}$, 727 (1961).

14. O.L. Curtis, Jr. and J.H. Crawford, Jr. Phys. Rev. $\underline{124}$, 1731 (1961).

15. S.M. Ryvkin and I.D. Yaroshetskii, Soviet Phys. - Solid State $\underline{2}$, 1771 (1961).

16. O.L. Curtis, Jr. and J.H. Crawford, Jr., Radiation Damage in Semiconductors (Dunod, Paris, 1965) p.143.

17. B.G. Streetman, J. Appl. Phys. 37, 3145 (1966).

18. T.V. Mashovets and R. Yu. Khanseverov, Soviet Phys. - Solid State 7, 245 (1965).

19. I.P. Akimechenko, V.S. Vavilov, and A.F. Plotnikov, Soviet Phys. - Solid State 8, 1577 (1967).

20. R.A. Logan, Phys. Rev. 91, 757 (1953); S. Mayburg, Phys. Rev. 95, 38 (1954).

21. J.W. Mac Kay and E.E. Klontz, J. Appl. Phys. 30, 1269 (1959); J. Phys. Soc. Japan 18 Supp.III, 216 (1963); T.A. Calcott and J.W. Mac Kay, Phys. Rev. 161, 698 (1967).

22. W.L. Brown, W.M. Augustynak, and T.R. Waite, J. Appl. Phys. 30, 1258 (1959).

23. J.C. Pigg and J.H. Crawford, Jr., Phys. Rev. 135, A 114 (1964); H. Saito, J.C. Pigg, J.H. Crawford, Jr., Phys. Rev. 144, 725 (1966).

24. R.E. Whan, Phys. Rev. 140, 19690 (1965); Appl. Phys. Lett. 6, 221 (1965).

25. J.W. Corbett, R.S. MacDonald, and G.D. Watkins, J. Phys. Chem. Solids 25, 873 (1964).

26. G.D. Watkins, J. Phys. Soc. Japan 18 Supp.III., 22 (1963).

27. G.D. Watkins, Symposium on Radiation Effects in Semiconductor Components, Tolouse, 1967.

28. G.D. Watkins, Radiation Damage in Semiconductors (Dunod, Paris, 1965) p. 97.

29. J.H. Crawford, Jr., in The Interaction of Radiation with Solids, K. Strumane, J. Nihaul, R. Givers, and S. Amelickx, Ed. (North Holland, Amsterdam, 1964) p. 421.

30. J.W. Corbett, Electron Radiation Damage in Semiconductors and Metals, Supp. 17 to Solid State Physics (Academic Press, New York, 1966).

31. W.G. Pfann, Zone Melting (Wiley, New York, 1958).

32. F. Aurich, H.P. Kleinknecht, A. Renz, K. Schuefgraf, and K. Seiler, Ann. Physik 11, 83 (1963).

33. R.N. Hall, R.D. Baertsch, T.J. Soltys, General Electric Report # S-68-1088, May, 1968.

34. J.A. Burton, R.C. Prim, and W.P. Slichter, J. Chem. Phys. 21, 1987 (1953).

35. C.D. Thurmond, Semiconductors, Ed. N.B. Hannay (Reinhold, New York, 1959) p. 160.

36. R.W. Hall, Phys. Rev. 88, 139 (1952); J.Phys. Chem. 57, 836 (1953).

37. J. Czochralski, Z. Phys. Chem. 92, 219 (1918).

38. G.K.Teal and J.B. Little, Phys.Rev. 78, 647 (1950).

39. W.R. Runyan, Rev. Sci, Instr. 30, 535 (1959).

40. W.C. Dash, Growth of Single Crystals, Ed. Doremus et al., (Chapman and Hall, London, 1958) p. 361.

41. C.L. Gallagher, Phys. Rev. 88, 721 (1952).

42. G.L. Pearson, W.T. Read, F.J. Morin, Phys. Rev. 93, 666 (1954).

43. W.T. Read, Phil. Mag. 45, 775 (1954); 45, 1119 (1954); 46, 111 (1955).

44. J.H.P. Von Wuren, G. Koopmans, and J. Block, Phys. Stat. Sol. 27, 219 (1968).

45. W. Schroter, Phys. Stat. Sol. 21, 211 (1967).

46. G.K. Wertheim and G.L. Pearson, Phys. Rev. 107, 694 (1957).

47. F.L. Vogel, W.T. Read, and L.C. Lovel, Phys. Rev. 94, 1791 (1954).

48. R.A. Logan, G.L. Pearson, and D.A. Kleinman, Bull. Am. Phys. Soc. 3, 261 (1958).

49. A.G. Tweet, J. Appl. Phys. 30, 2002 (1959).

50. H.Letaw, Jr., J. Phys. Chem. Sol. 1, 100 (1956).

51. A. Hiraki and Suita, J. Phys. Soc. Japan 18 Supp.III., 254 (1963).

52. C.S. Fuller and K.B. Wolfstirn, J. Phys. Chem. Sol. 26, 463 (1965).

53. P.Penning, Phillips Res. Rep. 13, 17 (1958).

54. T.V. Mashovets, S.M. Ryvkin, R. Yu. Khansevarov, Soviet Phys. - Solid State 9, 407 (1967).

55. M. Stojic and R.R. Hasiguti, Radiation Effects in Semiconductors, Ed. F.L. Vook, (Plenum, New York, 1968) p. 238.

56. M.L. Swanson, ibid., p.46.

57. J.A. Burton, E.D. Kolb, W.P. Slichter, J.D. Struthers, J. Chem. Phys. 21, 1991 (1953).

58. H.A. Schafft, S.G. Needham, NBS Technical Note 445, May, 1968.

59. E.M. Pell, National Academy of Sciences Pub. 871, 136 (1961).

60. A.J. Tavendale, Proc. Second International Symposium on Nuclear Electronics, Paris (IAEA, Vienna), November, 1963.

61. P.P. Webb, IEEE Trans. Nuc. Sci. NS- 15, 321 (1968).

62. S.M. Ryvkin, O.A. Mateev, N.B. Strokan, A.Kh. Khusainov, Soviet Phys. - Technical Physics 9, 1190 (1965).

63. L.V. Maslova, O.A. Mateev,,S.M. Ryvkin, N.B. Strokan, A. Kh. Khusainov, Proc. Panel on Lithium-Drifted Germanium Detectors (International Atomic Energy Commission, Vienna, 1966) p. 32. S.M. Ryvkin, L.L. Makovsky, N.B. Strokan, V.P. Subashieva, A. Kh. Khusainov, IEEE Trans Nuc. Sci. NS- 15, 351 (1968).

64. G.T. Ewan and A.J. Tavendale, Canadian J. Phys. 42, (1964).

65. H.W. Kraner and H.E. Wegner, Bull. Amer. Phys. Soc. 13, 360 (1968).

66. G. Kegal, IEEE Trans. on Nuc. Sci. NS- 15, 332 (1968).

67. J.E. Cline, IEEE Trans. on Nuc. Sci. NS- 15, 198 (1968).

68. S.M. Ryvkin, Soviet Phys. - Semiconductors $\underline{1}$, 1352 (1968).

69. L.B. Valdes, Proc. I.R.E. $\underline{42}$, 420 (1954).

70. F.L. Vogel, W.G. Pfann, H.E. Corey, E.E. Thomas, Phys. Rev. $\underline{90}$, 489 (1953).

71. F.J. Morin, Phys. Rev. $\underline{93}$, 62 (1954).

72. C.D. Thurmond, W.G. Gulder, A.L. Beach, J. Electrochem. Soc. $\underline{103}$, 603 (1956).

73. C.S. Fuller and F.H. Dolieden, J.Phys. Chem. Solids $\underline{19}$, 251 (1961).

74. GeO_2 is not stable at the melting point of germanium (940°C). GeO is highly volatile at this temperature. Using high purity material, no other stable oxides are expected to form in a reducing ambient (hydrogen).

75. W.G. Cochran, Proc. Camb. Phil. Soc. $\underline{30}$, 365 (1934).

76. A.J. Goss and R.E. Adlington, Marconi Rev. $\underline{22}$, 18 (1959).

77. JW. Cleland, J.H. Crawford, Jr., and D.K. Holmes, Phys. Rev. $\underline{102}$, 722 (1956).

78. R.F. Konopleva, S.R. Novikov, and S.M. Ryvkin, Soviet Phys. - Solid State $\underline{6}$, 1596 (1965).

79. E.M. Conwell and V.F. Weisskopf, Phys. Rev. $\underline{77}$, 388 (1950).

80. H. Reiss, C.S. Fuller, and F.J. Morin, Bell System Tech. J. $\underline{35}$, 535 (1956).

81. R.E. Williams, J.Phys. Chem. Sol. $\underline{12}$, 265 (1960).

82. W. Shockley and J.T. Last, Phys. Rev. $\underline{107}$, 392 (1957).

83. R. Dalven, Infrared Phys. $\underline{6}$, 129 (1966).

84. T.R. Waite, Phys. Rev. $\underline{107}$, 463, 471 (1957); J. Phys. Chem. Sol. $\underline{28}$, 103 (1958).

85. O. Lindberg, Proc. I.R.E. $\underline{40}$, 1414 (1952).

86. E.H. Putley, The Hall Effect and Related Phenomena (Butterworths, London, 1060).

87. N.A. Kitovskii, T.V. Mashovets, and S.M. Ryvkin, Soviet Phys. - Solid State $\underline{4}$, 2088 (1963).

88. I.R.E. Standards Committee, Proc. I.R.E. $\underline{49}$, 1293 (1961).

89. J.R. Haynes and W. Shockley, Phys. Rev. $\underline{81}$, 835 (1951).

90. D. Navon, R. Bray, H.Y. Fan, Proc. I.R.E. $\underline{40}$, 1342 (1952); H.Y. Fan, D. Navon, and H.Gebbie, Physica $\underline{20}$, 855 (1954).

91. A.Many, Proc. Phys. Soc. $\underline{67}$, 9 (1954).

92. J.P. Mc Kelvey and R.L. Longini, J. Appl. Phys. $\underline{25}$, 634 (1954).

93. J.A. Hornbeck and J.R. Haynes, Phys. Rev. $\underline{97}$, 311 (1955); Phys. Rev. $\underline{100}$, 606 (1955).

94. A. Smith, Phys. Rev. $\underline{116}$, 793 (1959).

95. J.C. Blakemore and K.C. Nomura, J. Appl. Phys. $\underline{31}$, 753 (1960).

96. W. Shockley and W.T. Read, Jr., Phys. Rev. $\underline{87}$, 835 (1952).

97. Chih-Tang Sah and W. Shockley, Phys. Rev. $\underline{109}$, 1103 (1958).

98. G.K. Wertheim, Phys. Rev. $\underline{109}$, 1086 (1958).

99. O.L. Curtis, Jr.,J. Appl. Phys. $\underline{36}$, 2094 (1965).

100. B.G. Streetman, J. Appl. Phys. $\underline{37}$, 3137 (1966).

101. C.A. Coulson, M.J. Kearsley, Proc. Roy. Soc. $\underline{241}$, 433 (1959).

102. P. Debye and E. Huckel, Physik. Z. $\underline{24}$, 195 (1923).

103. N. Bjerrum, Kgl. Danske Videnskab. Selskab, $\underline{7}$, 9 (1926).

104. R.M. Fuoss, Trans. Faraday Soc. $\underline{30}$, 967 (1934).

105.   H. Reiss, J. Chem. Phys. $\underline{25}$, 400 (1956).

106.   J.S. Prener, J. Chem. Phys. $\underline{25}$, 1294 (1956).

107.   R.H. Kingston, J. Appl. Phys. $\underline{27}$, 101 (1956).

108.   H.C. Gatos, Report on Visit to the U.S.S.R., 1968.

BIOGRAPHY

The author was born on December 2, 1943 in Birmingham Alabama. After graduating from Shades Valley High School in Birmingham, he entered the Massachusetts Institute of Technology in September, 1961 and received an S.B. degree from the Department of Metallurgy in June, 1965. During this period he was elected a member of Phi Lambda Upsilon and commissioned in the United States Air Force.

In September, 1965, the author entered graduate school in the Department of Metallurgy at the Massachusetts Institute of Technology, and engaged in a doctoral program emphasizing the physics of solids in the Electronic Materials Group. During this period he was elected a member of Sigma Xi.